RANGELAND INVENTORY AND MONITORING WITH UNMANNED AERIAL SYSTEM IMAGERY

by

Jeffrey K. Gillan

_____

A Dissertation Submitted to the Faculty of

SCHOOL OF NATURAL RESOURCES AND THE ENVIRONMENT

In Partial Fulfillment of the Requirements
For the Degree of

DOCTOR OF PHILOSOPHY
WITH A MAJOR IN NATURAL RESOURCE STUDIES

In the Graduate College
THE UNIVERSITY OF ARIZONA
2019

THE UNIVERSITY OF ARIZONA
GRADUATE COLLEGE

As members of the Dissertation Committee, we certify that we have read the dissertation prepared by Jeffrey K. Gillan titled, "Rangeland inventory and monitoring with unmanned aerial system imagery" and recommend that it be accepted as fulfilling the dissertation requirements of the Degree of Doctor of Philosophy.

_____ Date: April 15th, 2019
Willem J.D. van Leeuwen

_____ Date: April 15th, 2019
Mitchel P. McClaran
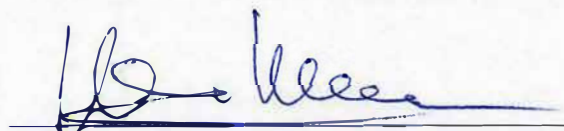
_____ Date: April 15th, 2019
Steve Archer

_____ Date: April 15th, 2019
Jason W. Karl

Final approval and acceptance of this dissertation is contingent upon the candidate's submission of the final copies of the dissertation to the Graduate College.

I hereby certify that I have read this dissertation prepared under my direction and recommend that it be accepted as fulfilling the dissertation requirement.

_____ Date: April 15th, 2019
Willem J.D. van Leeuwen
Dissertation Committee Chair
School of Natural Resources and the Environment

ACKNOWLEDGEMENTS

Those who helped me on this journey:
Connie Maxwell, Amy Slaughter, Brad Cooper, Justin Van Zee, Kyle Hartfield, Charlie Conley, Bailey Bellavance, Patrick Broxton, Andy Honaman, Tyson Swetnam, Phil Heilman, Mary Nichols, Michelle Cavanaugh, Meg Lota Brown, David Bradshaw, Katie Hughes, Lindsey Fera, Ashley Stewart, Byron Hempel, Sarah Noelle, Rachel Turner, Kelsey Landreville, Vanessa Prileson, Andrew Johnson, Eric Panebaker, Greg Barron-Gafford, and my dissertation committee.

TABLE OF CONTENTS

ABSTRACT

Publicly managed rangelands today are seeing higher demand from society for the goods and services they can provide, including livestock production, wildlife habitat, myriad forms of recreation, and ecosystem services. Adaptively managed multiple-use lands could benefit from more objective and synoptic data to evaluate ecosystem function and to carry out and defend land health assessments that allow or exclude certain land use activities. Field methods to measure critical soil and vegetation indicators are well-established and becoming standardized across jurisdictions. However, field methods have two main limitations: 1) most can only observe small portions of the landscape, which may produce an incomplete picture of the status and trend of rangeland health; and 2) field methods cannot measure some indicators very well or not at all. This research focused on developing methods to measure soil and vegetation characteristics from unmanned aerial system (commonly known as drones) imagery, which can observe significantly more land than their field counterparts. I demonstrated the measurement of one soil (erosion/deposition) and four vegetation (forage utilization, fractional cover, vegetation height, canopy gaps) indicators using drone imagery and compared each with established field methods. The results show that drone imagery methods can serve as a complement to field methods or even a replacement in some cases. I found that drone imagery methods can precisely map topographic change and forage utilization across extents not previously possible. Imagery methods can outperform field methods for vegetation heights and canopy gaps in some vegetation communities. Drone-imagery indicators have matured to the point where they can start being integrated into adaptive land management. An online space dedicated to sharing imagery workflows amongst the range community could quicken the pace of identifying best practices to facilitate the transition toward this technology. Adopting drone-based inventory and monitoring data, however, will not replace field skills in plant identification, knowledge of vegetation phenology and succession, and logical interpretation of the data for land health assessments.

INTRODUCTION

Intellectual Merit and Research Context

Rangelands are typically arid to semi-arid lands composed of indigenous vegetation usually characterized as grasslands, savannas, shrublands, and deserts (Society for Range Managment, 1998). What links these lands under common terminology is their marginal value for cultivating crops in their dry environments. Rangelands occur all over the world, but in North America, I am primarily referring to lands starting in the Great Plains in the center of the continent and stretching west to the Pacific Ocean. These lands are below the high elevation forests, where a large proportion are managed by public agencies due to their tendency to be remote and drought stricken. These lands were once thought only valuable for production of food and fiber in the form of livestock (Sayre, 2017). In more recent decades, society has assigned many more values to these lands including biodiversity, wildlife habitat, ecosystem services including water provisioning, clean air, carbon sequestration, and myriad forms of recreation (Havstad et al., 2007; Millennium Ecosystem Assessment, 2005; Yahdjian et al., 2015).

The beginning of the 20th century saw a recognition that western rangelands were degrading and producing less forage for livestock than previously. In reaction to this, the field of range science began in the West in an attempt to determine the carrying capacity of land and sustain natural grass production for the livestock industry (Sayre 2017). A century later, the goal of range science is still to try to keep lands useful and productive but for an expanding set of values and higher demand from society.

Rangeland landscapes today are a mosaic of vegetation communities impacted by disturbances such as herbivory (domestic and wild), fire, disease, and an array of human manipulation. Ownership and management of these lands is also a mosaic of public and private entities

sometimes with conflicting missions, and a general public with diverging opinions on how the land should be used and managed.

Rangeland managers today, especially on public lands, have a difficult task of managing for multiple use (FLPMA 1976). To manage for all desired uses, rangeland science and management has moved away from assessing site conditions relative to specific land uses (e.g., livestock grazing), and toward a more holistic ecosystem approach known as range health. Range health is the 'the degree to which the integrity of the soil and ecological processes of rangeland ecosystems are maintained' (NRC, 1994; Pellant et al., 2005) which is assessed through the ecological attributes of biotic integrity, soil and site stability, and hydrologic function (Pellant et al., 2005; Pyke et al., 2002).

Managers need information on the status and trend of rangeland health to make informed decisions on type and intensity of land use, as well as to prescribe corrective actions. Assessing the three aspects of rangeland health is carried out by measuring indicators. Indicators are vegetation or soil traits that are essential for tracking the basic functions and associated ecosystem services provided by rangelands (Herrick et al., 2010). Indicators can be qualitative or quantitative and include proportion of ground cover, species composition, presence of rills and soil pedestals, and vegetation heights as examples.

Rangeland health indicator data can be used in an adaptive management framework. Adaptive management is the scientific method applied to resource management: recurrent management while striving to reduce uncertainty in understanding mechanisms of ecosystem dynamics (Kendall and Moore, 2012). Depending how and when indicator data are collected, they can be used for inventory, monitoring, or assessments. An inventory is a point in time measurement of the resource to determine location or current condition (Elzinga et al. 1998), which can provide

the basis for management plans (West, 2003). For example, a species inventory could show a significant presence of an invasive species. Monitoring is the collection and analysis of repeated observations or measurements to evaluate changes in condition and progress toward meeting a management objective (Elzinga et al. 1998; Kendall and Moore 2012). Upon developing and implementing a plan of action to combat the invasive species, monitoring data are collected to inform progress or lack thereof toward the resource management goal. Monitoring data are perhaps the most important part of adaptive management because it tells us if actions are working or should be adapted. It completes the information feedback loop (Moir and Block, 2001) and primes another iteration of the adaptive management cycle with a bit more knowledge of the ecosystem. Assessments are point-in-time interpretations of monitoring and inventory data in relation to management objectives, benchmarks, or reference (i.e., ideal) condition (West, 2003). An example is a comparing a grazing allotment with land health standards for permit renewal (USDI Bureau of Land Management, 2001).

Methods refer to the mechanics of how to measure an indicator (Karl et al., 2017) and have been developing since range became a field of science in the early 20th century. There are often several methods for measuring the same indicator with nuance to the information they provide and their interpretability. For example, there are several methods to measure vegetation cover - along a step transect, via a continuous line transect, with point intercept techniques, or estimated in plot frames (Elzinga et al., 1998).

Field methods are able to generate very detailed data describing a site including species composition, presence of biological crusts, and fine-scale erosion. The fundamental limitation of field methods are that they are generally limited in geographic scope and cost-prohibitive to cover large areas (Booth and Cox, 2011). Data from small plots or key areas cannot be automatically scaled up to represent entire pastures or landscapes (West, 2003). Small sample sizes over large,

heterogeneous landscapes may lead to high degrees of uncertainty of indicator values and rangeland health.

There is never enough funding to collect ground-based inventory and monitoring data at the frequency, detail, or scale that would be ideal over a long time horizon (Booth and Cox, 2011). Remote sensing (aerial photography & satellite imagery) offers methods for collecting range data over larger extends and potentially reducing the cost of information. As of the year 2019, there are geospatial imagery platforms and products available to study rangelands at myriad grains and extents. From space-borne sensors capable of imaging entire continents to manned aerial photography capable of hyperspectral imaging with sub-meter resolution, the choice of remotely sensed data is large and growing. However, expanding the extent of data with remote sensing often has the tradeoff of detail loss and inferring/modeling indicator values instead of observing them. Additionally, many fine-scale soil and vegetation characteristics that indicate rangeland health, are not easily measured with satellite imagery because of coarse resolution and temporal infrequency (Tueller, 1996). Use of manned aerial photography is primarily limited by cost.

Research to develop monitoring methods from small unmanned aerial system (sUAS), commonly known as drones, is currently receiving a lot of attention to expand inventory and monitoring extents. There are currently several types of relatively inexpensive ready-to-fly drones that are small enough to be carried into the field and deployed by one person. They can capture very high resolution data (< 5 cm resolution) over dozens to hundreds of hectares on-demand. These tools have enabled rangeland scientists and managers to study the land at a new scale with inexpensively produced 2D and 3D imagery products. Drone imagery methods have the potential to replace field methods in some instances, expand or compliment others, and enable the development of new indicators (Cunliffe et al., 2016; Olsoy et al., 2018; Rango et al., 2009).

My research sought to develop methods of measuring important rangeland indicators with UAS color and multispectral imagery. My goals were to expand the extent of inventory and monitoring data and to measure indicators in ways not possible with traditional ground-based methods.

Rangeland Remote Sensing Literature Review
The first use of aerial photography to assess agricultural lands occurred in the 1930s (Monmonier, 2002; Rango et al., 2008). Widespread use began as a way for the USDA to monitor crop and pasture acreage to stabilize the over-supply of crops and support soil-conserving crops. Aerial photography for range science also began in the 1930's with the first images acquired in 1936 at Santa Rita Experimental Range, AZ (Browning et al., 2009), and in 1937 at Jornada Experimental Range, NM (Laliberte et al., 2004).

Over the following decades, there were many studies using aerial photography for rangeland applications, mostly through photo interpretation. For example, Dudzinski and Arnold (1967) located sheep from aerial imagery to infer grazing behavior. Driscoll (1970) demonstrated using color infrared imagery to photo interpret shrub species and measure foliar cover in Colorado rangelands.

The satellite sensor age beginning in the 1970s ushered in new digital imagery analysis and the ability to study rangelands on landscape, regional, and continental scales (Tueller, 1989). For example, Maxwell (1976) and Haas et al. (1975) each used Landsat MSS imagery to estimate green biomass in the Great Plains. Musick (1984) used spectral indices from Landsat MSS to estimate vegetation cover at Jornada Experimental Range in southern New Mexico. Despite these new capabilities, there was often a mismatch in the information satellite imagery could provide and the information range managers wanted (Hunt et al., 2003). Satellite imagery at the time had

relatively coarse spatial resolution, too coarse for many inventory and monitoring indicators and the ability to infer plant successional stages (Hunt et al., 2003).

Some range remote sensing research shifted back to aerial photography because of the capability of generating high-resolution imagery (< 1 m) which could produce more detailed information including percent bare-ground, and individual plant species (Tueller, 1996). Many digital image analysis techniques developed for satellite imagery began to be applied to aerial photography. Acquiring aerial imagery on film was still the most common practice meaning it had to be scanned or digitized before analysis. For example, Everitt et al. (1980) analyzed color infrared film photographs with a densitometer to separate 12 rangeland sites in a south Texas coastal prairie. Whiteman and Brown, (1998) used film aerial photographs, digitized to create 0.6 m pixels, where they estimated woody shrub density and cover in Mitchell grasslands in Queensland, Australia. Gong et al., (2000) digitized aerial film to 0.3 m resolution to estimate tree heights in a California oak woodland. Film was still being used as recently as 1999 when Petersen et al., (2005) used color and color infrared film to classify 3 willow species in southeastern Oregon after they digitized it to 7 cm pixels.

Acquiring aerial imagery with digital sensors began to appear in the rangeland remote sensing literature in mid-2000s (Booth et al., 2006; Booth and Cox, 2008). An all-digital workflow streamlined image processing and analysis for measuring range indicators such as vegetation cover (Duniway et al., 2012; Karl et al., 2014), canopy gaps (Karl et al., 2012b), vegetation heights (Gillan et al., 2014), and soil erosion (Gillan et al., 2016). In addition to all digital passive sensors, active sensors such as light distance and ranging (LiDAR) were shown to be useful tools for measuring 3-dimensional rangeland indicators. For example, airborne LiDAR was demonstrated to accurately measure the 3D structure of rangeland shrubs (Glenn et al., 2011; Streutker and Glenn, 2006) and erosion in dryland ecosystems (Perroy et al., 2010).

Collecting high-resolution imagery (or LiDAR) from manned airplanes typically requires contracting with a commercial provider, which can be expensive and inflexible in terms of short-notice scheduling. UAS were seen as a more affordable and safer option that could be brought in-house and deployed on-demand. One of the first published papers using UAS-based imagery for a rangeland application was with a fixed-wing drone used to estimate shrub utilization (Quilter and Anderson, 2001). Hardin et al. (2007) and Hardin and Jackson (2005) used fixed-wing UAS for monitoring knapweed in Utah. Researchers at the Jornada Experimental Range in New Mexico produced a large body of research which exposed the range community to the potential of UAS and advanced image analysis for range monitoring, assessments, and inventories (Laliberte et al., 2011; Rango et al., 2009). Those demonstrations, however, used relatively large and expensive drones and required a team of specialists. It was not easily replicated for public lands due to cost and aviation rules at the time (see Rango and Laliberte, 2010).

The arrival of inexpensive multi-rotors and sensors small enough to mount on them, has made the use of drone imagery much more practical in terms of cost and learning curve. Dandois and Ellis (2010) shifted the paradigm by being the first to measure the size and structure of vegetation in 2D and 3D with inexpensive digital cameras mounted on multi-rotor platforms. Multi-rotor copters can be easily operated by one person and programmed to conduct autonomous data collecting missions. At the heart of this new approach was a computer vision photogrammetry technique called structure-from-motion (Snavely et al., 2008; Westoby et al., 2012) that made it possible to produce very accurate point clouds and orthomosaics from drone-based digital imagery (see Appendix A for details). Anderson and Gaston (2013) predicted the merging of these hardware and software technologies would revolutionize spatial ecology.

In 2013, a Chinese company, DJI (www.dji.com), released the first ready-to-fly consumer multi-rotor called Phantom and in 2014 released Phantom 2 with an integrated camera. This signaled the beginning of mainstream awareness of the potential uses of drone imagery to impact research for natural resource and earth sciences. Demand has subsequently soared in the research community and many other sectors including agriculture, civil engineering, archeology, law enforcement, and real estate (Colomina and Molina, 2014; Floreano and Wood, 2015; Watts et al., 2012). Commercial companies have responded by continually improving airframes, global navigation satellite systems, autopilots, and image processing software.

Natural resource scientists are currently researching the use of drone imagery to measure a variety of soil and vegetation indicators. For example, Cunliffe et al., (2016) demonstrated the use of small multi-rotor imagery to 3D model semi-arid vegetation and estimate above ground biomass in New Mexico. Olsoy et al., (2018) used a Sensefly Ebee (www.sensefly.com), a small wing-shaped drone carrying an RGB sensor, to estimate the heights of sagebrush shrubs and relate it to pygmy rabbit habitat. Baena et al., (2017) identified dryland tree and shrub species in Peru with a modified RGB sensor flown on a Sensefly Ebee. Cox et al., (2018) tracked the size and pace of headcut erosion with a combination of historical aerial imagery and 3D modeling of recently collected drone imagery.

Additional research is required to meet the ultimate goal of integrating drone-based indicators within adaptive management of public rangelands. The research needs include: comparing imagery indicator values with traditional field methods across different vegetation communities; developing image-processing workflows that can efficiently estimate multiple indicators; and developing new image-based methods not previously published.

PRESENT STUDY

This dissertation consists of three research projects described in Appendices A, B, and C. Taken together, they demonstrate UAS imagery methods to geographically expand and enhance the ability to estimate one soil and four vegetation indicators. The following section describes each of the projects including their objectives, equipment and imagery methods, comparison with traditional field methods, major findings, and a description of my role in the research.

Appendix A: Fine-resolution Repeat Topographic Surveying of Dryland Landscapes using UAS-Based Structure-from-motion Photogrammetry: Assessing Accuracy and Precision against Traditional Ground-based Erosion Measurements

Jeffrey K. Gillan, Jason W. Karl, Ahmed Elaksher, and Michael C. Duniway

We used drone-based imagery to measure the vertical change of a rangeland soil surface to quantify and visualize soil erosion, deposition, and redistribution. Along thirty topographic transects we measured the soil surface height from digital elevations models (DEMs) created from aerial imagery from a large fixed-wing drone. We compared the heights to ground-based measurements taken from a laser range finder suspended from an erosion bridge and found strong vertical agreement (accuracy) between the methods (RMSE 2.9 and 3.2 cm in June 2014 and February 2015, respectively) and high vertical repeatability for creating DEMs (RMSE 2.8 cm). Our results suggest repeat UAV imagery and structure-from-motion photogrammetry processing could replace erosion bridges and provide for a more synoptic landscape assessment than field-based methods of shifting soil surfaces for some studies. Though we used a large and impractical drone (in terms of cost and aviation rules) in this study, the methods would be easier and the same results could be achieved with smaller and more affordable equipment.

I led the research including developing the concept for the study, reviewing literature on the topic, processing and analyzing the data, and preparing the manuscript. The erosion bridge measurements were collected by staff at Jornada Experimental Range as part of the 'Threshold Resistance and Connectivity' study originally developed by Michael Duniway and Jeffrey Herrick. Drone mission planning and operation was carried out by Connie Maxwell and Amy Slaughter, both of Jornada Experimental Range. Writing and editing of the final manuscript was aided by my co-authors, Jason Karl, Ahmed Elaksher, and Michael Duniway.

Appendix B: Estimating forage utilization with drone-based photogrammetric point clouds

Jeffrey K. Gillan, Mitchel P. McClaran, Tyson L. Swetnam, and Philip Heilman

Similar to my other research projects, I sought to compare and contrast a traditional field method with a drone imagery method that can observe larger land extents. We developed a point cloud differencing method to estimate forage utilization, an approach unique in published literature. We tested the method at Santa Rita Experimental Range, a semi-arid savanna in southern Arizona. We found strong agreement between field and point cloud estimates of forage utilization across 6 test plots. Additionally, our method allowed us to map and visualize utilization intensity across space, a potentially useful dataset for investigating grazing behavior. With minor workflow and technological improvements, it would be feasible to estimate forage utilization over the entire pasture (150 ha) and potentially even larger areas using drone-imagery point clouds. This was the first study I conducted using inexpensive multi-rotor drones for image collection. It was an

important step toward demonstrating that cost-effective tools could be useful for rangeland inventory and monitoring.

Mitch McClaran, Phil Heilman, and Tyson Swetnam conceived of the original idea to measure grass height change with drone-based point clouds. We equally developed the study and plot design. Rachel Turner and Sarah Noelle carried out ground-based measurements of biomass and utilization. I collected all of the drone imagery, processed the imagery into point clouds and orthomosaics, conducted the analysis, and interpreted the results. I was the primary manuscript author with input and writing from Mitch McClaran, Tyson Swetnam, and Phil Heilman.

Appendix C: Toward Operationalizing the use of low cost UAS as an imaging tool for rangeland inventory and monitoring

Jeffrey K. Gillan, Willem J.D. van Leeuwen, and Jason W. Karl

Formatted for *Environmental Monitoring and Assessment*

Transitioning from research demonstrations to a suite of monitoring methods that are useful for supporting management decisions (e.g., accurate, repeatable, and cost-effective) will require additional exploration to develop best practices for image acquisition and workflow specifications that can efficiently estimate multiple indicators. The objectives of this project were to: 1) develop a unified workflow to measure three common rangeland indicators from drone imagery, fractional cover of plant functional types, canopy gaps, and vegetation heights; and 2) assess agreement between imagery-based indicator values and field-measured values and investigate how fractional cover estimates differed between two sensor types (RGB v. multi-spectral). I embedded with a field monitoring crew in the Northern California District of the Bureau of Land Management to compare imagery-derived (using small drones) and field-measured indicator values. The indicator

values between imagery and field methods yielded encouraging agreement while revealing

systematic differences between the methods. There was minimal difference in fractional cover

accuracy between sensor types. Drone imagery will enable broader extent observations of

fractional cover, but with a tradeoff of detail loss. For canopy gaps and vegetation heights, drone

imagery was found to measure the indicators more thoroughly than field methods. Workflow best

practices for producing a suite of indicators is likely to vary by vegetation composition and

phenology. An online space dedicated to sharing imagery-based workflows could spur

collaboration among researchers and quicken the pace of integrating drone-imagery data with

adaptive management of rangelands.

I developed the concept for the project, collected the aerial imagery, processed all data, generated

indicator values, and interpreted results. I wrote the manuscript with input and guidance from

Wim van Leeuwen, Jason Karl, Mitch McClaran, and Kyle Hartfield. The Great Basin Institute,

in partnership with BLM, collected all field indicator data used in this study.

Conclusions and Future Directions
This research adds to the growing body of knowledge on using UAS-based imagery for rangeland

inventory and monitoring data collection. I demonstrated that drone-imagery can expand the

extent of each of the indicators I investigated (soil erosion, forage utilization, fractional cover,

canopy gaps, and vegetation heights) compared with traditional field methods. These larger

sampling extents can increase our confidence in indicators values and effectively reduce the cost

of collecting rangeland health information across landscapes. Despite the broader extent, drone

data will typically be used in a sampling framework instead of a landscape census (see Karl et al.,

2012a).

In addition to expanding the extent of some indicators, drone-imagery methods produce maps, facilitating spatial analyses and visualizations of indicator value patterns that are not possible with field data alone. Spatially explicit data can foster tangential ecological inquiries not currently possible with field data. For example, pairing livestock movement data (via GPS or accelerometers) with dense point cloud representations of their grazing environment and utilized forage, could enable interesting grazing behavior studies. Quantifying and visualizing soil movement can reveal erosional processes related to vegetation, gaps, slope, and soil type, in ways not easily discerned from field transects.

Drone-imagery will enable us to measure some indicators more thoroughly than field methods. This was best demonstrated with vegetation heights. Photogrammetry can extract hundreds of measurements per individual plant, revealing the complex nature of vegetation structure and improving our ability to assess wildlife habitat, compute biomass, and calculate carbon storage. Drone-imagery will empower us to develop new indicators, features of the land that cannot be measured at all from the ground. These could include landscape-style metrics describing the connectivity of wind and water forces, and fragmentation of vegetation communities or habitat.

Expanding the extent of data, however, is often a tradeoff with observation detail. For fractional cover, distinguishing grasses and other herbaceous species as well as identifying rare plants and biological crusts is a significant challenge from imagery at any scale. This limitation will prevent imagery-based monitoring from completely replacing field-based observation. For forage utilization, detecting light grazing will be difficult with a point cloud approach. Similarly, detecting small amounts of soil surface change (1-2 cm) would not be possible with the imagery scale we used. However, management scenarios requiring levels of grazing or erosion detection

more precise than thresholds in this research are exceedingly rare, and not likely to impede the methods' utility.

The next step in this research is to leave the plot realm (where most drone imagery research has so far occurred) and scale-up to pastures and landscapes while maintaining rapid data processing and product turnaround. Creating image products faster and cheaper will be aided by two technologies. The first is leveraging differential GNSS technology onboard the drones. Real time kinematic GNSS is becoming more common for precisely recording drone position at image exposure time. Through direct georeferencing, the need for ground control targets is reduced or eliminated (Forlani et al., 2018; Turner et al., 2014), which will accelerate data collection efforts and streamline reference identification during photogrammetric processing. The current model of using a single powerful desktop computer to process individual drone-collected images into point clouds, elevation models, and orthomosaics is not a time- or cost-effective approach to producing image products from thousands of aerial images. The second technology that will enable scaling up of drone-based monitoring of rangelands is using distributed network processing or many high-performance computing nodes to speed dense point cloud generation (Goff et al., 2011; Gorelick et al., 2017; Jones et al., 2018).

Drone imagery-indicators have matured to the point where they can start being integrated into adaptive land management. An online space dedicated to sharing imagery workflows amongst the range community could quicken the pace of identifying best practices to facilitate the transition toward this technology. Drone-based aerial photography and ground data offer different lines of evidence for some pattern or process and an additional stream of information to help us understand what is happening on the land and insights into how we can keep it healthy and productive.

REFERENCES

Anderson, K., Gaston, K.J., 2013. Lightweight unmanned aerial vehicles will revolutionize spatial ecology. Front. Ecol. Environ. 11, 138–146. https://doi.org/10.1890/120150

Baena, S., Moat, J., Whaley, O., Boyd, D.S., 2017. Identifying species from the air: UAVs and the very high resolution challenge for plant conservation. PLoS One 12, e0188714. https://doi.org/10.1371/journal.pone.0188714

Booth, D., Cox, S., 2011. Art to science: Tools for greater objectivity in resource monitoring. Rangelands 33, 27–34. https://doi.org/10.2111/1551-501x-33.4.27

Booth, D.T., Cox, S.E., 2008. Image-based monitoring to measure ecological change in rangeland. Front. Ecol. Environ. 6, 185–190. https://doi.org/10.1890/070095

Booth, D.T., Cox, S.E., Berryman, R.D., 2006. Precision measurements from very-large scale aerial digital imagery. Environ. Monit. Assess. 112, 293–307. https://doi.org/10.1007/s10661-006-1070-0

Browning, D.M., Archer, S.R., Byrne, A.T., 2009. Field validation of 1930s aerial photography: What are we missing? J. Arid Environ. 73, 844–853. https://doi.org/10.1016/j.jaridenv.2009.04.003

Colomina, I., Molina, P., 2014. Unmanned aerial systems for photogrammetry and remote sensing: A review. ISPRS J. Photogramm. Remote Sens. 92, 79–97. https://doi.org/10.1016/j.isprsjprs.2014.02.013

Council, N.R., 1994. Rangeland Health: new methods to classify, inventory, and monitor rangelands. National Academy Press, Washington DC.

Cox, S.E., Doncaster, D.L., Godfrey, P.E., Londe, M.D., 2018. Aerial and terrestrial-based monitoring of channel erosion, headcutting, and sinuosity. Environ. Monit. Assess. 190, 717. https://doi.org/10.1007/s10661-018-7091-7

Cunliffe, A.M., Brazier, R.E., Anderson, K., 2016. Ultra-fine grain landscape-scale quantification

of dryland vegetation structure with drone-acquired structure-from-motion photogrammetry. Remote Sens. Environ. 183, 129–143. https://doi.org/10.1016/j.rse.2016.05.019

Dandois, J.P., Ellis, E.C., 2010. Remote sensing of vegetation structure using computer vision. Remote Sens. 2, 1157–1176. https://doi.org/10.3390/rs2041157

Driscoll, R.S., 1970. Identification and measurement of shrub type vegetation on large-scale aerial photograps, in: Third Annual Earth Resources Program Review, Vol II, Agriculture and Sensor Studies. NASA manned spacecraft Center, Houston, TX.

Dudzinski, M.L., Arnold, G.W., 1967. Management Aerial Photography and Statistical Analysis for Studying Behaviour Patterns of Grazing. J. Range Manag. Manag. 20, 77–83.

Duniway, M.C., Karl, J.W., Schrader, S., Baquera, N., Herrick, J.E., 2012. Rangeland and pasture monitoring: an approach to interpretation of high-resolution imagery focused on observer calibration for repeatability. Environ. Monit. Assess. 184, 3789–804. https://doi.org/10.1007/s10661-011-2224-2

Elzinga, C.L., Salzer, W., Willoughby, J.W., 1998. Measuring and Monitoring Plant Populations. U.S. Department of the Interior, Bureau of Land Management, Denver, CO.

Everitt, J.H., Gerbermann, A.H., Alaniz, M.A., Bowen, R.L., 1980. Using 70-mm aerial photography to identify rangeland sites. Photogramm. Eng. Remote Sens. 46, 1339–1348. https://doi.org/10.1038/nnano.2013.174

Floreano, D., Wood, R.J., 2015. Science, technology and the future of small autonomous drones. Nature 521, 460–466. https://doi.org/10.1038/nature14542

Forlani, G., Dall'Asta, E., Diotri, F., Cella, U.M. di, Roncella, R., Santise, M., 2018. Quality Assessment of DSMs Produced from UAV Flights Georeferenced with On-Board RTK Positioning. Remote Sens. 10, 311. https://doi.org/10.3390/rs10020311

Gillan, J.K., Karl, J.W., Barger, N.N., Elaksher, A., Duniway, M.C., 2016. Spatially Explicit Rangeland Erosion Monitoring Using High-Resolution Digital Aerial Imagery. Rangel. Ecol. Manag. 69, 95–107. https://doi.org/10.1016/j.rama.2015.10.012

Gillan, J.K., Karl, J.W., Duniway, M., Elaksher, A., 2014. Modeling vegetation heights from high resolution stereo aerial photography: an application for broad-scale rangeland monitoring. J. Environ. Manage. 144, 226–35. https://doi.org/10.1016/j.jenvman.2014.05.028

Glenn, N.F., Spaete, L.P., Sankey, T.T., Derryberry, D.R., Hardegree, S.P., Mitchell, J.J., 2011. Errors in LiDAR-derived shrub height and crown area on sloped terrain. J. Arid Environ. 75, 377–382. https://doi.org/10.1016/j.jaridenv.2010.11.005

Goff, S.A., Vaughn, M., McKay, S., Lyons, E., Stapleton, A.E., Gessler, D., Matasci, N., Wang, L., Hanlon, M., Lenards, A., Muir, A., Merchant, N., Lowry, S., Mock, S., Helmke, M., Kubach, A., Narro, M., Hopkins, N., Micklos, D., Hilgert, U., Gonzales, M., Jordan, C., Skidmore, E., Dooley, R., Cazes, J., McLay, R., Lu, Z., Pasternak, S., Koesterke, L., Piel, W.H., Grene, R., Noutsos, C., Gendler, K., Feng, X., Tang, C., Lent, M., Kim, S.-J., Kvilekval, K., Manjunath, B.S., Tannen, V., Stamatakis, A., Sanderson, M., Welch, S.M., Cranston, K.A., Soltis, P., Soltis, D., O'Meara, B., Ane, C., Brutnell, T., Kleibenstein, D.J., White, J.W., Leebens-Mack, J., Donoghue, M.J., Spalding, E.P., Vision, T.J., Myers, C.R., Lowenthal, D., Enquist, B.J., Boyle, B., Akoglu, A., Andrews, G., Ram, S., Ware, D., Stein, L., Stanzione, D., 2011. The iPlant Collaborative: Cyberinfrastructure for Plant Biology. Front. Plant Sci. 2, 34. https://doi.org/10.3389/fpls.2011.00034

Gong, P., Biging, G.S., Standiford, R., 2000. Technical Note: Use of Digital Surface Model for Hardwood Rangeland Monitoring. J. range Manag. 53, 622–626. https://doi.org/10.2307/4003157

Gorelick, N., Hancher, M., Dixon, M., Ilyushchenko, S., Thau, D., Moore, R., 2017. Google Earth Engine: Planetary-scale geospatial analysis for everyone. Remote Sens. Environ. 202, 18–27. https://doi.org/10.1016/j.rse.2017.06.031

Haas, R.H., Deering, D.W., Rouse Jr., J.W., Schell, J.A., 1975. Monitoring vegetation conditions from Landsat for use in range management, in: NASA Earth Resource Symposium. Houston, TX.

Hardin, P., Jackson, M., Anderson, V., Johnson, R., 2007. Detecting Squarrose Knapweed (

    Centaurea virgata Lam. Ssp. squarrosa Gugl.) Using a Remotely Piloted Vehicle: A Utah

    Case Study. GIScience Remote Sens. 44, 203–219. https://doi.org/10.2747/1548-

    1603.44.3.203

Hardin, P.J., Jackson, M.W., 2005. An Unmanned Aerial Vehicle for Rangeland Photography.

    Rangel. Ecol. Manag. 58, 439–442. https://doi.org/10.2111/1551-

    5028(2005)058[0439:AUAVFR]2.0.CO;2

Havstad, K.M., Peters, D.P.C., Skaggs, R., Brown, J., Bestelmeyer, B., Fredrickson, E., Herrick,

    J., Wright, J., 2007. Ecological services to and from rangelands of the United States. Ecol.

    Econ. 64, 261–268. https://doi.org/10.1016/j.ecolecon.2007.08.005

Herrick, J.E., Lessard, V.C., Spaeth, K.E., Shaver, P.L., Dayton, R.S., Pyke, D. a, Jolley, L.,

    Goebel, J.J., 2010. National ecosystem assessments supported by scientific and local

    knowledge. Front. Ecol. Environ. 8, 403–408. https://doi.org/10.1890/100017

Hunt, E.R., Everitt, J.H., Ritchie, J.C., Moran, M.S., Booth, D.T., Anderson, G.L., Clark, P.E.,

    Seyfried, M.S., 2003. Applications and Research Using Remote Sensing for Rangeland

    Management. Photogramm. Eng. Remote Sens. 69, 675–693.

    https://doi.org/10.14358/PERS.69.6.675

Jones, M.O., Allred, B.W., Naugle, D.E., Mestas, J.D., 2018. Innovation in rangeland

    monitoring : annual , 30 m , plant functional type percent cover maps for U . S . rangelands ,

    1984 – 2017 9. https://doi.org/10.1002/ecs2.2430

Karl, J.W., Duniway, M.C., Nusser, S.M., Opsomer, J.D., Unnasch, R.S., 2012a. Using Very-

    Large-Scale Aerial Imagery for Rangeland Monitoring and Assessment: Some Statistical

    Considerations. Rangel. Ecol. Manag. 65, 330–339. https://doi.org/10.2111/REM-D-11-

    00102.1

Karl, J.W., Duniway, M.C., Schrader, T.S., 2012b. A Technique for Estimating Rangeland

    Canopy-Gap Size Distributions From High-Resolution Digital Imagery. Rangel. Ecol.

Manag. 65, 196–207. https://doi.org/10.2111/REM-D-11-00006.1

Karl, J.W., Gillan, J.K., Barger, N.N., Herrick, J.E., Duniway, M.C., 2014. Interpretation of high-resolution imagery for detecting vegetation cover composition change after fuels reduction treatments in woodlands. Ecol. Indic. 45. https://doi.org/10.1016/j.ecolind.2014.05.017

Karl, J.W., Herrick, J.E., Pyke, D.A., 2017. Monitoring Protocols: Options, Approaches, Implementation, Benefits, in: Briske, D. (Ed.), Rangeland Systems: Processes, Management and Challenges. Springer, p. 664.

Kendall, W.L., Moore, C.T., 2012. Maximizing the utility of monitoring to the adaptive management of natural resources, in: Gitzen, R.A., Milspaugh, J.J., Cooper, A.B., Licht, D.S. (Eds.), Design and Analysis of Long-Term Ecological Monitoring Studies. University of Cambridge Press.

Laliberte, A.S., Rango, A., Havstad, K.M., Paris, J.F., Beck, R.F., McNeely, R., Gonzalez, A.L., 2004. Object-oriented image analysis for mapping shrub encroachment from 1937 to 2003 in southern New Mexico. Remote Sens. Environ. 93, 198–210. https://doi.org/10.1007/978-3-319-42019-6_13

Laliberte, A.S., Winters, C., Rango, A., 2011. UAS remote sensing missions for rangeland applications. Geocarto Int. 26, 141–156. https://doi.org/10.1080/10106049.2010.534557

Maxwell, E.L., 1976. A remote rangeland analysis system. J. Range Manag. 29, 66–73.

Millennium Ecosystem Assessment, 2005. Ecosystems and Human Well-Being: desertification synthesis, Ecosystems and human well-being. https://doi.org/ISBN: 1-56973-590-5

Moir, W.H., Block, W.M., 2001. Adaptive Management on Public Lands in the United States : Commitment or Rhetoric ? Environ. Manage. 28, 141–148. https://doi.org/10.1007/s002670010213

Monmonier, M., 2002. Aerial Photography at the Agricultural Adjustment Administration: Acreage Controls, Conservation Benefits, and Overhead Surveillance in the 1930s. Photogramm. Eng. Remote Sens. 68, 1257–1261.

Musick, H.B., 1984. Assessment of Landsat Multispectral Scanner spectral indexes for

    monitoring arid rangeland. IEEE Trans. Geosci. Remote Sens. GE-22, 512–519.

    https://doi.org/10.1109/TGRS.1984.6499162

Olsoy, P.J., Shipley, L.A., Rachlow, J.L., Forbey, J.S., Glenn, N.F., Burgess, M.A., Thornton,

    D.H., 2018. Unmanned aerial systems measure structural habitat features for wildlife across

    multiple scales. Methods Ecol. Evol. 9, 594–604. https://doi.org/10.1111/2041-210X.12919

Pellant, M., Shaver, P., Pyke, D.A., Herrick, J.E., 2005. Interpreting Indicatiors of Rangeland

    Health, version 4, Technical Reference 1734-6. https://doi.org/10.1007/s13398-014-0173-

    7.2

Perroy, R.L., Bookhagen, B., Asner, G.P., Chadwick, O. a., 2010. Comparison of gully erosion

    estimates using airborne and ground-based LiDAR on Santa Cruz Island, California.

    Geomorphology 118, 288–300. https://doi.org/10.1016/j.geomorph.2010.01.009

Petersen, S.L., Stringham, T.K., Laliberte, A.S., 2005. Classification of willow species using

    large-scale aerial photography. Rangel. Ecol. Manag. 58, 582–587.

    https://doi.org/10.2111/04-129R1.1

Pyke, D., Herrick, J., Shaver, P., Pellant, M., 2002. Rangeland health attributes and indicators for

    qualitative assessment. J. range Manag. 55, 584–597. https://doi.org/10.2307/4004002

Quilter, M.C., Anderson, V. a L.J.O., 2001. A proposed method for determining shrub utilization

    using (LA / LS) imagery. J. Range Manag. 54, 378–381.

Rango, A., Laliberte, A., Herrick, J.E., Winters, C., Havstad, K., Steel, C., Browning, D., 2009.

    Unmanned aerial vehicle-based remote sensing for rangeland assessment, monitoring, and

    management. J. Appl. Remote Sens. 3, 033542. https://doi.org/10.1117/1.3216822

Rango, A., Laliberte, A., Winters, C., 2008. Role of aerial photos in compiling a long-term

    remote sensing data set. J. Appl. Remote Sens. 2, 023541.

    https://doi.org/10.1117/1.3009225

Rango, A., Laliberte, A.S., 2010. Impact of flight regulations on effective use of unmanned

aircraft systems for natural resources applications. J. Appl. Remote Sens. 4, 043539.

https://doi.org/10.1117/1.3474649

Sankey, T.T., McVay, J., Swetnam, T.L., McClaran, M.P., Heilman, P., Nichols, M., 2017. UAV

hyperspectral and lidar data and their fusion for arid and semi-arid land vegetation

monitoring. Remote Sens. Ecol. Conserv. 1–14. https://doi.org/10.1002/RSE2.44

Sayre, N.F., 2017. The Politics of Scale. The University of Chicago Press.

Snavely, N., Seitz, S.M., Szeliski, R., 2008. Modeling the world from Internet photo collections.

Int. J. Comput. Vis. 80, 189–210. https://doi.org/10.1007/s11263-007-0107-3

Society for Range Managment, 1998. Glossary of terms used in range management, in: Bedell,

T.E. (Ed.), Glossary of Terms Used in Range Management.

Streutker, D.R., Glenn, N.F., 2006. LiDAR measurement of sagebrush steppe vegetation heights.

Remote Sens. Environ. 102, 135–145. https://doi.org/10.1016/j.rse.2006.02.011

Tueller, P.T., 1996. Near-earth monitoring of range condition and trend. Geocarto Int. 11, 53–62.

https://doi.org/10.1080/10106049609354548

Tueller, P.T., 1989. Remote Sensing technology for rangeland management applications. J. Range

Manag. 42, 442–453. https://doi.org/10.2307/3899227

Turner, D., Lucieer, A., Wallace, L., 2014. Direct georeferencing of ultrahigh-resolution UAV

imagery. IEEE Trans. Geosci. Remote Sens. 52, 2738–2745.

https://doi.org/10.1109/TGRS.2013.2265295

USDI Bureau of Land Management, 2001. H-4180-1 Rangeland Health Standards.

Watts, A.C., Ambrosia, V.G., Hinkley, E. a., 2012. Unmanned Aircraft Systems in Remote

Sensing and Scientific Research: Classification and Considerations of Use. Remote Sens. 4,

1671–1692. https://doi.org/10.3390/rs4061671

West, N.E., 2003. History of Rangeland Monitoring in the U.S.A. Arid L. Res. Manag. 17, 495–

545. https://doi.org/10.1080/713936110

Westoby, M.J., Brasington, J., Glasser, N.F., Hambrey, M.J., Reynolds, J.M., 2012. 'Structure-

from-Motion' photogrammetry: A low-cost, effective tool for geoscience applications.

Geomorphology 179, 300–314. https://doi.org/10.1016/j.geomorph.2012.08.021

Whiteman, G., Brown, J.R., 1998. Assessment of a method for mapping woody plant density in a

grassland matrix. J. Arid Environ. 38, 269–282. https://doi.org/10.1006/jare.1997.0325

Yahdjian, L., Sala, O.E., Havstad, K.M., 2015. Rangeland ecosystem services: Shifting focus

from supply to reconciling supply and demand. Front. Ecol. Environ. 13, 44–51.

https://doi.org/10.1890/140156

APPENDIX A:

FINE-RESOLUTION REPEAT TOPOGRAPHIC SURVEYING OF DRYLAND LANDSCAPES USING UAS-BASED STRUCTURE-FROM-MOTION PHOTOGRAMMETRY: ASSESSING ACCURACY AND PRECISION AGAINST TRADITIONAL GROUND-BASED EROSION MEASUREMENTS

Jeffrey K. Gillan[1], Jason W. Karl[1], Ahmed Elaksher[2], and Michael Duniway[3]

[1]US Department of Agriculture-Agricultural Research Service Jornada Experimental Range, New Mexico State University, Las Cruces, NM 88001, USA

[2]Civil Engineering Department, College of Engineering, California Polytechnical State University, Pomona, CA, 91766, USA

[3]US Geological Survey, Southwest Biological Science Center, Moab, UT 84532, USA

Abstract

Structure-from-motion (SfM) photogrammetry from unmanned aerial system (UAS) imagery is an emerging tool for repeat topographic surveying of dryland erosion. These methods are particularly appealing due to the ability to cover large landscapes compared to field methods and at reduced costs and finer spatial resolution compared to airborne laser scanning. Accuracy and precision of high-resolution digital terrain models (DTMs) derived from UAS imagery have been explored in many studies, typically by comparing image coordinates to surveyed check points or LiDAR datasets. In addition to traditional check points, this study compared 5 cm resolution DTMs derived from fixed-wing UAS imagery with a traditional ground-based method of measuring soil surface change called erosion bridges. We assessed accuracy by comparing the elevation values between DTMs and erosion bridges along thirty topographic transects each 6.1 m long. Comparisons occurred at two points in time (June 2014, February 2015) which enabled us to assess vertical accuracy with 3314 data points and vertical precision (i.e., repeatability) with 1657 data points. We found strong vertical agreement (accuracy) between the methods (RMSE 2.9 and 3.2 cm in June 2014 and February 2015, respectively) and high vertical precision for the DTMs (RMSE 2.8 cm). Our results from comparing SfM-generated DTMs to check points, and strong agreement with erosion bridge measurements suggests repeat UAS imagery and SfM processing could replace erosion bridges for a more synoptic landscape assessment of shifting soil surfaces for some studies. However, while collecting the UAS imagery and generating the SfM DTMs for this study was faster than collecting erosion bridge measurements, technical challenges related to the need for ground control networks and image processing requirements must be addressed before this technique could be applied effectively to large landscapes.

Introduction

Repeat topographic surveys are an important tool for studying and managing dryland ecosystems, particularly for tracking soil erosion and gully formation (D'Oleire-Oltmanns et al., 2012; Eltner et al., 2014; Gillan et al., 2016; Martinez-Casasnovas et al., 2003; Marzolff and Poesen, 2009). Other applications include hydrologic erosion modeling (Al-Hamdan et al., 2014; Goodrich et al., 2011), formulating ecohydrologic models (Vivoni et al., 2014), predicting plant species occurrence via topographic attributes (Lassueur et al., 2006), and delineating watersheds at a very fine scale to improve studies of water and energy cycling in water-limited ecosystems (Templeton et al., 2014).

An emerging tool for repeat topographic surveying is structure-from-motion (SfM) photogrammetry derived from unmanned aerial system (UAS) imagery (Eltner et al., 2014; Harwin and Lucieer, 2012; Lucieer et al., 2013; Niethammer et al., 2010; Rosnell and Honkavaara, 2012). Use of this tool has increased dramatically due to the proliferation of low-cost and easily accessible consumer UAS, the availability of many off-the-shelf sensors small enough to be carried aboard small aircraft (Pajares, 2015), and advances in computer vision and software to process imagery (Gonçalves and Henriques, 2015; Snavely et al., 2008). SfM differs from traditional photogrammetry in that it can reconstruct 3-dimensional scenes based purely on a large number (typically millions) of automatically detected ground points in many overlapping images independent of ground references (Fonstad et al., 2013). This allows it to be very flexible in terms of accepting images with inconsistent overlap, rotation between successive images, and images from different angles (i.e. nadir and oblique) (Ai et al., 2015). SfM can also handle images collected with consumer grade cameras with unknown or unstable lens characteristics (Westoby et al., 2012). Traditional photogrammetry is less flexible in that it requires consistent image overlap, minimal rotation between successive images, and calibrated sensors (Ai et al., 2015). The flexibility of SfM is ideal for UAS-based topography surveying. Scientists and land

managers now have the ability to make on-demand imagery products, often at finer spatial and temporal resolutions along with reduced costs compared to imagery from satellite or manned aircraft (Anderson and Gaston, 2013).

A typical product of image-based reconstructions are digital terrain models (DTMs; i.e., bare ground). Differencing a time-series of DTMs constructed from UAS imagery enables quantification and visualization of soil movement (i.e., erosion and deposition) in more detail and over a larger area compared to field methods such as erosion bridges (Shakesby, 1993), erosion pins (Fanning, 1994; Sirvent et al., 1997), and total station surveying (Martínez-Casasnovas et al., 2002; Wheaton et al., 2009). Additionally, high-resolution SfM DTMs can be produced at a finer resolution and lower cost compared to airborne laser scanning (Wallace et al., 2016) and can cover a larger geographic extent but with a reduction in detail compared with terrestrial laser scanning (Neugirg et al., 2016).

Knowing the expected accuracy (i.e., correctly representing the terrain) and precision (i.e., repeatability of terrain measurements) are critical aspects of using this tool effectively for repeat topographic surveys. Past research has shown that high-resolution (< 10 cm ground sampling distance) DTMs from UAS can be created with vertical accuracy < 5 cm (Clapuyt et al., 2015; D'Oleire-Oltmanns et al., 2012; Eltner and Schneider, 2015; Gonçalves and Henriques, 2015; Lucieer et al., 2014; Stöcker et al., 2015). Quantifying vertical repeatability is essential to separate model error from actual surface change (Milan et al., 2011; Wheaton et al., 2009). Past studies of high-resolution DTMs have found repeatability to be on average 1.7–6 cm (Clapuyt et al., 2015; Lucieer et al., 2013).

Many research papers have reported accuracy and precision of SfM DTMs by using surveyed check points or comparison with LiDAR derived DTMs. None, however, have directly compared

the results with concurrent erosion bridges, a common field method that has been demonstrated to effectively measure small topography changes for many natural resource applications including livestock impacts (Nash et al., 2003), post-fire erosion (Sankey et al., 2010; Shakesby et al., 2002; White et al., 2006; White and Loftin, 2000), erosion rates in cultivated fields (Van De et al., 2008), and impacts of recreational trails (Eagleston and Rubin, 2013). Though they can detect micro changes in soil surface with high precision, erosion bridges measure linear topographic profiles usually at lengths between 1 and 10 m, making it possible only to sample small portions of the landscape. Additionally, the choice of where to locate erosion bridges in a study area requires a priori knowledge and anticipation of where soil movement will occur. Unexpected consequences of the disturbance or process of interest may cause soil erosion to occur in places not sampled by the erosion bridges. Alternatively, measuring soil surface change via UAS photography and SfM methods provides synoptic observation of entire study areas and the ability to spatially locate sources and sinks of sediment movement, including areas with unexpected results.

In this paper, we directly compare SfM DTMs with erosion bridge data to demonstrate that the method of UAS-based SfM DTMs, though more technically challenging, can provide additional benefits of increasing sampling area. Included are analyses showing the differences in accuracy and precision that can be expected between the field and aerial methods. We demonstrate these methods in the context of investigating erosional impacts of unpaved road networks across the landscape.

The proliferation of unpaved road networks on public lands is a persistent and pressing problem for land managers globally (Okayasu et al., 2007), particularly in the western USA (Brooks and Lair, 2005; Watts et al., 2007). These unpaved roads present a challenge for soil conservation (Duniway and Herrick, 2011), with assessments of road erosion often relying on modelling that is

not well parameterized to highly disturbed conditions (Grismer, 2007; Laflen and Forest, 1997). Many immediate and pronounced impacts from roads and related disturbances are associated with altered erosion and hydrology (Duniway et al., 2010; Duniway and Herrick, 2013) which are not well captured by common rangeland monitoring methods (e.g., Herrick et al.(Herrick and Van Zee, 2009)). The USDA-Agricultural Research Service Jornada Experimental Range (JER) is conducting a long-term controlled experiment called Threshold Resistance and Connectivity (TRAC) to investigate further the effect of road networks on rangeland health. Across an 870 ha watershed, a series of unpaved roads were constructed with a road grader and received vehicle driving treatments several times per year which consisted of driving on the roads with a 4WD pick-up truck to simulate traffic. The soil erosion and compaction component of the TRAC study is currently being measured with a series of erosion bridges which sample a small portion of the experimental roads. A UAS-based DTM differencing approach to measuring soil erosion from roads could greatly expand and improve data collection for this study, as well as provide an important tool for land managers tasked with monitoring conditions on unpaved road networks. Though we test this technology over a relatively small area (15 ha), we view the results in terms of expanding the geographic extent and discuss the opportunities and challenges of scaling-up this approach.

The objectives of this project were to: 1) create high-resolution SfM DTMs from UAS-acquired imagery and assess their accuracy by comparing surface elevation profiles from the DTM with in situ close-range laser measurements from erosion bridges; 2) assess precision (i.e., repeatability) of SfM DTMs between image acquisition dates in order to quantify the level of topographic change that is detectable; 3) conduct DTM differencing to quantify and visualize soil movement over a 9 month time-span; and 4) assess the feasibility of applying these methods to large landscapes (> 200 ha).

Materials and Methods

Study Area

We conducted this study at the JER north of Las Cruces, NM (32°36'19.30" N, 106°37'12.14" W; 1420 m). The JER lies on the northern end of the Chihuahuan Desert and has a semi-arid climate. The study area received 293 mm of precipitation during the study period from June 2014 to February 2015 with more than half of the precipitation falling as the late summer monsoon rains. The TRAC study is located on a broad alluvial fan emanating from the western flank of the San Andres Mountains. The study area slopes gently from east to west with an average of slope of 2°. The soil was characterized as shallow gravelly loam (Ecological Site ID R042XB010NM). Shrubs dominated by *Larrea tridentata (*Creosote), *Prosopis glandulosa (*Mesquite), *Flourensia cernua* (Tarbush), and *Parthenium incanum* (Mariola) cover approximately 40–50% of the study, while an understory of grasses and forbs is nearly non-existent.

The TRAC project has a total of 47 plots (50 × 50 m) spread out over 870 ha (Figure 1). We selected a subset of six test plots within a 15 ha strip to compare UAS-based topographic surveying with erosion bridge measurements. The layout of the plots was chosen to be along a north-south line, which facilitated image acquisition.

Field Measurements

As part of the TRAC project, soil surface elevation profiles were measured in June 2014 and February 2015 along 5 linear transects in each plot using a laser range finder mounted on an erosion bridge (Figures 2, 3). The erosion bridge consisted of a metal beam suspended approximately 1.5 m above the ground using tripods on each side for support. Permanent nails in the ground marked the beginning and end of each transect and also provided a guide to set up the bridge identically each time. A laser range finder (Leica Disto D8) was slid along the beam in a rolling carriage and the distance from the beam to the ground was recorded every 10 cm along the

6.1 m erosion bridge for a total of 62 measurements. The laser had footprint of ~ 0.1 mm. Adjustments were made to account for slight sag in the middle of the beam. The vertical repeatability of this method was estimated to be ± 2.5 mm based on consecutive surveys without terrain change. Manufacturer reported accuracy was ± 1.0 mm. Since the primary objective for the erosion bridge measurements was measuring the terrain change, vegetation encountered along the transects was delicately pulled aside to ensure the laser was striking the ground.

Image Acquisition

We acquired UAS imagery in June 2014 and February 2015 within a few days of the erosion bridge measurements using an MLB BAT4 fixed-wing (Figure 2; Table 1) which weighs 59 kg and has a 4 m wingspan. The aircraft was powered by an 110 cc 2-stroke engine and required a runway (152 m minimum) for take-off and landing. The BAT4 has a telemetry range of over 16 km and has an endurance of approximately five hours before refueling. These characteristics make it an ideal platform to image large landscapes and flight tests have shown that it can image nearly 13 km^2 (1300 ha) in 2.5 h at 213 m above ground level (AGL). Operation of the UAS in national and restricted airspace was conducted under a Federal Aviation Administration certificate of authorization held by New Mexico State University Physical Science Laboratory.

For this study, the aircraft flew on average 152 m AGL which yielded a ground sampling distance of ~ 2.7 cm and an image footprint of 156×104 m. The onboard sensor was a 21 megapixel Canon EOS 5D Mark II DSLR and a Canon EF 35 mm lens. It was mounted within the fuselage with a lens hole cut on the bottom of the aircraft. The entire acquisition mission was executed autonomously using Cloud Cap Piccolo autopilot and the mission planning and flight software Piccolo Command Center (www.cloudcaptech.com). Both acquisitions used the same flight plan. Planned image forward overlap was 66% and image sidelap was 66%. The forward overlap was lower than typical (~ 80%) due to camera triggering speed. All images were intended to be

vertical (nadir). Three parallel flight lines were in north-south orientation and eighteen parallel

flight lines were in east-west orientations (Figure 2c) to ensure multiple views for all surfaces.

For each acquisition date, the flight plan was executed twice to ensure target coverage and image

overlap in case of camera triggering problems or slight variations in roll, pitch, and yaw at the

time of exposure. Each point on the ground was captured on average in 20 images. Images were

captured in RAW format and converted to 16-bit TIFF for image processing. Images were taken

within a few hours of solar noon to minimize shadowing. There was more shadowing, however,

in the February 2015 acquisition because of the lower winter sun angle.

Repeat DTM surveys require highly accurate spatial references to ensure proper scaling, rotation,

and georeferencing of the 3D model. Though direct georeferencing with onboard GNSS and

inertial measurement units (IMU) has become common, imagery products are still generally more

accurate and precise using a network of surveyed ground control points (GCPs)(D'Oleire-

Oltmanns et al., 2012; Turner et al., 2014). In terms of GCP patterns, recent literature has

suggested that GCP networks should be evenly distributed (Harwin and Lucieer, 2012) and

generally surround the area of interest due to DTM quality deteriorating outside of GCP

envelopes (Javernick et al., 2014; Smith et al., 2014). Regarding GCP density (quantity per area),

references from traditional aerial photogrammetry suggest locating GCPs at the beginning and

end of each flight line along with interior GCPs located every 3–5 images (Eltner et al., 2016;

Kraus, 2007; McGlone, 2013). Some SfM studies have reported the highest accuracies with GCPs

densities similar to the traditional approach (Clapuyt et al., 2015; Harwin and Lucieer, 2012).

Beyond this density, there appears to be a saturation point where additional GCPs offer no further

improvement (Long et al., 2016; Tonkin and Midgley, 2016; Turner et al., 2012). Other research

has shown that GCPs quantities can be greatly reduced with a well-defined camera model and

proper weighting of tie point and marker accuracy (James et al., 2017).

We surveyed 12 GCPs in each plot with a Leica TS02 total station (http://leica-geosystems.com).

Comparative analysis showed that there was no significant difference in image product quality

using 3 GCPs and 12 GCPs. Accordingly, we used 3 GCPs per plot as ground referencing during

SfM processing and used the remaining 9 locations as check points (Figure 3b). Our main sources

of errors were centering the prism pole at the GCP locations and the uncertainties in angle and

distance measurements observed with the total station. Following the procedure described by

Baykal et al. (Baykal et al., 2005), with a 1.0 mm centering error for the prism pole (Franklin and

Meyer, 2016) and the published accuracy of the Leica TS02 total station (Leica Geosystems,

n.d.), the estimated relative positional uncertainty of the GCPs is approximately 1.5–1.7 mm.

Each plot was surveyed separately in its own local coordinate system. We then converted the

local coordinates into universal transverse Mercator (UTM) coordinate system by determining the

x, y, z position of the 3 GCPs in each plot using a Trimble GeoXH 6000 GNSS receiver. We

differential corrected the coordinates with data from a Continuously Operating Reference Station

(CORS) using the Trimble's GPS Pathfinder Office (http://www.trimble.com/) (3D positional

accuracy of 10 cm). The local coordinates of the check points were projected into UTM using

ArcGIS 10.2 (ESRI, Redlands, CA). This total station/GNSS method of referencing was done to

have the accuracy of a total station survey but in a real world coordinate system making it GIS

ready for future analysis with additional data sets. The GCP/check point targets were 17 cm

diameter black plastic lids with a 5×5 cm white square in the center. For each flight, ten GCPs

were placed on the permanent nails that mark the ends of each erosion bridge (Figure 3b). Two

additional targets were placed near the center of each plot, attached to PVC stakes in the ground.

The same GCP/check points were used for 2014 and 2015 imagery. Image exposure location and

orientation information recorded by the BAT4's onboard GNSS/IMU was not used for

referencing because of large positional errors due to time synchronization problems between the

camera shutter and the GNSS/IMU.

Image Processing

We used SfM photogrammetry software Agisoft Photoscan version 1.1.6 build 2038 (http://www.agisoft.ru) to create 3D point clouds, digital surface models (DSMs), and orthomosaics for each plot individually. The first step consisted of photo alignment and creation of sparse point clouds. Agisoft Photoscan uses algorithms similar to Scale Invariant Features Transform (SIFT) (Lowe, 2004) to search for features that are identifiable in multiple images and through an iterative bundle adjustment determines the location and orientation of all cameras in the block as well as calculates 3D coordinates of the features in a sparse point cloud. Internal camera parameters were not known a priori, however, self-calibration provided by Agisoft Photoscan was used as it has been shown to produce accuracy results similar to pre-calibration approaches (Harwin et al., 2015). No erroneously located sparse points were detected (e.g., sinkers and flyers) so no manual point filtering was conducted. Next, we manually identified GCPs in 2 images for each plot which enabled Agisoft Photoscan to estimate the locations of the GCPs in all other images based on the scene geometry. The estimated GCP locations were checked and adjusted to the center of each GCP. Coded targets that Agisoft Photoscan can automatically identify were experimented with but were unreliable at this image scale. We performed the linear Helmert transformation to convert the scene's arbitrary coordinates into UTM Zone 13, WGS84 (the coordinates of the GCPs), then potential non-linear errors were removed by optimizing the scene with another bundle adjustment using the GCP coordinates (Agisoft, 2014). Within the bundle adjustment we specified the following measurement accuracies: marker accuracy, 3 cm; marker accuracy, 0.1 pixels; and tie point accuracy, 4 pixels. The latter two parameters were default in Agisoft Photoscan, while the first parameter was an estimate of accuracy using the total station/GNSS workflow. The lens parameters we optimized included focal length (f), principal point coordinates (cx, cy), radial distortion parameters (k1, k2, k3), affinity and non-orthogonal (b1, b2), tangential distortion (p1, p2). We specified "ultra-high" density and "mild filtering" settings for dense point cloud creation which generated an average

density of 1444 points·m^{-2} (Table 1, Figure 3c). A more detailed description of the SfM

workflow can be found in Snavely et al. (Snavely et al., 2008), Westoby et al. (Westoby et al.,

2012), Smith et al. (Smith et al., 2015), and Eltner et al. (Eltner et al., 2016).

In repeat topographic surveys, the presence of shrubs and other vegetation can confound our

ability to quantify soil change. Accordingly, we identified and filtered out all vegetation in the

point clouds. We used the "Classify Ground Points" tool in Agisoft Photoscan to identify ground

and non-ground points based on their topographic position compared to surrounding points. The

point cloud was first divided into a grid of equally sized cells, and the point with the lowest

elevation was identified as being ground. Additional ground points were identified based on a

user specified distance and angle from the original ground point. After testing each of the

parameters we found the best results had a cell size of 0.75 m, a maximum angle to other ground

points of 1 degree, and maximum distance of 5 cm from the originally identified ground point.

See also Cunliffe et al. (Cunliffe et al., 2016) for similar a methodology used to filter vegetation

in a semi-arid shrubland. To have greater control over the interpolation process (Agisoft

Photoscan does not publish full methods), we exported only the ground points into Log ASCII

Standard (LAS) files, then imported them into ArcGIS 10.2 as ESRI LASD files. We converted

the point clouds to DTMs) using natural neighbor interpolation with a spatial resolution of 5 cm.

Areas where the points had been removed because they were identified as vegetation, became

gaps in the DTMs represented as "no data". Some manual editing was necessary to completely

remove vegetation areas from the DTMs due to omission by the ground point classification in

Agisoft Photoscan. We assessed the quality of the DTMs by comparing northing, easting, and

elevation coordinates with the 9 check points in each plot. We subtracted the 2014 DTM from the

2015 DTM on a cell by cell basis to make a DTM difference image for each of the six plots.

Because this was a methodological test and because minimal erosion was expected between

acquisition dates, we did not transform the DTM difference measurements into estimates of soil

volume and mass. Dense point clouds, DSMs, and orthomosaics with the vegetation still present were also generated and exported from Agisoft Photoscan for visualization purposes.

Assessing Agreement between Erosion Bridge and DTMs

Using the colored point clouds to visual identify the ends of the topographic transects (marked with targets), we extracted elevations from the DTMs using the "interpolation line" tool available in ArcMap 3D Analyst toolbar. The extracted profile is intended to be the exact area measured by the erosion bridge to facilitate direct comparison between the two methods (Figure 3d). The erosion bridge laser measurements (originally distance to ground) were converted to elevation in the same UTM coordinate system as the DTMs by assigning the first laser measurement (nail) the same GNSS coordinate as the GCP. The rest of the erosion bridge elevation values were calculated as a vertical deviation from the beginning nail elevation. Using this methodology, the erosion bridge topographic profiles were not a completely independent "check" data set and testable only for z-value elevation. This was done deliberately to compare the photogrammetric DTM methods with erosion bridge methods independent from the inherent inaccuracies of referencing tools such as GNSS.

Erosion bridge measurements were taken every 10 cm, while DTMs had 5 cm cell sizes. Using an R script (R version 3.1.1.; (Karl and Gillan, n.d.), we paired a DTM height with its corresponding erosion-bridge height every 10 cm along the transect. The remaining DTM heights that were not paired (half) were removed from the analysis. There were a total of 62 pairs per transect and 1860 pairs across all transects in the 6 plots. Because the measurements were taken twice (June 2014, February 2015) the total number of comparative height pairs was 3720. We removed from the analysis the height pairs corresponding to the nails at both ends of the transects because they were used to convert the erosion bridge data to UTM coordinates, and thus not independent. On several of the transects, shrubs were present. To make the erosion-bridges directly comparable with the

DTMs, we removed any height pairs that had the presence of vegetation (i.e., vegetation pulled aside to laser the ground) because vegetation areas were already removed from the DTMs. After removing height pairs influenced by vegetation and nail pairs, we had 3314 pairs for analysis.

Assessing DTM Repeatability

A common method for quantifying repeatability is propagating accuracy error in each digital elevation model (DEM; a generic term encompassing both DTMs and DSMs; see Lane et al. 2003(Lane et al., 2003)). For example, Brasington et al. (Brasington et al., 2003) and Wheaton et al. (Wheaton et al., 2009) showed how individual errors in a DEM can be propagated in a DEM difference as:

$$\delta u_{DoD} = \sqrt{(\delta z_{new})^2 + (\delta z_{old})^2}, \tag{1}$$

where δu_{DoD} is the propagated error in the differenced DEM, and δz_{new} and δz_{old} are the individual errors in the first and second DEM, respectively. Another method measures the height of unchanged features during the time-series which could include natural features such as rocks or a network of validation points (Derose et al., 1998; Gessesse et al., 2010). Comparison of DEM change to change measured by the erosion bridge offers a third method of quantifying repeatability. Deviation of the DEM change estimates from the erosion bridge change measurements ("true change" for the purposes of this study) is an indication of the repeatability of the DEM method. Using this method produced 1657 estimate of repeatability, far more than the check point dataset (n = 54) or locating invariant features (e.g., rocks) in the imagery of each plot. Because photogrammetric processing was separate for each plot, we assessed repeatability for each plot individually.

Based on the quantified repeatability error we used a statistical threshold to separate model error in DTM differencing from actual surface change. We used a *t*-distribution 95% confidence

interval where the upper and lower 2.5 percentiles (i.e., < 2.5 percentile and > 97.5 percentiles) were considered to be actual surface change. Values > 2.5 percentile and < 97.5 percentile were discarded as model error. This method of thresholding represents a conservative estimate of change which limits type I errors (i.e. reporting soil movement when it did not occur). Setting a threshold level of detection should reflect the specific application of the repeat topographic survey and the potential costs of false positives and false negatives. For our application, we did not want to wrongly attribute soil erosion to vehicular driving on dirt roads if it did not actually happen.

Results
DTM Comparison with Check Points

We assessed the easting, northing, and elevation accuracy of the DTMs through a traditional method of comparing image coordinates with independent check point coordinates. The easting and northing RMSE for all plots was 1.1 cm and 1.5 cm, respectively for the June 2014 acquisition (Table 2). The easting and northing RMSE for the Feb. 2015 acquisition was nearly identical with RMSE of 1.1 cm and 1.1 cm, respectively.

The elevation RMSE for all plots was 2.3 cm in the June 2014 acquisition and February 2015 acquisition. DTM precision (repeatability) between acquisition dates was determined by subtracting 2014 check point ground coordinates from 2015 check point ground coordinates. Precision RMSE was estimated to be 1.4, 1.6, and 1.7 cm for easting, northing, and elevation, respectively (Table 3).

Agreement between Aerial DTMs and Erosion Bridges (Accuracy)

Comparing the topographic transects measured by the aerial DTMs and the erosion bridges produced vertical RMSE of 2.9 cm and 3.2 cm for all plots in June 2014 and Feb. 2015,

respectively (Table 4). Except for plot 5, the DTMs in each of the plots in both 2014 and 2015 were reconstructed with a slight systematic higher elevation on average compared with the erosion bridges. DTM and erosion bridge elevation profiles for Plot 5 for each year along with the topographic change from one year to the next are shown in Figure 4a (graphs for remaining plots are in the supplemental material).

DTM Repeatabilty

Across all plots the vertical repeatability of the DTMs, as measured by the difference between erosion bridge change and DTM change, had an average RMSE of 2.8 cm (Table 5). In individual plots, RMSE ranged from 2.2 cm to 4.4 cm. Applying the 95% C.I. threshold, the average vertical error (undetectable surface change) was between −4.7 cm and 6.1 cm. Vertical surface change detectability varied between individual plots. The lower 95th percentile threshold ranged between −2.0 cm and −8.8 cm while the upper 95th percentile threshold ranged between 4.6 cm and 8.6 cm.

The only anomalies in the repeatability results occurred in Plot 4 where 8 measurements from the erosion bridge showed deepening of a narrow rill that was not detected in the DTMs (Figure A4). Therefore the difference between the erosion bridge change and DTM change at this site was much larger than all other repeatability measures in the study. These values had a disproportionately large effect on the threshold of this plot but were retained in the analysis to demonstrate some of the discrepancies between the two methods of topographic measurement.

In comparison with the check point benchmark, accuracy and precision using the erosion bridge benchmark was slightly worse. This was not altogether unexpected because the check point benchmark was a comparison of DTMs with survey grade positioning of flat discs. The erosion bridge benchmark method was more challenging given the range of surface roughness of the

transects. In addition, there was a small spatial mismatch in the way the terrain was measured between DTMs and erosion bridge laser measurements. The erosion bridge laser measured a point on the ground less than a millimeter in size while the DTM was an interpolation of 3-4 points within a 5 cm cell.

Topographic Change

Over the 9 month span between data collections there was very little soil movement. The erosion bridge measurement showed an average positive vertical change of only 4 mm (Table 5). The DTMs showed an average change of −2 mm between acquisitions. This indicates that there is a small but systematic shift between the ground and imagery methods. The cause of this shift is unknown in this case, but can easily be corrected if the offset remains stable in further investigations. Maps of DTM differencing showed very little surface change within the area enclosed by the GCPs deep enough to cross the threshold of true surface change (Figure 4b as example; other maps are in Appendix A). Only a few areas within arroyos (dry water channels) experienced significant soil change. An exception to this can be seen in the northwest corner of plot 5 where there is indication of significant soil deposition. This is not true surface change but are instead DTMs errors that will be described in more detail in the discussion.

Discussion
Comparison with Other Studies

The vertical accuracy of our UAS-based SfM DTMs were quite similar to other studies using very fine spatial resolution imagery. Gonçalves and Henriques (Gonçalves and Henriques, 2015) had a vertical RMSE of 2.7–4 cm comparing DTMs to independent check points measured with GNSS. Lucieer et al. (Lucieer et al., 2014) reported a vertical RMSE of 4.4 cm comparing DTMs to ground check points measured with GNSS. Stöcker et al. (Stöcker et al., 2015) comparing DTMs to ground check points measured with a total station found RMSE of Z coordinates to be 1.6 cm. Eltner and Schneider (Eltner and Schneider, 2015) reported a 3D RMSE of 9 mm

compared to ground check points measured with a total station and 3D RMSE of 8.7 mm compared to terrestrial laser scanning. Glendell et al. (Glendell et al., 2017) compared vertically differenced DEMs using terrestrial laser scanning methods against UAS image reconstructions, both with 2 cm GSD. They found vertical difference RSMEs as low as 5 and 6 cm.

Directly comparing the accuracy of different studies is generally not possible due to the multitude of acquisition and processing specifications. Some of the differences included the original scale of the imagery, overlap, the density of the point clouds, and the methods they used to create a benchmark that have varying levels of inherent accuracies (i.e., GNSS, Total Station, Laser Scanning). However, even with minor mismatches comparing accuracy between studies, it is clear from the literature and this study that fine-scale terrain can be surveyed from UAS-based SfM to accuracies within a few centimeters.

Repeatability of UAS-based SfM DTMs is less reported in the literature for very fine spatial resolution image studies. Our DTMs (absolute mean difference ± 1.8 cm) were quite similar to a study by Lucieer et al. (Lucieer et al., 2013) who looked at static ground areas totaling 205,000 pixels and found the absolute mean difference between two DTMs to be ± 1.7 cm. Clapuyt et al. (Clapuyt et al., 2015) created replications of DTMs using different image sets at one point in time and found mean vertical precision to be ± 6 cm. This lower precision was possibly due to less precise GNSS coordinates of check points and sparser point clouds, so it is not directly comparable to our study. Neugirg et al. (Neugirg et al., 2016) reported repeatability of DTMs having a standard deviation of 6.2 cm which was less precise than our DTMs (2.3 cm).

Topographic Surveying for Soil Erosion
Our results from comparing SfM-generated DTMs to check points, and strong agreement with erosion bridge measurements suggests repeat UAS imagery and SfM processing could replace

erosion bridges for a more synoptic landscape assessment of shifting soil surfaces for some

studies. For example, with soil surface DTM differencing it may be possible to view landscape-

scale effects of the TRAC driving treatments including cumulative effects downstream of the

disturbance. Gillan et al. (Gillan et al., 2016), using DTM differencing to estimate soil erosion

across the study area following vegetation removal treatments in southern Utah, USA, showed

that soil movement to neighboring treatments potentially violated assumptions of treatment

independence and was not adequately captured by in-situ soil-surface sampling. The ability to

map areas of soil erosion and deposition in landscapes could help increase understanding of soil

loss patterns due to road networks and potentially improve our ability to model these dynamic

processes. Owing to the difficulty in setting up and calibrating erosion bridges, it is possible only

to sample a small portion of the same landscape. Even then, it takes much longer to set up the

erosion bridges and take measurements than it does to acquire and process UAS images of the

same plots.

However, there is tradeoff between geographic extent and pixel size (i.e., spatial resolution) for

surveying soil elevation change. The ability to discern topographic change from UAS-based SfM

DTM differencing is lower than that of erosion bridge measurements, meaning SfM DTM

differencing requires a larger vertical change of soil to be detectable as it was implemented in this

study. Using our strict change threshold (95% CI), we could detect soil erosion greater than 4.7

cm and deposition greater than 6.1 cm from UAS-based DTM differencing at this image scale.

Whether this level of precision is suitable for studying or monitoring dryland soil erosion depends

on the objective and the cost of making Type I and Type II errors (Mudge et al., 2012). For the

TRAC study, our implementation of a strict threshold was appropriate to avoid Type I errors (i.e.,

falsely attributing a linkage between vehicle driving and erosion processes). In a monitoring

context, the cost of not detecting soil movement may be great enough to warrant relaxing the

threshold (i.e., accepting a lower C.I.), thereby improving the detectability of soil movement. An

approach that leverages the advantages of both the aerial and ground methods could be workable in some situations. For example, the aerial DTM differencing method we employed could be used to cover a large geographic extent to identify potential problem areas at a coarse resolution. Once the areas have been identified, more precise erosion monitoring methods (lower flying UAS; in situ measurements) could be used to more closely monitor those areas.

DTM Errors

Our calculated DTM differences showed that errors fell into two categories. The first were areas of erroneous soil surface change in the edges or corners of some plots (e.g., Figure 4B, northwest corner of Plot 5). This vertical error is likely due to a combination of sources. First, these errors could be caused by slight "doming" affect as described by James and Robson (James and Robson, 2014) and Eltner and Schneider (Eltner and Schneider, 2015) who showed that nadir-only image acquisitions coupled with SfM self-calibration can lead to poor modeling of camera radial distortion expressed as incorrect lower elevations in the periphery of the 3D scene. Alternatively, our observed areas of incorrect soil surface change could be due to the absence of ground control in the scene periphery and illustrates decay of DTM accuracy outside the area enclosed by the ground control network (Jaud et al., 2016; Javernick et al., 2014; Smith et al., 2014; Tonkin and Midgley, 2016). For our study plots, there does not appear to be a consistent distance outside the enclosed area where accuracy begins to rapidly decline. Some plots displayed increased error immediately outside enclosed area while other plots showed little DTM difference errors for 10's of meters. Variation amongst plots could be due to slight differences in image overlap, accuracy of GCPs, or differences in the original photo alignment.

The second source of error in our DTM differences came from imperfect filtering of vegetation and was expressed as large gains or losses of elevation immediately adjacent to shrubs (i.e., one or both of the DTMs still contained vegetation and when differenced created large changes in

elevation). Vegetation filtering is still a significant challenge at this very fine scale and reduces our ability to automate DTM difference processing. Our approach was to use the topographic position of points in the cloud to identify ground points, however, other SfM studies have used a variety of methods to filter vegetation with no clear consensus on a superior workflow (Cunliffe et al., 2016; Javernick et al., 2014; Jensen and Mathews, 2016; Smith et al., 2014; Wallace et al., 2016). In our semi-arid shrubland study area, there is a distinct difference in color between the creosote/mesquite shrubs and the bare ground. Coupling color separation with our current use of topographic position filtering could be very successful in terms of separating vegetation from ground.

Limitations for Large Landscapes

There are two main technical constraints to currently adopting UAS-based DTM differencing over large landscapes (> 200 ha) in an operational capacity. The first challenge is the ground control requirements. We achieved accuracy and precision RMSE < 3 cm within the envelope of 3 GCPs for each of our 50×50 m plots, but expanding this methodology over the entire TRAC study area would necessitate hundreds of GCPs to achieve this same level accuracy and precision. To make quality data collection over large landscapes a more cost effective endeavor, GCP demand needs to be reduced or eliminated. Fortunately, recent research is showing that direct georeferencing using onboard GNSS differentially corrected with base station data can produce similar (Rehak et al., 2013) or slightly worse (Hugenholtz et al., 2016; Turner et al., 2014) image product accuracy compared with GCPs. More testing is needed with this technology to see if vertical accuracy and precision RMSE < 3 cm is possible. Ground control demand may also be reduced by the addition of oblique imagery (Harwin et al., 2015; James and Robson, 2014), well-defined camera models, and proper weighting of tie point and marker accuracy during bundle adjustments (Carbonneau and Dietrich, 2016; James et al., 2017).

Additionally, the time and computing resources required to replicate our method over the entire TRAC study would also be prohibitive. Even with powerful desktop computers with high-end CPUs, GPUs, and abundant RAM, SfM processing is computationally intensive and can take many days to produce dense point clouds from a large imagery dataset. Additional research into optimization of the number and type (i.e., nadir vs. oblique) of images for high-quality products from SfM is needed. As we continue to collect remotely sensed data at an ever finer resolution and greater extents, cyberinfrastructure that leverages high-performance computing (Goff et al., 2011) and distributed network processing (i.e. cloud computing) such as Google Earth Engine (https://earthengine.google.com) will become increasingly necessary for storing, processing, and interpreting data for natural resource management in the age of big data.

Conclusions

Our results demonstrated the utility of SfM DTM differencing using UAS imagery for monitoring changes in soil surface as an alternative to in situ measurements from traditional erosion bridges. Accuracy of the DTMs as measured against erosion bridge was high (RMSE 2.9 cm and 3.2 cm in 2014 and 2015, respectively), and correspondence with change as measured by the erosion bridges was also in high agreement (RMSE 2.8 cm). The technique we presented allows for a synoptic view of soil movement which provides information on the spatial distribution of erosion and deposition processes that was difficult and expensive to generate previously. However, while collecting the UAS imagery and generating the SfM DTMs for this study was faster than collecting erosion bridge measurements, technical challenges related to the need for ground control networks and image processing requirements must be addressed before this technique could be applied effectively to large landscapes.

Acknowledgements

References

Agisoft, 2014. Agisoft PhotoScan User Manual: Professional Edition, Version 1.2.

Ai, M., Hu, Q., Li, J., Wang, M., Yuan, H., Wang, S., 2015. A Robust Photogrammetric Processing Method of Low-Altitude UAV Images. Remote Sens. 7, 2302–2333. https://doi.org/10.3390/rs70302302

Al-Hamdan, O.Z., Hernandez, M., Pierson, F.B., Nearing, M. a., Williams, C.J., Stone, J.J., Boll, J., Weltz, M. a., 2014. Rangeland hydrology and erosion model (RHEM) enhancements for applications on disturbed rangelands. Hydrol. Process. 29, 445–457. https://doi.org/10.1002/hyp.10167

Anderson, K., Gaston, K.J., 2013. Lightweight unmanned aerial vehicles will revolutionize spatial ecology. Front. Ecol. Environ. 11, 138–146. https://doi.org/10.1890/120150

Baykal, O., Tari, E., Coşkun, M.Z., Erden, T., 2005. Accuracy of Point Layout with Polar Coordinates. J. Surv. Eng. 131, 87–93. https://doi.org/10.1061/(ASCE)0733-9453(2005)131:3(87)

Brasington, J., Langham, J., Rumsby, B., 2003. Methodological sensitivity of morphometric estimates of coarse fluvial sediment transport. Geomorphology 53, 299–316. https://doi.org/10.1016/S0169-555X(02)00320-3

Brooks, M.L., Lair, B., 2005. Ecological Effects of Vehicular Routes in a Desert Ecosystem. Western Ecological Research Center, Las Vegas, NV, USA.

Carbonneau, P.E., Dietrich, J.T., 2016. Cost-effective non-metric photogrammetry from consumer-grade

sUAS: implications for direct georeferencing of structure from motion photogrammetry. Earth Surf. Process. Landforms 42, 473–486. https://doi.org/10.1002/esp.4012

Clapuyt, F., Vanacker, V., Van Oost, K., 2015. Reproducibility of uav-based earth topography reconstructions based on structure-from-motion algorithms. Geomorphology 260, 4–15. https://doi.org/10.1016/j.geomorph.2015.05.011

Cunliffe, A.M., Brazier, R.E., Anderson, K., 2016. Ultra-fine grain landscape-scale quantification of dryland vegetation structure with drone-acquired structure-from-motion photogrammetry. Remote Sens. Environ. 183, 129–143. https://doi.org/10.1016/j.rse.2016.05.019

D'Oleire-Oltmanns, S., Marzolff, I., Peter, K., Ries, J., 2012. Unmanned Aerial Vehicle (UAV) for Monitoring Soil Erosion in Morocco. Remote Sens. 4, 3390–3416. https://doi.org/10.3390/rs4113390

Derose, R.C., Gomez, B., Marden, M., Trustrum, N.A., 1998. Gully erosion in Mangatu Forest, New Zealand, estimated from digital elevation models. Earth Surf. Process. Landforms 23, 1045–1053. https://doi.org/10.1002/(SICI)1096-9837(1998110)23:11<1045::AID-ESP920>3.0.CO;2-T

Duniway, M.C., Herrick, J.E., 2013. Assessing Impacts of Roads: Application of a Standard Assessment Protocol. Rangel. Ecol. Manag. 66, 364–375. https://doi.org/10.2111/REM-D-11-00130.1

Duniway, M.C., Herrick, J.E., 2011. Disentangling road network impacts: The need for a holistic approach. J. Soil Water Conserv. 66, 31A–36A. https://doi.org/10.2489/jswc.66.2.31A

Duniway, M.C., Herrick, J.E., Pyke, D. a., Toledo P., D., 2010. Assessing Transportation Infrastructure Impacts on Rangelands: Test of a Standard Rangeland Assessment Protocol. Rangel. Ecol. Manag. 63, 524–536. https://doi.org/10.2111/REM-D-09-00176.1

Eagleston, H., Rubin, C., 2013. Non-motorized winter recreation impacts to snowmelt erosion, tronsen basin, eastern cascades, Washington. Environ. Manage. 51, 167–181. https://doi.org/10.1007/s00267-012-9963-x

Eltner, A., Baumgart, P., Maas, H.-G., Faust, D., 2014. Multi-temporal UAV data for automatic measurement of rill and interrill erosion on loess soil. Earth Surf. Process. Landforms 40, 741–755. https://doi.org/10.1002/esp.3673

Eltner, A., Kaiser, A., Castillo, C., Rock, G., Neugirg, F., Abellan, A., 2016. Image-based surface reconstruction in geomorphometry – merits, limits and developments of a promising tool for

geoscientists. Earth Surf. Dyn. Discuss. 1445–1508. https://doi.org/10.5194/esurfd-3-1445-2015

Eltner, A., Schneider, D., 2015. Analysis of Different Methods for 3D Reconstruction of Natural Surfaces from Parallel-Axes UAV Images. Photogramm. Rec. 30, 279–299. https://doi.org/10.1111/phor.12115

Fanning, P., 1994. Long-term contemporary erosion rates in an arid rangelands environment in western New South Wales, Australia. J. Arid Environ. 28, 173–187. https://doi.org/10.1016/s0140-1963(05)80055-2

Fonstad, M.A., Dietrich, J.T., Courville, B.C., Jensen, J.L., Carbonneau, P.E., 2013. Topographic structure from motion: A new development in photogrammetric measurement. Earth Surf. Process. Landforms 38, 421–430. https://doi.org/10.1002/esp.3366

Franklin, K.D., Meyer, T.H., 2016. Centering Error for Range Poles. Surv. L. Inf. Sci. 75, 77–84.

Gessesse, G.D., Fuchs, H., Mansberger, R., Klik, A., Rieke-Zapp, D.H., 2010. Assessment of ersosion, deposition and rill development on irregular soil surfaces using close range digital photogrammetry. Photogramm. Rec. 25, 299–318.

Gillan, J.K., Karl, J.W., Barger, N.N., Elaksher, A., Duniway, M.C., 2016. Spatially Explicit Rangeland Erosion Monitoring Using High-Resolution Digital Aerial Imagery. Rangel. Ecol. Manag. 69, 95–107. https://doi.org/10.1016/j.rama.2015.10.012

Glendell, M., McShane, G., Farrow, L., James, M.R., Quinton, J., Anderson, K., Evans, M., Benaud, P., Rawlins, B., Morgan, D., Jones, L., Kirkham, M., DeBell, L., Quine, T.A., Lark, M., Rickson, J., Brazier, R.E., 2017. Testing the utility of structure from motion photogrammetry reconstructions using small unmanned aerial vehicles and ground photography to estimate the extent of upland soil erosion. Earth Surf. Process. Landforms. https://doi.org/10.1002/esp.4142

Goff, S.A., Vaughn, M., McKay, S., Lyons, E., Stapleton, A.E., Gessler, D., Matasci, N., Wang, L., Hanlon, M., Lenards, A., Muir, A., Merchant, N., Lowry, S., Mock, S., Helmke, M., Kubach, A., Narro, M., Hopkins, N., Micklos, D., Hilgert, U., Gonzales, M., Jordan, C., Skidmore, E., Dooley, R., Cazes, J., McLay, R., Lu, Z., Pasternak, S., Koesterke, L., Piel, W.H., Grene, R., Noutsos, C., Gendler, K., Feng, X., Tang, C., Lent, M., Kim, S.-J., Kvilekval, K., Manjunath, B.S., Tannen, V., Stamatakis, A., Sanderson, M., Welch, S.M., Cranston, K.A., Soltis, P., Soltis, D., O'Meara, B., Ane,

C., Brutnell, T., Kleibenstein, D.J., White, J.W., Leebens-Mack, J., Donoghue, M.J., Spalding, E.P., Vision, T.J., Myers, C.R., Lowenthal, D., Enquist, B.J., Boyle, B., Akoglu, A., Andrews, G., Ram, S., Ware, D., Stein, L., Stanzione, D., 2011. The iPlant Collaborative: Cyberinfrastructure for Plant Biology. Front. Plant Sci. 2, 34. https://doi.org/10.3389/fpls.2011.00034

Gonçalves, J.A., Henriques, R., 2015. UAV photogrammetry for topographic monitoring of coastal areas. ISPRS J. Photogramm. Remote Sens. 104, 101–111. https://doi.org/10.1016/j.isprsjprs.2015.02.009

Goodrich, D.C., Guertin, D.P., Burns, I.S., Nearing, M. a., Stone, J.J., Wei, H., Heilman, P., Hernandez, M., Spaeth, K., Pierson, F., Paige, G.B., Miller, S.N., Kepner, W.G., Ruyle, G., McClaran, M.P., Weltz, M., Jolley, L., 2011. AGWA: The Automated Geospatial Watershed Assessment Tool to Inform Rangeland Management. Rangelands 33, 41–47. https://doi.org/10.2111/1551-501X-33.4.41

Grismer, M.E., 2007. Soil Restoration and erosion control: quantitative assessment and direction. Trans. ASABE 50, 1619–1626.

Harwin, S., Lucieer, A., 2012. Assessing the Accuracy of Georeferenced Point Clouds Produced via Multi-View Stereopsis from Unmanned Aerial Vehicle (UAV) Imagery. Remote Sens. 4, 1573–1599. https://doi.org/10.3390/rs4061573

Harwin, S., Lucieer, A., Osborn, J., 2015. The Impact of the Calibration Method on the Accuracy of Point Clouds Derived Using Unmanned Aerial Vehicle Multi-View Stereopsis. Remote Sens. 7, 11933–11953. https://doi.org/10.3390/rs70911933

Herrick, J.E., Van Zee, J.W. Van, 2009. Monitoring Manual for grassland, shrubland, and savanna ecosystems: Volume II.

Hugenholtz, C., Brown, O., Walker, J., Barchyn, T., Nesbit, P., Kucharczyk, M., Myshak, S., 2016. Spatial Accuracy of UAV-Derived Orthoimagery and Topography: Comparing Photogrammetric Models Processed with Direct Geo-Referencing and Ground Control Points. GEOMATICA 70, 21–30. https://doi.org/10.5623/cig2016-102

James, M.R., Robson, S., 2014. Mitigating systematic error in topographic models derived from UAV and ground-based image networks. Earth Surf. Process. Landforms 39, 1413–1420. https://doi.org/10.1002/esp.3609

James, M.R., Robson, S., D'Oleire-Oltmanns, S., Niethammer, U., 2017. Optimising UAV topographic

surveys processed with structure-from-motion: Ground control quality, quantity and bundle

adjustment. Geomorphology 280, 51–66. https://doi.org/10.1016/j.geomorph.2016.11.021

Jaud, M., Passot, S., Le Bivic, R., Delacourt, C., Grandjean, P., Le Dantec, N., 2016. Assessing the

Accuracy of High Resolution Digital Surface Models Computed by PhotoScan® and MicMac® in

Sub-Optimal Survey Conditions. Remote Sens. 8, 465. https://doi.org/10.3390/rs8060465

Javernick, L., Brasington, J., Caruso, B., 2014. Modeling the topography of shallow braided rivers using

Structure-from-Motion photogrammetry. Geomorphology 213, 166–182.

https://doi.org/10.1016/j.geomorph.2014.01.006

Jensen, J.L.R., Mathews, A.J., 2016. Assessment of Image-Based Point Cloud Products to Generate a Bare

Earth Surface and Estimate Canopy Heights in a Woodland Ecosystem. Remote Sens. 8.

https://doi.org/10.3390/rs8010050

Karl, J., Gillan, J., n.d. R Code [WWW Document]. URL https://github.com/jkarl/photogrammetry

(accessed 4.1.17).

Kraus, K., 2007. Photogrammetry: Geometry from Images and Laser Scans, 2nd ed. De Gruyter, Berlin,

Germany.

Laflen, J.M., Forest, S., 1997. WEPP-Predicting water erosion using a process-based model. J. Soil Water

Conserv. 52, 96–102.

Lane, S.N., Westaway, R.M., Murray Hicks, D., 2003. Estimation of erosion and deposition volumes in a

large, gravel-bed, braided river using synoptic remote sensing. Earth Surf. Process. Landforms 28,

249–271. https://doi.org/10.1002/esp.483

Lassueur, T., Joost, S., Randin, C.F., 2006. Very high resolution digital elevation models: Do they improve

models of plant species distribution? Ecol. Modell. 198, 139–153.

https://doi.org/10.1016/j.ecolmodel.2006.04.004

Leica Geosystems, n.d. Leica FlexLine TS02plus Data sheet. Heerbrugg, Switzerland.

Long, N., Millescamps, B., Pouget, F., Dumon, A., Lachaussée, N., Bertin, X., 2016. Accuracy assessment

of coastal topography derived from UAV images. Int. Arch. Photogramm. Remote Sens. Spat. Inf.

Sci. - ISPRS Arch. 2016–Janua, 1127–1134. https://doi.org/10.5194/isprsarchives-XLI-B1-1127-

2016

Lowe, D.G., 2004. Distinctive image features from scale invariant keypoints. Int'l J. Comput. Vis. 60, 91–110. https://doi.org/http://dx.doi.org/10.1023/B:VISI.0000029664.99615.94

Lucieer, A., Jong, S.M.D., Turner, D., 2013. Mapping landslide displacements using Structure from Motion (SfM) and image correlation of multi-temporal UAV photography. Prog. Phys. Geogr. 38, 97–116. https://doi.org/10.1177/0309133313515293

Lucieer, A., Turner, D., King, D.H., Robinson, S.A., 2014. Using an Unmanned Aerial Vehicle (UAV) to capture micro-topography of Antarctic moss beds Using an Unmanned Aerial Vehicle (UAV) to capture micro-topography. Int. J. Appl. Earth Obs. Geoinf. 27, 53–62. https://doi.org/10.1016/j.jag.2013.05.011

Martinez-Casasnovas, J.A., Anton-Fernandez, C., Ramos, M.C., 2003. Sediment production in large gullies of the Mediterranean area (NE Spain) from high-resolution digital elevation models and geographical information systems analysis. Earth Surf. Process. Landforms 28, 443–456. https://doi.org/10.1002/esp.451

Martínez-Casasnovas, J.A., Ramos, M.C., Ribes-Dasi, M., 2002. Soil erosion caused by extreme rainfall events: mapping and quantification in agricultural plots from very detailed digital elevation models. Geoderma 105, 125–140. https://doi.org/10.1016/S0016-7061(01)00096-9

Marzolff, I., Poesen, J., 2009. The potential of 3D gully monitoring with GIS using high-resolution aerial photography and a digital photogrammetry system. Geomorphology 111, 48–60. https://doi.org/10.1016/j.geomorph.2008.05.047

McGlone, J.C., 2013. Manual of photogrammetry, 6th ed. American Society for Photogrammetry and Remote Sensing, Bethesda, MD, USA.

Milan, D.J., Heritage, G.L., Large, A.R.G., Fuller, I.C., 2011. Filtering spatial error from DEMs: Implications for morphological change estimation. Geomorphology 125, 160–171. https://doi.org/10.1016/j.geomorph.2010.09.012

Mudge, J.F., Baker, L.F., Edge, C.B., Houlahan, J.E., 2012. Setting an optimal α that minimizes errors in null hypothesis significance tests. PLoS One 7, e32734. https://doi.org/10.1371/journal.pone.0032734

Nash, M.S., Jackson, E., Whitford, W.G., 2003. Soil microtopography on grazing gradients in Chihuahuan desert grasslands. J. Arid Environ. 55, 181–192. https://doi.org/10.1016/S0140-1963(02)00251-3

Neugirg, F., Stark, M., Kaiser, A., Vlacilova, M., Della Seta, M., Vergari, F., Schmidt, J., Becht, M., Haas, F., 2016. Erosion processes in calanchi in the Upper Orcia Valley, Southern Tuscany, Italy based on multitemporal high-resolution terrestrial LiDAR and UAV surveys. Geomorphology 269, 8–22. https://doi.org/10.1016/j.geomorph.2016.06.027

Niethammer, U., Rothmund, S., James, M.R., Travelletti, J., Joswig, M., 2010. UAV-based remote sensing of landslides. Int. Arch. Photogramm. Remote Sens. Spat. Inf. Sci. - ISPRS Arch. 38, 496–501.

Okayasu, T., Muto, M., Jamsran, U., Takeuchi, K., 2007. Spatially heterogeneous impacts on rangeland after social system change in Mongolia. L. Degrad. Dev. 18, 555–566. https://doi.org/10.1002/ldr.796

Pajares, G., 2015. Overview and Current Status of Remote Sensing Applications Based on Unmanned Aerial Vehicles (UAVs). Photogramm. Eng. Remote Sens. 81, 281–330. https://doi.org/10.14358/PERS.81.4.281

Rehak, M., Mabillard, R., Skaloud, J., 2013. a Micro-Uav With the Capability of Direct Georeferencing. Int. Arch. Photogramm. Remote Sensing, Beijing, China XL, 4–6. https://doi.org/10.5194/isprsarchives-XL-1-W2-317-2013

Rosnell, T., Honkavaara, E., 2012. Point cloud generation from aerial image data acquired by a quadrocopter type micro unmanned aerial vehicle and a digital still camera. Sensors 12, 453–480. https://doi.org/10.3390/s120100453

Sankey, J.B., Glenn, N.F., Germino, M.J., Gironella, A.I.N., Thackray, G.D., 2010. Relationships of aeolian erosion and deposition with LiDAR-derived landscape surface roughness following wildfire. Geomorphology 119, 135–145. https://doi.org/10.1016/j.geomorph.2010.03.013

Shakesby, R.A., 1993. The soil erosion bridge: a device for micro-profiling soil surfaces 18, 823–827. https://doi.org/10.1002/esp.3290180906

Shakesby, R.A., Coelho, C.O.A., Ferreira, A.J.D., Walsh, R.P.D., 2002. Ground-level changes after wildfire and ploughing in eucalyptus and pine forests, Portugal: Implications for soil microtopographical development and soil longevity. L. Degrad. Dev. 13, 111–127. https://doi.org/10.1002/ldr.487

Sirvent, J., Desir, G., Gutierrez, M., Sancho, C., Benito, G., 1997. Erosion rates in badland areas recorded by collectors, erosion pins and profilometer techniques (Ebro Basin, NE-Spain). Geomorphology 18,

61–75. https://doi.org/10.1016/S0169-555X(96)00023-2

Smith, M.W., Carrivick, J.L., Hooke, J., Kirkby, M.J., 2014. Reconstructing flash flood magnitudes using "Structure-from-Motion": A rapid assessment tool. J. Hydrol. 519, 1914–1927. https://doi.org/10.1016/j.jhydrol.2014.09.078

Smith, M.W., Carrivick, J.L., Quincey, D.J., 2015. Structure from motion photogrammetry in physical geography. Prog. Phys. Geogr. 40, 247–275. https://doi.org/10.1177/0309133315615805

Snavely, N., Seitz, S.M., Szeliski, R., 2008. Modeling the world from Internet photo collections. Int. J. Comput. Vis. 80, 189–210. https://doi.org/10.1007/s11263-007-0107-3

Stöcker, C., Eltner, A., Karrasch, P., 2015. Measuring gullies by synergetic application of UAV and close range photogrammetry — A case study from Andalusia, Spain. Catena 132, 1–11. https://doi.org/10.1016/j.catena.2015.04.004

Templeton, R.C., Vivoni, E.R., Méndez-Barroso, L.A., Pierini, N.A., Anderson, C.A., Rango, A., Laliberte, A.S., Scott, R.L., 2014. High-resolution characterization of a semiarid watershed: Implications on evapotranspiration estimates. J. Hydrol. 509, 306–319. https://doi.org/10.1016/j.jhydrol.2013.11.047

Tonkin, T.N., Midgley, N.G., 2016. Ground-Control Networks for Image Based Surface Reconstruction : An Investigation of Optimum Survey Designs Using UAV Derived Imagery and. Remote Sens. 8, 16–19. https://doi.org/10.3390/rs8090786

Turner, D., Lucieer, A., Wallace, L., 2014. Direct georeferencing of ultrahigh-resolution UAV imagery. IEEE Trans. Geosci. Remote Sens. 52, 2738–2745. https://doi.org/10.1109/TGRS.2013.2265295

Turner, D., Lucieer, A., Watson, C., 2012. An Automated Technique for Generating Georectified Mosaics from Ultra-High Resolution Unmanned Aerial Vehicle (UAV) Imagery, Based on Structure from Motion (SfM) Point Clouds. Remote Sens. 4, 1392–1410. https://doi.org/10.3390/rs4051392

Van De, N., Douglas, I., Mcmorrow, J., Lindley, S., Thuy Binh, D.K.N., Van, T.T., Thanh, L.H., Tho, N., 2008. Erosion and nutrient loss on sloping land under intense cultivation in Southern Vietnam. Geogr. Res. 46, 4–16. https://doi.org/10.1111/j.1745-5871.2007.00487.x

Vivoni, E., Rango, A., Anderson, C., 2014. Ecohydrology with unmanned aerial vehicles. Ecosphere 5, 1–14. https://doi.org/10.1890/ES14-00217.1

Wallace, L., Lucieer, A., Malenovský, Z., Turner, D., Vopěnka, P., 2016. Assessment of Forest Structure

Using Two UAV Techniques: A Comparison of Airborne Laser Scanning and Structure from Motion (SfM) Point Clouds. Forests 7, 62. https://doi.org/10.3390/f7030062

Watts, R.D., Compton, R.W., Mccammon, J.H., Rich, C.L., M, S., Owens, T., Ouren, D.S., 2007. Roadless space of the conterminous United States. Science (80-.). 316, 736–738. https://doi.org/10.1126/science.1138141

Westoby, M.J., Brasington, J., Glasser, N.F., Hambrey, M.J., Reynolds, J.M., 2012. 'Structure-from-Motion' photogrammetry: A low-cost, effective tool for geoscience applications. Geomorphology 179, 300–314. https://doi.org/10.1016/j.geomorph.2012.08.021

Wheaton, J.M., Brasington, J., Darby, S.E., Sear, D. a., 2009. Accounting for uncertainty in DEMs from repeat topographic surveys: improved sediment budgets. Earth Surf. Process. Landforms 156, 136–156. https://doi.org/10.1002/esp.1886

White, C.S., Loftin, S.R., 2000. Response of 2 semiarid grasslands to cool-season pre-scribed fire. J. Range Manag. 53, 52–61. https://doi.org/10.2307/4003392

White, C.S., Pendleton, R.L., Pendleton, B.K., 2006. Response of two semiarid grasslands to a second fire application. Rangel. Ecol. Manag. 59, 98–106. https://doi.org/10.2111/04-153R2.1

Figures and Tables
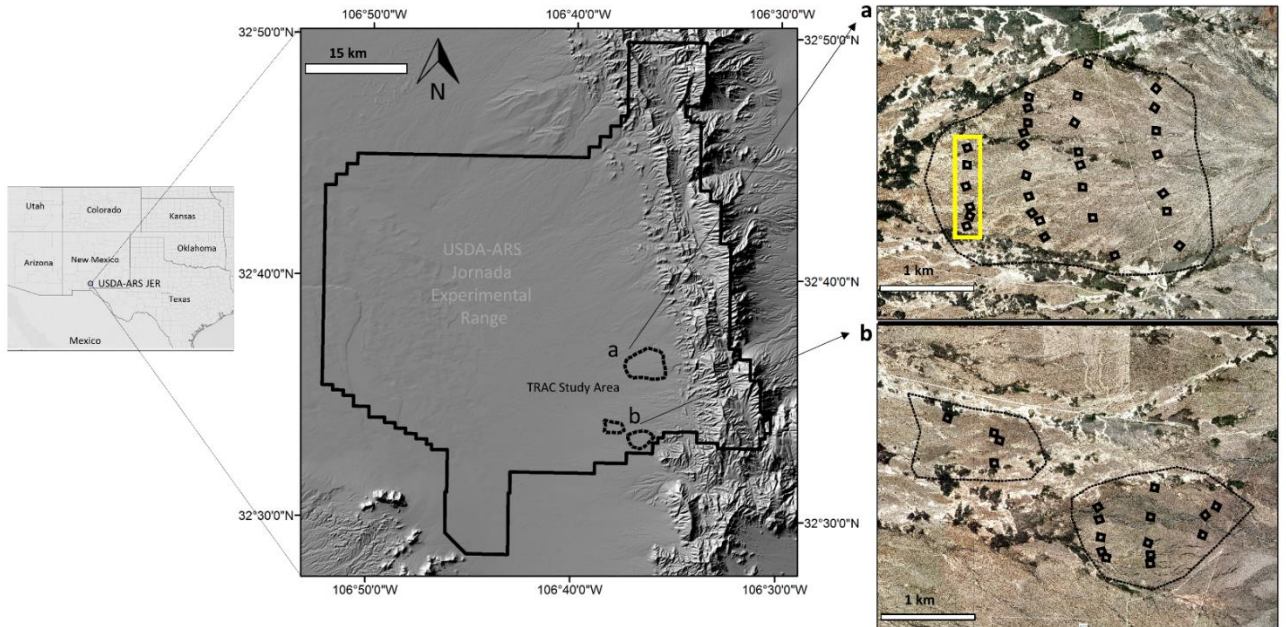
Fig. 1. This study was conducted at the USDA-Agricultural Research Service Jornada Experimental Range outside of Las Cruces, NM. Our six test plots (within yellow box) are a subset of the threshold resistance and connectivity (TRAC) project which is investigating the impact of roads and vehicular traffic on dryland landscapes.
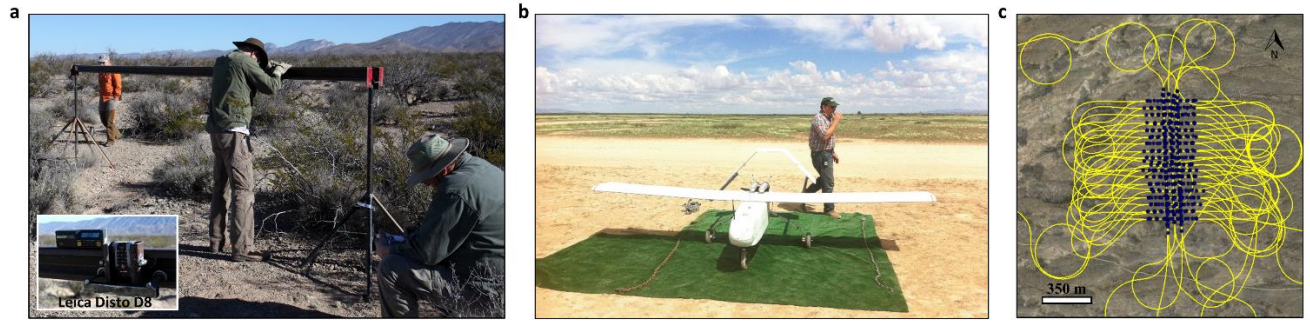
Fig. 2. (**a**) We measured surface elevation profiles using a laser range finder (inset map) attached and slid along a 6.1 m erosion bridge. (**b**) We acquired high-resolution imagery using an MLB BAT4 fixed-wing unmanned aerial vehicle. (**c**) The flight path for the image acquisition in June 2014 and February 2015. The yellow line is the flight path and the blue dots represent the image locations.
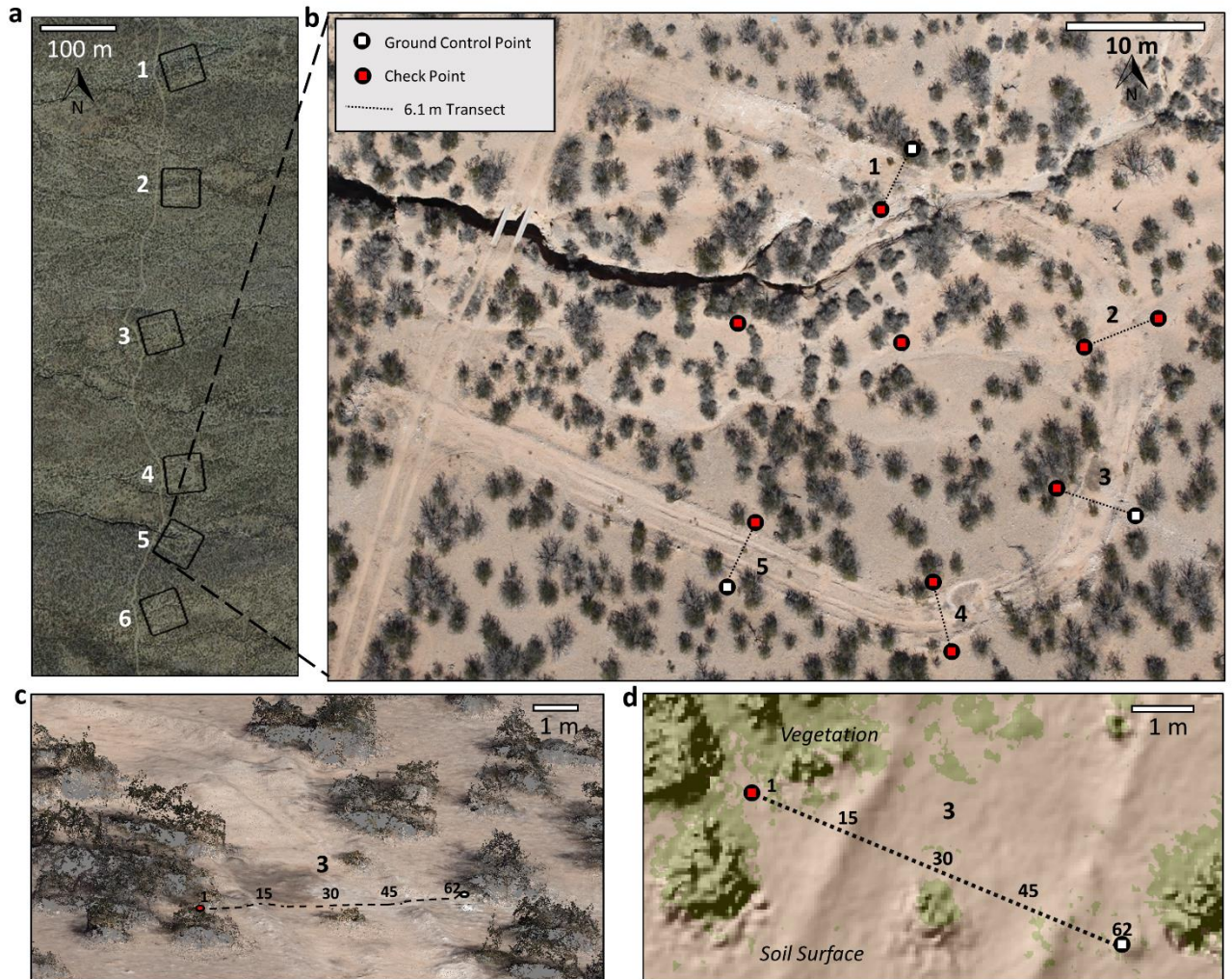
Fig. 3. (**a**) Six 50x50 m test plots were chosen to compare laser range finder (erosion bridge) and UAS-based digital terrain model (DTM) methods for representing surface topography. (**b**) For each plot we measured surface elevation profiles along 5 transects using both methods. The DTMs were reconstructed using structure-from-motion photogrammetry methods referenced with 3 ground control points and were assessed with 9 check points. (**c**) Point clouds were created for each plot as an intermediate step to build DTMs. (**d**) Along each transect we compared the elevations between the erosion bridge and DTM 62 times (10 cm spacing).

a

June 2014   Feb. 2015   Change

Transect 1
Transect 2
Transect 3
Transect 4
Transect 5

Surface Height (cm)

Distance Along Transect (m)

—— Laser Erosion Bridge   —— DTM Soil Surface   —— DEM Vegetation

b

Plot 5

DTM Difference (cm)

Deposition
- >10.0
- 6.1 - 10.0
- 4.7 - 6.0

Repeatability Error {
- 0 - 4.6
- -3.9 - 0

Erosion
- -5.9 - -4.0
- -9.9 - -6.0
- <-10.0

◻ Ground Control Point
● Check Point
······· 6.1 m Transect

10 m
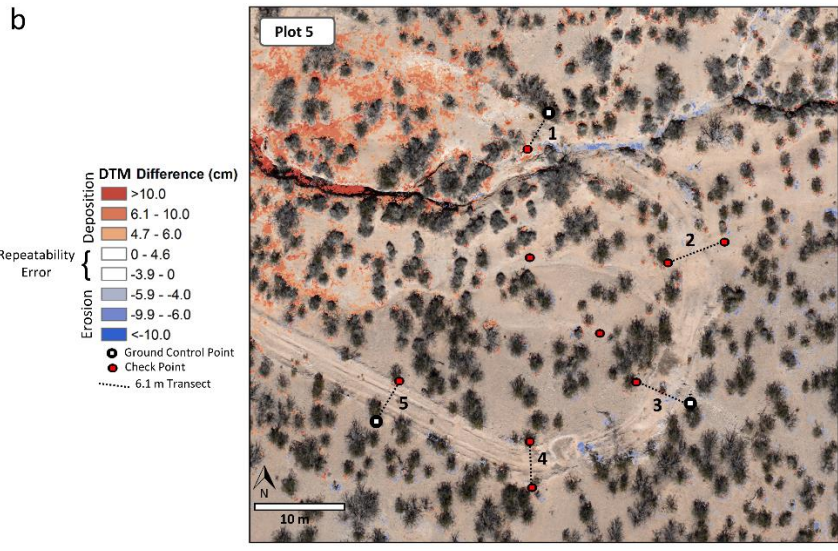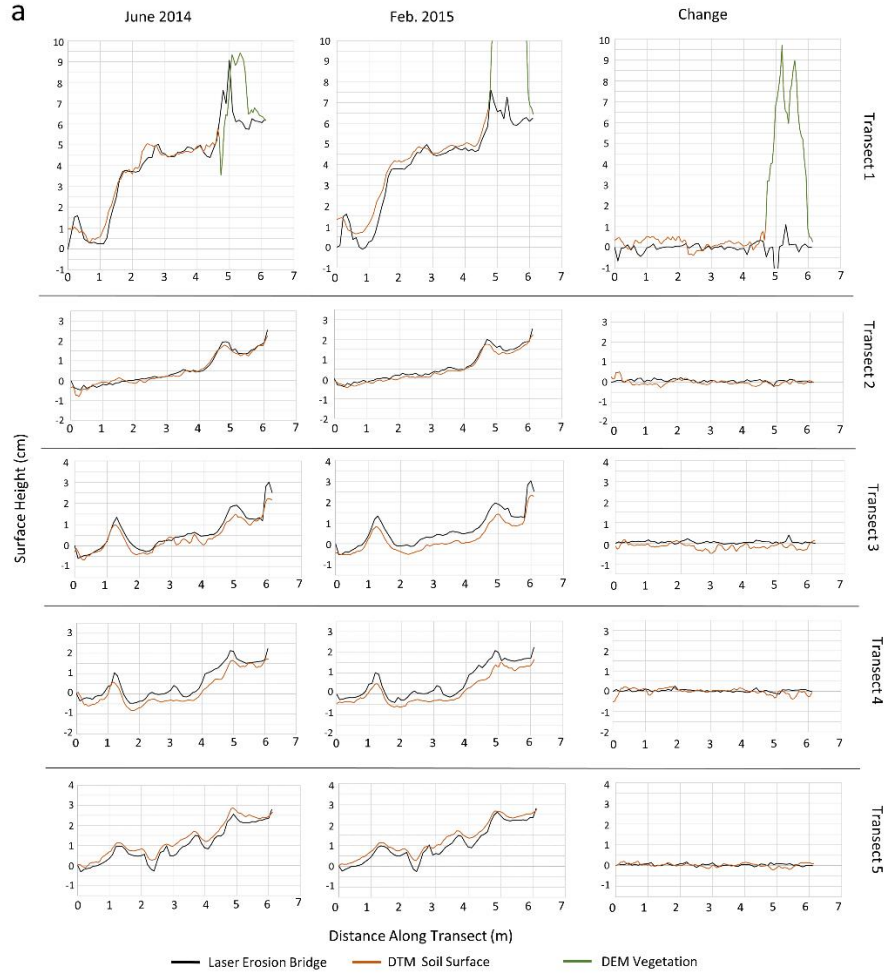
Fig. 4. (**a**) Surface topographic profiles from Plot 5 measured with erosion bridges and digital elevation models (DSMs) reconstructed from UAS imagery. The surface heights (y-axis) are shown as a vertical difference from the first erosion bridge height for easier interpretation and comparison across graphs. The large differences between erosion bridge and DSM surface height measurements at the end of Transect 1 were due to the presence of vegetation. All height pairs with vegetation influence were not included in the accuracy and precision analyses. (**b**) DTM difference image for plot 5 overlaid on UAS-based orthophotos. Blue colors represent elevation decrease (erosion) and the red colors represent elevation increase (deposition) from June 2014 to February 2015. Transparent areas are within the threshold of repeatability error as determined by the difference between the erosion bridge change and DTM change along the transects. The indicated deposition in the northwest corner of the plot is likely DTM error caused by 'doming' effect outside of the GCP envelope, as opposed to real surface change.

Table 1. Acquisition and processing specifications for June 2014 and February 2015 imagery

Aircraft	Bat 4 Fixed-Wing
Sensor	Canon EOS 5D Mark II, 21 megapixels
	Canon EF 35 mm lens
Flying height above ground level (m)	~ 152 AGL
Image Forward Overlap (%)	66
Image Side Overlap (%)	66
Image Ground Footprint (m)	156 × 104
Ground sampling distance (cm)	~ 2.7
Image Count	25–35 images per plot
Avg. Point density (points·m^{-2})	1444
DTM cell size (cm)	5

Table 2. Check point coordinates minus DTM coordinates.

Plot	Acquisition Date	Check Points n	Mean Difference (cm)			Absolute Mean Difference (cm)			RMSE (cm)		
			Easting	Northing	Elevation	Easting	Northing	Elevation	Easting	Northing	Elevation
1	June 2014	9	−0.1	−0.9	−0.2	1.0	0.9	1.7	1.1	1.1	2.2
	Feb. 2015	9	0.0	−1.0	0.2	0.8	1.3	0.9	1.0	1.8	1.2
2	June 2014	9	−0.4	0.8	−1.0	1.0	1.1	3.0	1.7	1.7	4.0
	Feb. 2015	9	−0.5	0.2	−1.1	1.1	0.4	2.5	1.4	0.5	3.8
3	June 2014	9	−0.4	0.1	−0.2	0.9	0.7	0.9	1.1	0.9	1.2
	Feb. 2015	9	−0.6	−0.0	0.1	0.9	0.6	1.3	1.3	0.9	1.4
4	June 2014	9	0.2	0.1	0.1	0.3	0.6	1.1	0.4	0.9	1.4
	Feb. 2015	9	0.6	−0.5	1.0	0.6	0.9	1.1	0.7	1.1	1.3
5	June 2014	9	0.4	0.3	1.7	0.8	1.4	2.0	1.0	2.6	2.7
	Feb. 2015	9	−0.5	0.3	2.0	1.2	1.0	2.9	1.3	1.1	3.5
6	June 2014	9	−0.3	0.3	0.0	0.7	0.6	0.9	0.9	0.7	1.1
	Feb. 2015	9	0.1	0.2	0.1	0.6	0.8	0.4	0.8	0.9	0.5
All	June 2014	54	−0.1	0.1	0.0	0.8	0.9	1.6	1.1	1.5	2.3
	Feb. 2015	54	−0.1	−0.1	0.4	0.9	0.8	1.5	1.1	1.1	2.3

Table 3. DTM precision (repeatability) calculated by subtracting 2014 check point image coordinates from 2015 check point image coordinates.

Plot	Check Points n	Mean Difference (cm)			Absolute Difference (cm)			RMSE (cm)		
		Easting	Northing	Elevation	Easting	Northing	Elevation	Easting	Northing	Elevation
1	9	−0.2	0.1	−0.5	1.0	1.2	1.4	1.2	1.7	2.0
2	9	0.0	0.6	0.1	1.5	1.0	1.1	1.9	1.5	1.4
3	9	0.1	0.1	−0.3	0.9	0.9	1.4	1.1	1.2	1.6
4	9	−0.3	0.6	−0.9	0.5	1.2	1.4	0.6	1.3	1.7
5	9	1.0	0.0	−0.3	1.7	1.5	1.6	1.8	2.3	2.1
6	9	−0.5	0.0	−0.1	0.8	0.6	0.9	1.0	0.7	1.0
All	54	0.0	0.2	−0.3	1.1	1.1	1.0	1.4	1.6	1.7

Table 4. Erosion bridge vertical measurements minus digital terrain model measurements.

Plot	Acquisition Date	Sample Size n	Mean Difference (cm)	Absolute Mean Difference (cm)	RMSE (cm)
1	June 2014	249	−2.2	2.5	2.9
	February 2015	249	−1.1	1.7	2.3
2	June 2014	292	−1.2	1.6	2.1
	February 2015	292	−0.9	1.9	3.0
3	June 2014	298	−2.1	2.2	2.6
	February 2015	298	−0.3	1.5	2.2
4	June 2014	278	−1.7	2.6	3.4
	February 2015	278	−1.7	2.5	4.8
5	June 2014	285	0.4	2.4	3.0
	February 2015	285	0.7	3.1	3.7
6	June 2014	255	−2.5	2.6	3.1
	February 2015	255	−1.7	2.0	2.4
All	June 2014	1657	−1.5	2.3	2.9
	February 2015	1657	−0.8	2.1	3.2

Table 5. Digital elevation model (DTM) vertical repeatability error as measured by comparing the DTM change with erosion bridge change (erosion bridge change minus DTM change). Because structure-from-motion processing was carried out separately for each plot to create DTMs, we assessed repeatability error individually for each plot.

Plot	Sample n	Mean Erosion Bridge Change (cm)	Absolute Mean Erosion Bridge Change (cm)	Mean DTM Change (cm)	Absolute Mean DTM Change (cm)	Erosion Bridge Change Minus DTM Change (cm)	Standard Deviation (cm)	Absolute Erosion Bridge Change Minus DTM Change (cm)	Change Difference RMSE (cm)	95% Confidence Interval (cm)	
										Lower	Upper
1	249	0.3	0.5	−0.7	1.9	1.0	2.4	2.0	2.6	−3.6	5.8
2	292	0.5	0.7	0.2	1.4	0.2	2.4	1.6	2.4	−4.4	5.0
3	298	0.8	1.0	−0.8	1.5	1.7	1.9	2.1	2.6	−2.0	5.5
4	278	−0.1	1.1	−0.1	1.9	0.0	4.4	2.3	4.4	−8.8	8.6
5	285	0.4	0.7	0.0	1.3	0.3	2.1	1.6	2.2	−3.9	4.6
6	255	0.6	0.7	−0.1	1.6	0.8	2.1	1.9	2.2	−3.4	5.0
All	1657	0.4	0.8	−0.2	1.6	0.7	2.7	1.9	2.8	−4.7	6.1

Supplemental Material
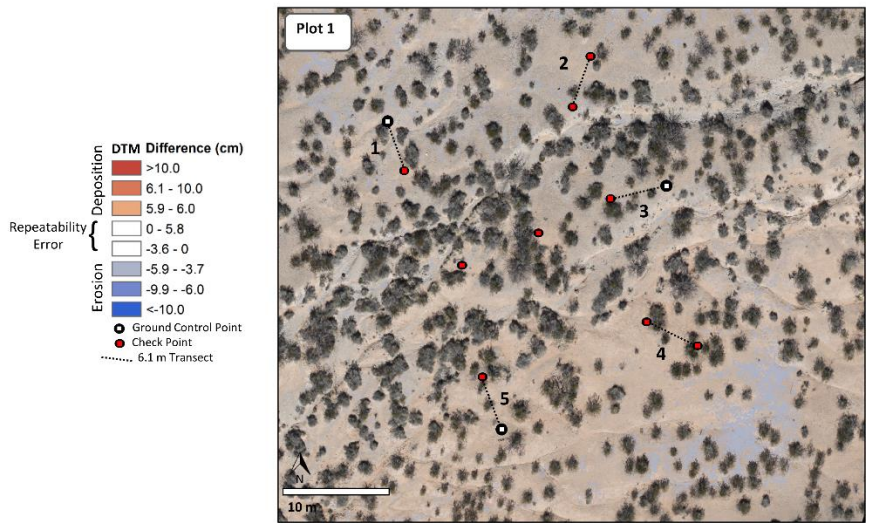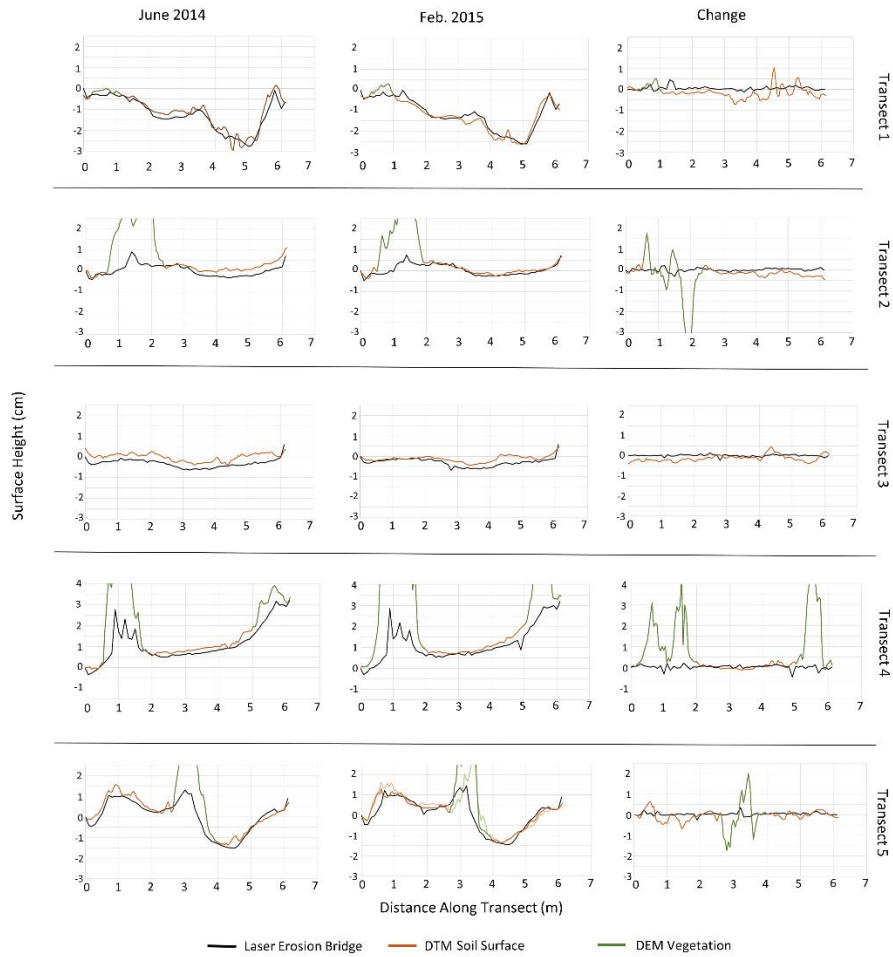
Supplemental Fig. 1. Plot 1 DTM differences and topographic profiles
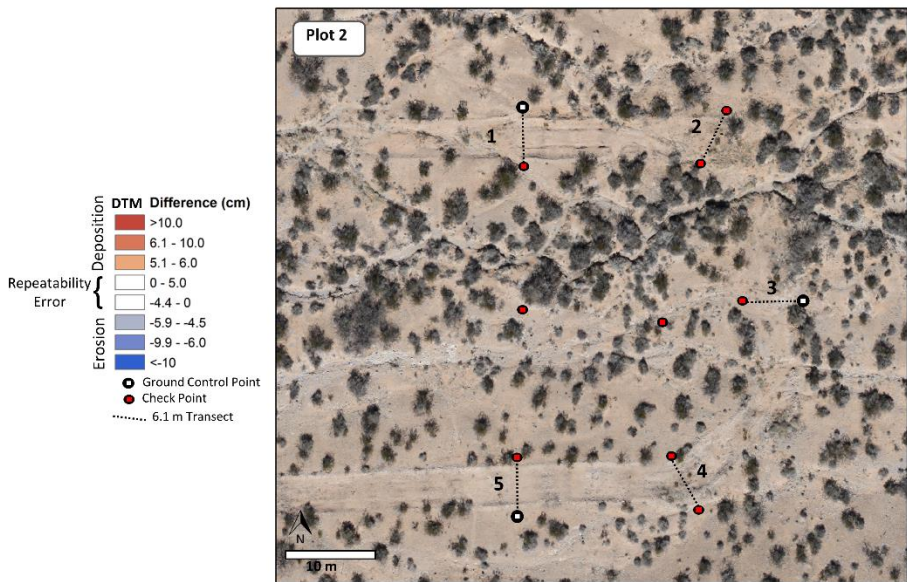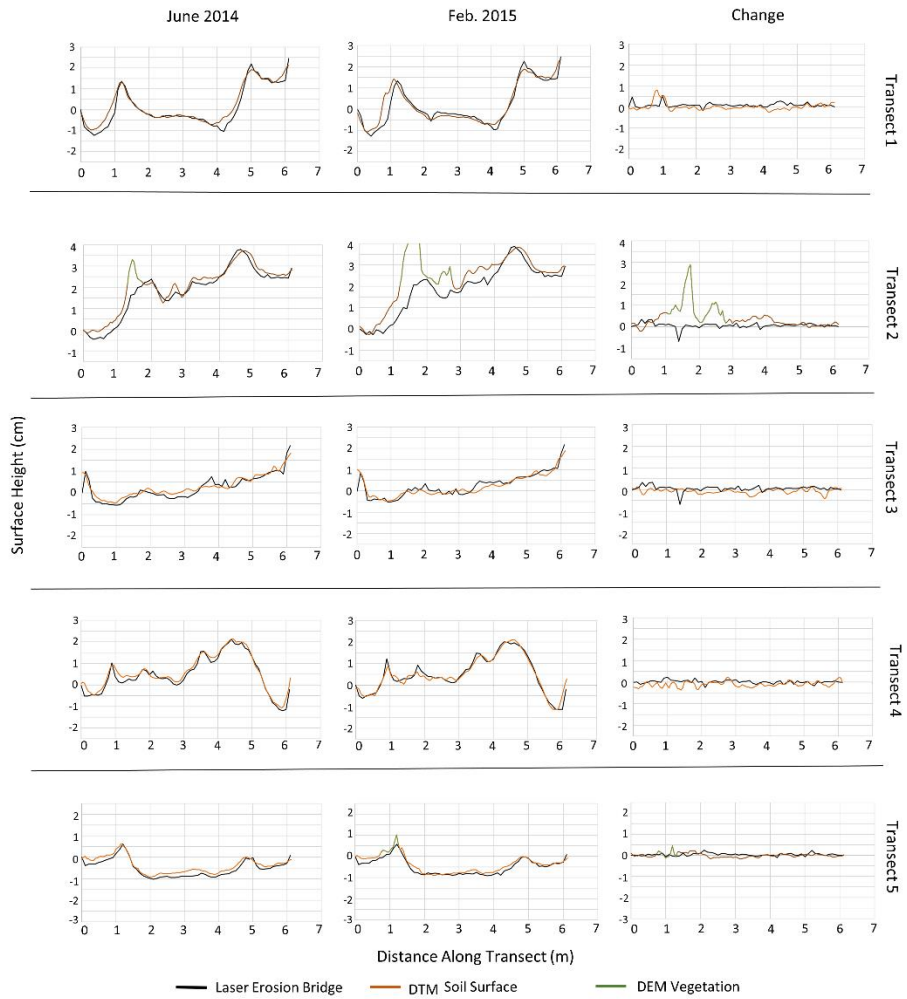
Supplemental Fig. 2. Plot 2 DTM differences and topographic profiles
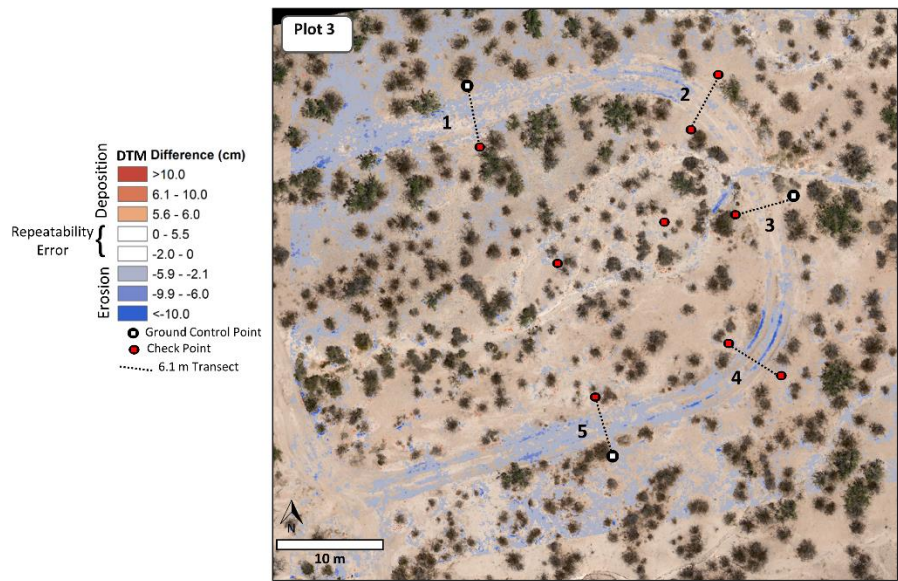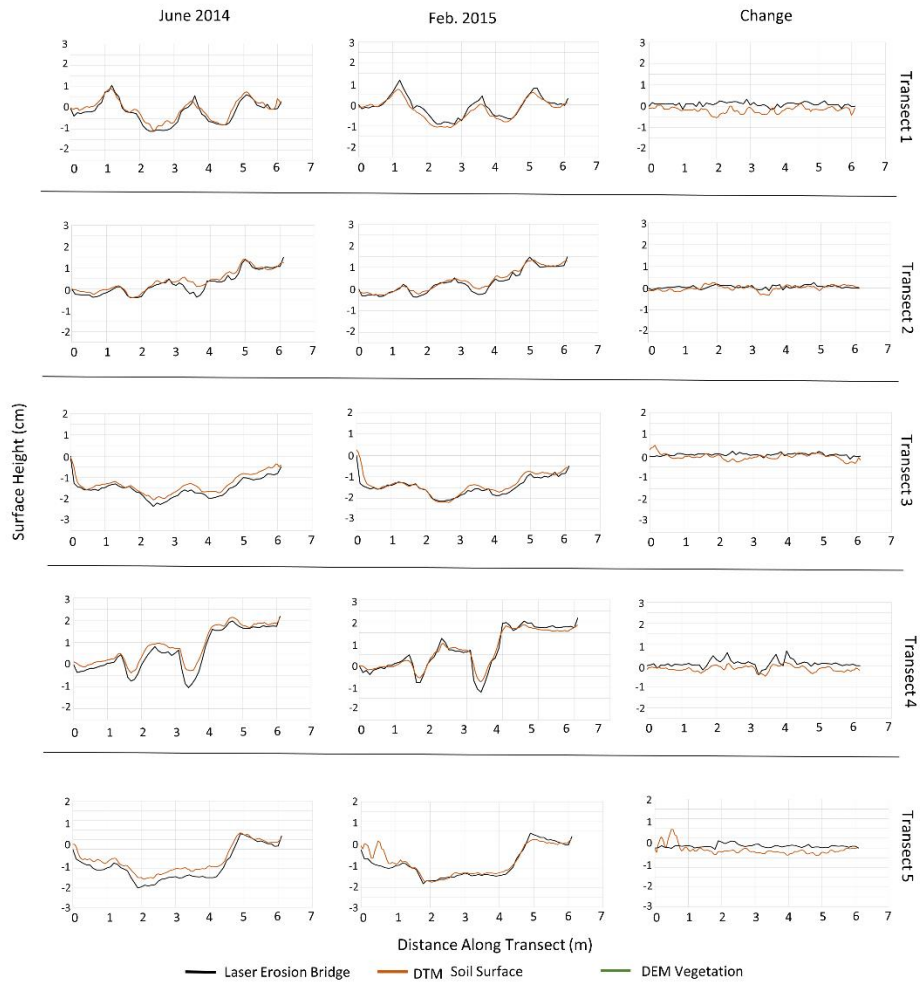
Supplemental Fig. 3. Plot 3 DTM differences and topographic profiles
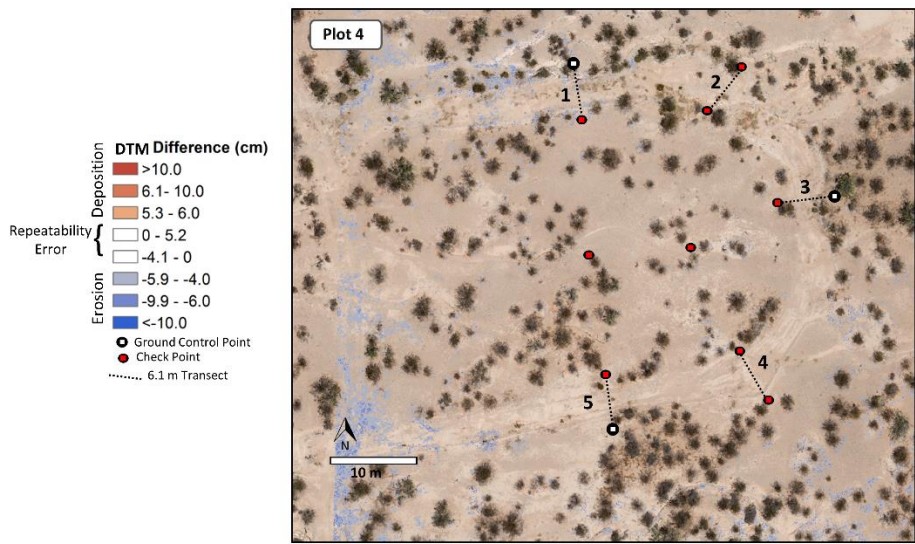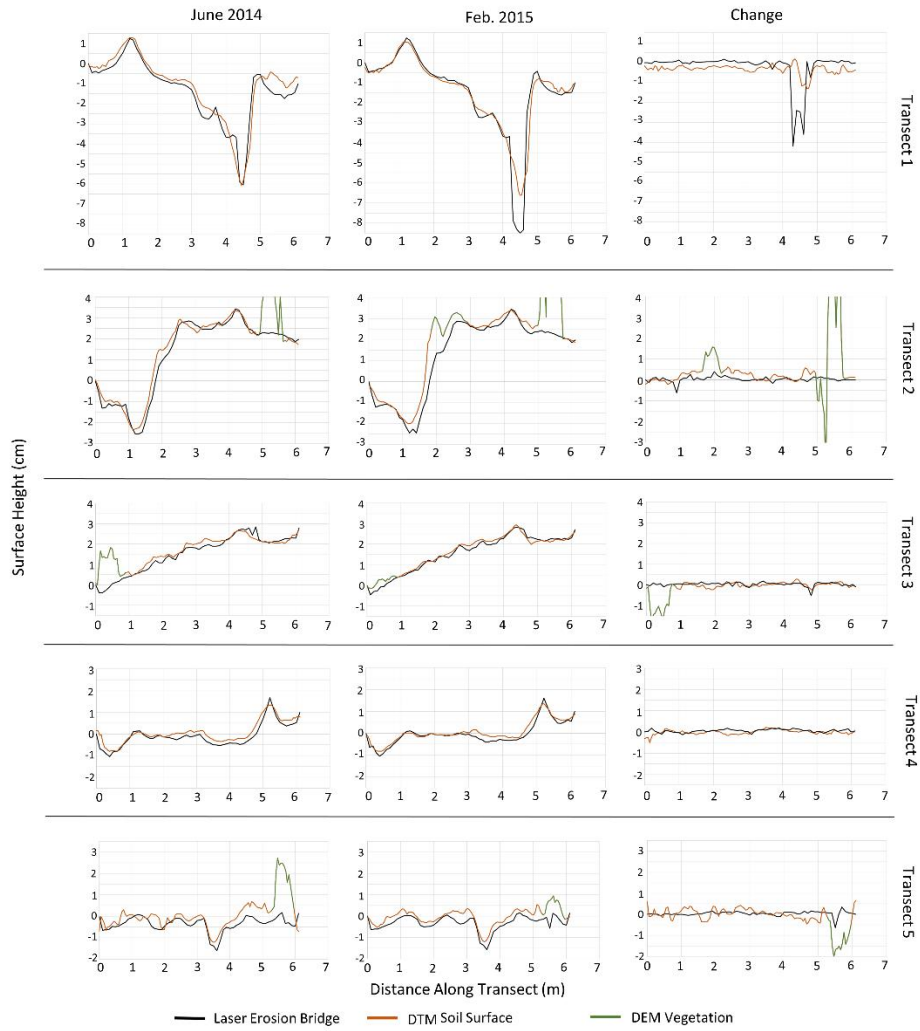
Supplemental Fig. 4. Plot 4 DTM differences and topographic profiles
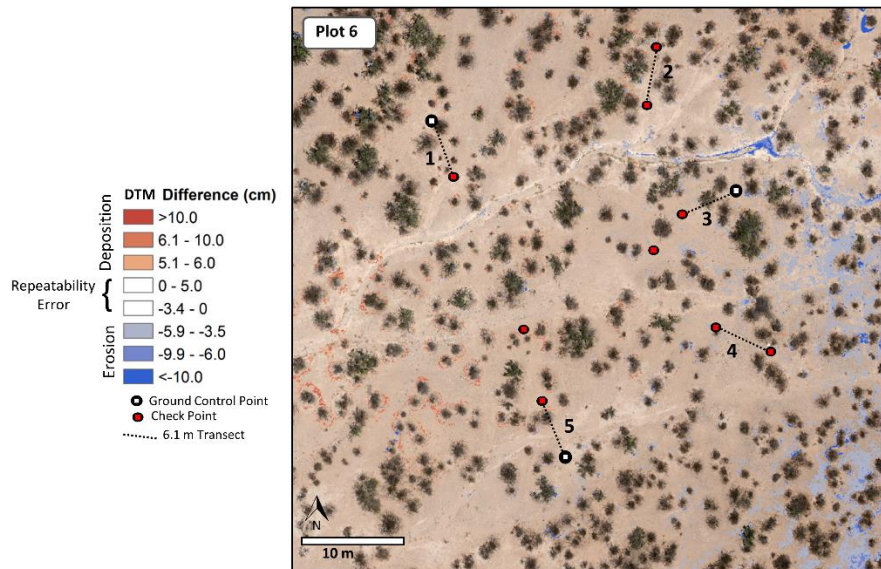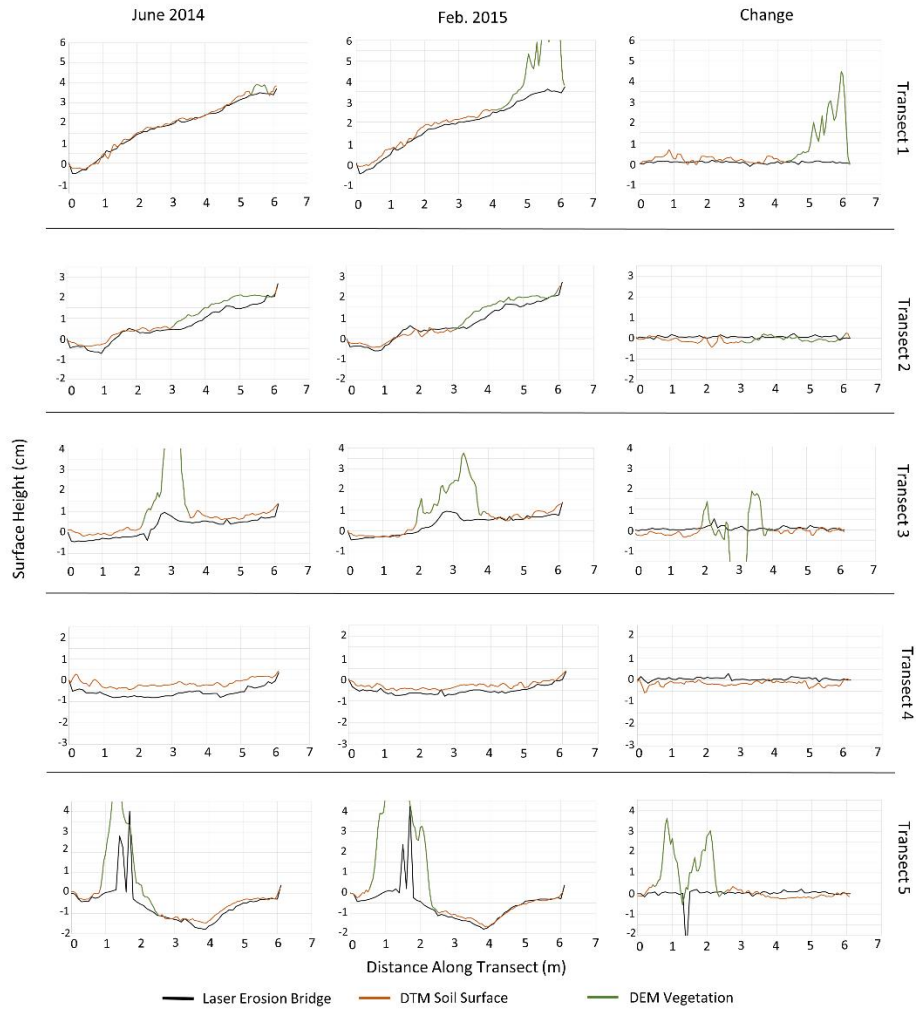
Supplemental Fig. 5. Plot 6 DTM differences and topographic profiles

APPENDIX B:

ESTIMATING FORAGE UTILIZATION WITH DRONE-BASED PHOTOGRAMMATRIC POINT CLOUDS

Jeffrey K. Gillan[1], Mitchel P. McClaran[1], Tyson L. Swetnam[2], and Philip Heilman[3]

[1]University of Arizona – School of Natural Resources and the Environment, Tucson, AZ 85721

[2]University of Arizona – BIO5 Institute, Tucson, AZ 85721

[3]USDA Agricultural Research Service – Southwest Watershed Research Center, Tucson, AZ 85719

Abstract

Monitoring of forage utilization typically occurs at sample locations, or key areas, selected for their presumed potential to represent utilization across pastures. However, utilization can vary greatly across landscapes and may not be well represented by traditional ground-based sampling without great effort. Remote sensing from satellite and manned airborne platforms offer spatial coverage at landscape scale but their poor spatial resolution (satellite) and cost (manned airborne) may limit their use in monitoring forage utilization. High-resolution photogrammetric point clouds obtained from small unmanned aerial systems (sUAS), represent an appealing alternative. We developed a method to estimate utilization by observing the height reduction of herbaceous plants represented by 3-dimensional point clouds. We tested our method in a semi-arid savanna in southern Arizona by comparing utilization estimates with ground-based methods after a month-long grazing duration. In six plots, we found strong correlation between imagery and ground-based estimates ($r^2 = 0.78$) and similar average estimate of utilization of across all plots (ground-based = 18%, imagery = 20%). With a few workflow and technological improvements, we think it is feasible to estimate point cloud utilization over the entire pasture (150 ha) and potentially even larger areas. These improvements include optimizing the number of images collected and used, equipping drones with more accurate global navigation satellite systems (e.g., GPS), and processing images with cloud-based parallel processing. We show proof of concept to provide confident estimates of forage utilization patterns over large pastures and landscapes, at levels of spatial precision that are consistent with ground-based methods. The adoption of drone-based monitoring of utilization of forage on rangelands could follow the paradigm shift already demonstrated by GPS and GIS technologies, where the initial high computing costs were reduced, use became the norm, and the availability of more precise spatial patterns was applied to prescribe and evaluate management practices.

Keywords: Drone, UAS, remote sensing, structure-from-motion photogrammetry, rangelands

Introduction

Forage utilization, defined as the proportion of current year's production by weight consumed or destroyed by animals (Heady, 1949), can indicate levels of use and potential impacts from grazing. Managers often establish maximum levels of utilization to ensure sustainability of use and establish monitoring protocols to detect those levels of utilization (Smith et al., 2016; USDI Bureau of Land Management, 1997). Monitoring of grazing pasture and rangelands, however, is time-consuming and therefore the area sampled is limited by the availability of time and resources.

Monitoring typically occurs at a handful of sample locations, or key areas, selected for their presumed potential to represent utilization across larger pasture and landscape-scale management units. However, utilization can vary greatly across a pasture due to livestock preference for specific forage species, terrain barriers, sun exposure, and distance to water (Bailey et al., 1996). As a result, patchy distribution of utilization may not be well represented by traditional ground-based sampling, and therefore levels of utilization could be poorly represented across the large landscapes typical of western rangelands (Veblen et al., 2014). Finding more efficient methods of collecting monitoring data at pasture and landscape scales should help improve understanding of conditions and their response to management across the vast rangelands in the western U.S. and world (Booth and Tueller, 2003).

Remote sensing from satellite and manned airborne platforms offer spatial coverage at landscape scale (Booth and Cox, 2011), but their poor spatial resolution (satellite) and cost (manned airborne) may limit their use in monitoring forage utilization. High-resolution imagery from small unmanned aerial systems (sUAS), commonly known as drones, represent an alternative (Anderson and Gaston, 2013; Rango et al., 2009). The availability of low cost sensor-carrying sUAS and the advancement of photogrammetric software has made on–demand 3-dimensional

(3D) depictions of rangeland vegetation relatively easy to produce. Further, sUAS have the potential for frequent on-demand deployments yielding imagery at scales sufficiently fine to resolve low stature herbaceous vegetation. Though sUAS imagery cannot be expected to cover the large geographic extents available from satellites or manned aircraft, they can easily exceed the extent of area covered by most ground-based campaigns. These new tools and the imagery products we can create with them have the potential to address a number of management concerns regarding forage use by livestock and wildlife, quality of wildlife habitat, and amount of wildfire fuels.

There has been very little research using remote sensing to measure forage utilization from any platform or scale. The only known study to explicitly estimate utilization did so by relating simulated browse (manually removed winterfat leaves to simulate livestock browsing) with UAS imagery spectra (Quilter and Anderson, 2001). There is, however, a large and growing body of literature on remotely sensing forage biomass where one could presumably estimate utilization with biomass measures at two points in time. The most common method relies on the relationship between ground-based measures of biomass with co-registered imagery spectra. This method has been demonstrated with satellite imagery (Edirisinghe et al., 2011; Feng and Zhao, 2011; Kawamura et al., 2005; Marsett et al., 2006; Schucknecht et al., 2017; Todd et al., 1998), manned airborne imagery (Beeri et al., 2007), and sUAS imagery (Wang et al., 2014). However, seasonal and phenological changes in spectra may limit the general application of this approach given the need for multi-temporal estimates of biomass.

Alternatively, 3D representation of vegetation can estimate biomass and should be robust across the seasons when spectra is likely to change. Cunliffe et al. (2016), for example, estimated biomass of grass (*Bouteloua eriopoda*) with grass volume derived from UAS-obtained photogrammetric point clouds. While this method overcomes the limitation of relating spectral

76

properties to biomass, it has a new challenge of accurately measuring herbaceous vegetation height. This is usually achieved by subtracting a digital terrain model (DTM) from a digital surface model (DSM). However, using a photogrammetric approach to make a DTM is challenging because it cannot 'see' underneath dense vegetation and thus the ground elevation under grasses must be interpolated from nearby ground elevations (Swetnam et al., 2018). In a natural rangeland environment, unbroken extents of vegetation and/or sloped terrain can lead to incorrect estimation of ground elevations under vegetation. These challenges often introduce vertical errors in canopy height models which can make a big difference in the volume and biomass estimates of low statue vegetation such as forage grasses. Studies in crop fields have produced accurate DTMs when the vegetation is not present (Bendig et al., 2014). This strategy does not work in many rangeland environments where perennial grasses (albeit dormant) are present year-round.

We report a "proof of concept" assessment of a remotely acquired photogrammetric method for estimating utilization without having to estimate biomass. Forage utilization in rangeland settings can be determined from the proportion of plants whose height has been reduced by grazing (Roach 1950). We can mimic this method by measuring change in plant height using point cloud analysis. We evaluated this method in a mixed shrub-grass savanna by comparing ground-based estimates and sUAS point cloud estimates of forage utilization following a month-long grazing event. This is the first study to use remotely sensed data to directly estimate forage utilization by grazing cattle.

The objectives for this study were: 1) Estimate forage utilization by differencing pre-grazed and post-grazed sUAS photogrammetric point clouds, 2) Compare imagery-derived utilization with ground measurements of utilization at transect and plot scales, and 3) Identify critical improvements that will extend this method to cover pasture-sized areas.

Methods

Study Area

The experimental area (pasture UA-C) is an 147 ha fenced pasture on the Santa Rita

Experimental Range (SRER) in southern Arizona (31° 48' 36" N, 110° 50'51" W, elevation 1174

m; Fig. 1; http://cals.arizona.edu/srer). SRER soils are characterized as clay loams, sandy loams,

and limey upland soils. This semi-arid area experiences a typical Sonoran Desert bimodal pattern

of precipitation where most moisture falls in late summer, the rest primarily in December and

January (McClaran and Wei, 2014). Mean annual temperature and precipitation are 19°C and

35.8 cm year^{-1}, respectively. The pasture lies on a sandy loam upland ecological site within

Sonoran Desert grassland savanna (MLRA 41-3). The dominant herbaceous forage species

included *Eragrostis lehmanniana* (Lehmann lovegrass), *Digitaria californica* (Arizona

cottontop), *Muhlenbergia porteri*. (bush muhly), and *Aristid*a ssp. (threeawn). Woody species

consisted of *Prosopis velutina* (mesquite), *Gutierrezia sarothrae* (broom snakeweed)*, Zinnia

pumila, Opuntia ssp.* (prickly pear)*,* and *Cylindropuntia ssp.* (cholla)*.*

In calendar year 2016, there was 39.5 cm of precipitation in the study pasture, 77% of which fell

in July, August, and September. Herbaceous grass production follows the late summer monsoon

rain. At peak greenness (mean Landsat 8 NDVI = 0.45) as a proxy for peak forage production, 80

animal units consisting of cow/calf pairs entered the pasture on August 22, 2016, and remained

until September 23, 2016. At the time of withdrawal, herbaceous vegetation had already begun

senescence indicated by lower NDVI values (mean = 0.36) and a lighter green color. This timing

near the end of the growing season minimized the amount of re-growth following defoliation

compared to a timing earlier in the growing season.

Ground Methods

Within the study pasture, we chose six randomly placed points to compare ground-based and sUAS imagery estimates of utilization (Fig. 1). From the random points, we chose a random azimuth to orient the rectangular plot. The baseline of the plots were oriented at 220° azimuth from the plot point. Perpendicular from the baseline, we established 5 sampling transects, each 30 m long. Transects were spaced approximately 20 m apart, but that distance varied depending on the ability to navigate through or around mesquite and cactus. The plot size was ~ 0.27 ha or 100 m x 30 m.

Following the removal of cattle from the pasture we measured utilization using the 'ungrazed plant' method along each transect. The method (Roach, 1950) was developed at the SRER and is based on the grazing habits of cattle. With ample available forage, cattle are likely to graze a grass clump once and move on to the next. Because of this behavior, there is a relationship between the percentage of ungrazed clumps and utilization of forage. At every other pace along the transect (20 total observations), the observer recorded the nearest herbaceous plant as 'grazed' or 'ungrazed'. Classifying very lightly grazed plants as 'grazed' is likely to over-estimate forage use because the tops of grass plants generally contain a small proportion of the plants biomass. To identify these very lightly grazed plants, we employed the grazed class method (Schmutz et al., 1963) which consists of species specific photo-guides for estimating biomass use. Plants with ≤ 10% use were classified as 'ungrazed'. The percent of ungrazed observations was entered as x in the linear formula.

$$\% \ utilization = 79.9451 - 0.8705x \qquad\qquad \textbf{[1]}$$

Utilization was calculated for each transect and for each plot (aggregate of 5 transects).

Additionally, we estimated utilization with before and after grazing measures of forage biomass, a method that is commonly used in other rangeland systems. Immediately before and immediately after the grazing period, we estimated forage production along each transect using the comparative yield method (USDI Bureau of Land Management, 1999). For each plot, forage was clipped, dried, and weighed from three calibration frames (40 x 40 cm) representing low, medium, and high amounts of forage. These frames were given scores of 1, 3, and 5, respectively. These calibration frames are used to train the observer to visually interpret all additional frames with a score of 0 to 5. This method allowed for quicker data collection and the ability to cover a larger area than destructive sampling methods. We estimated forage production in 20 frames along each transect for a total of 100 frames per plot. From the forage production data, we calculated utilization as:

$$\% \ utilization = 1 - \left(\frac{biomass_{post-grazed}}{biomass_{pre-grazed}}\right)$$
[2]

where utilization is calculated from the ratio of biomass measured pre-grazed to post-grazed. We refer to this as the 'biomass change' method hereafter. We calculated utilization with the biomass change method at only the plots (aggregate of 5 transects) because we did not record pre-grazed estimates for each transect.

Image Acquisition

Immediately before and after cattle grazing, we acquired very high-resolution drone imagery of each plot with DJI Phantom 3 Professional and Phantom 4 multi-rotor drones (See Table 1 for image acquisition specifications). These drones weigh ~ 3 lbs, have electric motors, and typically have 20 minute flight endurance. The Phantom series are the most ubiquitous drones on the market and are off-the-shelf ready to fly with modest price points around $1500. We acquired the

imagery for each plot using autonomous grid pattern missions programmed in Ipad application

Altizure v 3.0 (https://next.altizure.com). We flew low to the ground (20 m above ground level)

in order to get very high-resolution imagery (8-10 mm) capable of resolving low stature

herbaceous plants. In the structure-from-motion (SfM) photogrammetry approach we employed, a

high number of overlapping images is recommended to reconstruct complex features (Smith et

al., 2015; Westoby et al., 2012). However, the optimized number of images needed to reconstruct

perennial dryland grasses was unknown prior to this study. Consequently, we blanketed each plot

with 900-1000 images with high-overlap (80%), likely more imagery than what is necessary for

reconstruction. We acquired imagery at nadir and 42° oblique angles because the inclusion of

oblique images in the sparse point cloud step has been shown to improve scene geometry

compared with only nadir images (James and Robson, 2014). It was hypothesized that oblique

images might also improve reconstruction of herbaceous vegetation at the base of mesquite trees,

areas that are less visible from nadir only imagery. Each plot took approximately 45 minutes to

fly including two battery changes. Wind speed during the flights typically ranged from 5-10 mph,

not strong enough to disrupt operations.

Because the expected positional accuracy of the drone global navigation satellite system (GNSS)

is poor (1-2 meters horizontally and 5-10 m vertically from true location), we surveyed ground

control points (GCPs) to be used in the photogrammetry processing. On each plot, we surveyed

13 GCPs. Ten were used in the photogrammetry processing, and three were held back as x, y, z

check points. The GCPs were located on the ends of each vegetation transect (Fig. 1). Each GCP

consisted of a 17 cm diameter round plastic lid mounted on a 0.5 m rebar stake. The lids were

painted black & white in an iron cross pattern. We experimented with but ultimately abandoned

the use of coded targets, patterns that can be detected automatically by software, because it could

not reliably locate GCPs in oblique imagery. We surveyed the GCPs with a Trimble R10 real-

time kinematic GNSS, a setup consisting of a base station and rover. Points were surveyed in

NAD 83 UTM Zone 12 N projection with a horizontal precision of 5-7 mm vertical precision 6-16 mm.

Point Cloud Generation

We used image-based 3D reconstruction software Agisoft Photoscan v 1.3 (http://www.agisoft.ru) for point cloud generation. Each point in the cloud is an x, y, z location of a surface feature with its natural color assigned to it. The SfM process of making point clouds is well documented (Eltner et al., 2016; Smith et al., 2015; Snavely et al., 2008; Westoby et al., 2012) so it will be abbreviated here. All image processing was carried out on a Windows machine with two Intel Xeon CPUs (2.4 GHz;16 logical processors each), two EVGA GeForce GTX 1080 video cards, and 256 GB RAM.

We did 'high quality' initial alignment using the GNSS and time stamp metadata of each image to expedite the process. During this process, camera physical dimensions and lens distortion parameters were calculated with self-calibration. The pose of each exposure station was determined and a sparse point cloud was generated. Any images that did not align or were misaligned were realigned.

After initial alignment, we located all 10 GCPs and 3 check points and marked them in the images. By locating a GCP on two overlapping images, the software estimated the locations of the GCP on all other overlapping images. We went through every image and adjusted the estimated location of the GCPs to the center of the targets. Each GCP was visible on 100 to 400 images. Points in the center of the plot generally had more image projections and vegetation blocked the view of the GCP in some images. Manually adjusting GCPs locations was the most time-consuming aspect of the point cloud generation.

We used the GCPs for a bundle adjustment optimization procedure. Following the recommendation of James et al. (2017) we optimized parameters focal length (f), principal point coordinates (cx, cy), radial distortion (k1, k2), and tangential distortion (p1, p2). We also optimized to correct for rolling shutter effect present in Phantom sensors (Vautherin, 2016). Next, we used the 'gradual selection' tool to identify and remove low-quality sparse points with the following criteria: reprojection error >0.5 pixels, reconstruction uncertainty >30, and projection error > 3. The sparse cloud was optimized (bundle adjustment) after each removal of low quality points.

We created dense point clouds using ultra high density setting, which attempts to create a point for every image pixel, a desirable behavior for very fine-scale vegetation. For this step, we sought to optimize the number of images needed to reconstruct grass with high detail while limiting processing time. On one plot we experimented with the number of images used in dense reconstruction testing a model using only nadir images (150-200) and a model using nadir + all oblique images (900-1000) for dense reconstruction. The nadir only dense point cloud had ~27 million points and took approximately 5-6 hours to process. Comparatively, the nadir + oblique point cloud had ~87 million points and took upwards of a week to process. However, higher point density does not necessarily indicate better or more detailed grass height reconstruction. We tested grass height difference of the two point clouds by subtracting one from the other using M3C2 tool in CloudCompare. A detailed description of these methods is in the '*Point Cloud Filtering*' and '*Point Cloud Differencing*' sections of this paper. The nadir only point cloud was on average only 1 cm lower in height than the nadir + oblique point cloud, which suggests nadir only imagery is a more efficient approach.

Another concern of eliminating oblique images was losing the ability to detect and model herbaceous vegetation under mesquite trees. We evaluated this concern on one plot and found

herbaceous vegetation to be visible and reconstructed at the base of nearly all mesquites. We are, however, giving up some ability to model grass at the base of some mature mesquite trees that have wide obscuring canopies. These were rare occurrences in our study plots that we assume should not significantly alter utilization estimates. We proceeded to carry out dense point cloud reconstruction for all the plots using nadir images only (Fig. 2A). The plot point clouds typically had between 25 and 50 million points with density ranging from 3000-5000 points·m^{-2}.

Point Cloud Filtering

The goal of filtering is to remove any points that are not of interest in the analysis. For this study, we were interested in only herbaceous vegetation. Using the 'classify points' tool in Photoscan, we identified and removed points representing tall woody trees and shrubs while retaining low stature vegetation such as grasses and forbs (Fig. 2B). Cunliffe et al. (2016) and Gillan et al. (2017) both demonstrated the use of this type of filtering approach in semi-arid shrublands in New Mexico. This point filtering tool is a type of maximum local slope filter (Montealegre et al., 2015) where the lowest elevation point within a user defined grid cell is assumed to be ground. All additional ground points are identified based on a user defined maximum angle and distance from the origin ground point. To identify and remove woody trees and shrubs we found the best combination of parameter values were a grid size of 2 m, a maximum angle of 18°, and a max distance of 0.5 m. However, no filter is perfect so some tree stems and small shrubs were likely to remain. We exported the point clouds in log ASCII format (las) format, in projection NAD 83 UTM Zone 12 N.

In the open source program CloudCompare (Girardeau-Montaut 2011), we further filtered the point clouds to remove non-herbaceous vegetation points (i.e., bare-ground, rocks, woody vegetation stems) with a color threshold (Fig. 2C). We calculated a green leaf algorithm

($\frac{G*2-R-B}{G*2+R+B}$; Louhaichi et al. 2001) on the colorized points and applied a simple threshold to

separate the herbaceous vegetation from all other surface features. We found that that a green leaf

algorithm value > 0.035 was an appropriate threshold for identifying vegetation points. This cut-

off value varied slightly between plots due to nuanced soil and vegetation color as well as

illumination differences. We removed the non-herbaceous points leaving point clouds consisting

of only herbaceous vegetation before and after grazing.

Point Cloud Differencing

We used Multiscale Model to Model Cloud Comparison (M3C2) point cloud differencing tool

(Lague et al. 2013; James et al. 2017) in CloudCompare to subtract pre-grazed herbaceous points

from post-grazed herbaceous points in the vertical (z) plane only. This type of analysis is very

similar to the well-established method of digital elevation model differencing (Brasington et al.,

2003; Wheaton et al., 2009), but uses points instead of gridded raster surfaces. Doing the analysis

with points removes the step of having to interpolate the points into an elevation surface. Before

differencing, we thinned and smoothed the pre- and post-grazed point clouds to reduce noise and

absorb horizontal co-registration error (see Table 2). M3C2 calls this subset of points 'core

points'. We applied a 6 cm horizontal distance between core points, effectively removing 96% of

the total points within a cloud, resulting in 120-200 core points·m^{-2}. The elevation values of the

core points were calculated as an average of all points within a 3 cm spherical radius of the core

point. In the vertical (z) plane only, the algorithm measures the distance from the averaged core

point in pre-grazed cloud to the average core point in the post-grazed cloud (Fig. 2D). If there are

not core points from both clouds in the same vertical cylinder, then no differencing occurs.

We performed point cloud differencing for each transect and for entire plots (minimum convex

polygon surrounding the 5 transects). We isolated each transect in CloudCompare using the

'cross-section' tool. We set the width of the transects at 1 m, an area we thought would contain the 40 cm wide frame measurements with some additional space for possible spatial registration errors. We then exported the M3C2 point data to .csv format. We deleted any point difference values < -1.0 m or >1.0 because grass could not have been grazed or grown a meter in the one-month duration of the study. The sporadic existence of such erroneous values is due to some kind of error, most likely an unfiltered tree or shrub point differenced from underlying grass points. For each plot, the existence of these points was typically <0.5%.

Repeatability Error and Threshold for Detecting Vegetation Height Change

Because we estimate vertical differences between point clouds at two points in time, it is essential to quantify the repeatability (precision) error of point cloud reconstructions in order to separate true grass height change from measurement error. Good point cloud reconstruction requires finding the same surface features in multiple images. This can be an easier task for solid features (e.g., bare-ground, rocks) that are visible from several angles. For vegetative surfaces, even very slight differences in image perspectives or illumination can cause features to be obscured or have altered texture between successive images. This phenomenon can cause point cloud reconstructions of vegetation to be less repeatable. For each plot we measured the repeatability between the before and after grazing point clouds by looking initially at the check points. With perfect repeatability, the check point modeled coordinates should not change between two points in time. The observed change can be used to estimate repeatability error primarily due to scene geometry, lens calibrations, or reference quality. In addition to the check point analysis, we developed an herbaceous vegetation reconstruction error term. We did so by reconstructing a 3D scene twice using two independent image sets acquired within 30 minutes of each other (plot 5 on Sept 6, 2016). We used M3C2 to vertically difference the point clouds (same methods described previously). In theory, there should be no vertical difference between the point clouds, so any difference is due to reconstruction error. The standard deviation of check point differences was

3.0 cm. As expected, the standard deviation of herbaceous points (using same filtering methods) was larger at 7.7 cm. We calculated the total repeatability error for each plot as the standard deviation of the check point vertical repeat error plus 4.7 cm (7.7 cm herbaceous height SD minus 3.0 check point SD) for herbaceous reconstruction error (Fig. 2E; Table 2). Based on this two-part error assessment, the vegetation vertical repeatability error among plots ranged from 5.2 to 7.5 cm (Table 2).

We added a 90% confidence interval to the repeatability error to set a grass height change detection threshold that reduces type I errors (false positive for grazing designations).

$$\text{Grass height change detection threshold} = (\text{check point SD} + 4.7 \text{ cm}) * 1.645 \qquad \textbf{[3]}$$

Using plot 5 as an example, the repeatability SD of the check points was 1.1 cm. We added the grass reconstruction error of 4.7 cm for a total of 5.8 cm. The $CI_{90} = 5.8 * 1.645 = 9.5$ cm. Using this logic, grass height must be reduced by 9.5 cm in this plot for it to be considered grazed. Vegetation height change detection thresholds ranged from 8.5 cm to 12.3 cm (Table 2).

We applied the vegetation height change detection threshold to all core points in the differenced point clouds and labeled each point as grazed or ungrazed (Fig. 2E). We then calculated the percentage of ungrazed core points within the total forage core points and used that value in the 'ungrazed plant' method equation (Eq. 1; Fig. 2F) to estimate forge utilization. We then compared these values of utilization with ground-based estimates of utilization at transect scale, plot scale aggregated from 5 transects, and plot scale with all measurements within a polygon surrounding the transects (Fig. 2F). Transect 5 of plot 4 was omitted from the study because we failed to image the entire plot during August acquisition. Our comparative analysis contained 29 transects within 6 plots.

Accuracy of point cloud maximum plant heights

Accuracy in this case, refers to how well we can create a point cloud to capture the 'true' vegetation heights. This differs from the previous section that was primarily concerned with the repeatability of point cloud generation. Knowing how well point cloud reconstructions represented the true structure of the grass indicates how sensitive our methods are to detecting a change in height. It may also provide an explanation for differences between the ground and point cloud methods for estimating utilization. Prior to this the study, the accuracy of photogrammetrically reconstructing herbaceous vegetation from UAS imagery was unknown in our study ecosystem. To quantify vegetation maximum height accuracy, we used a hand-held tape to measure the maximum height of 21 herbaceous plants (grasses and forbs) immediately prior to the August image acquisition. We then compared the ground-based measured heights with the point cloud heights of those same 21 plants using CloudCompare.

Results

Agreement between imagery and ungrazed plant method of estimating utilization

At the transect scale, there was a poor linear relationship between point cloud and 'ungrazed plant' methods of utilization ($R^2 = 0.011$; Fig. 3A), and differences ranged from an overestimation (below 1:1 line) of 38% to an underestimation (above 1:1 line) of 34% of ground-based value. The median absolute difference between the methods was 13% (Fig. 3D). At the aggregated transect scale, the agreement between the point cloud and ungrazed plant method was much stronger than the transect scale ($R^2 = 0.78$; $b = 0.41$; Fig. 3B). Method differences ranged from an overestimation of 8% to an underestimation of 6% and median absolute difference was 5.2% (Fig. 3D). Agreement at the plot scale was also strong ($R^2 = 0.81$; b= 0.49; Fig. 3B); and ranged from an overestimation of 8% to an underestimation of 3%, and the median absolute difference was 6%

(Fig. 3D). Interestingly, at both the aggregated transect and entire plot scales, the ground-based estimate of utilization was underestimated when the point cloud estimate was <15% utilization and overestimated when >15% (Fig. 3B).

The average utilization of all 6 plots combined was estimated at 18.5% using the ungrazed plant method (Table 3). The point cloud method with 5 aggregated transects had utilization of 20.8%, while the entire plot point cloud method estimated a total utilization of 22.8% for all 6 plots. In terms of plot rank order (most to least), the point cloud methods were similar to the ungrazed plant method with some slightly different ordering (Table 3). The discrepancy in rank order between the ground-based and point cloud methods was the result of only a few percentage points.

Agreement between imagery and biomass change method of estimating utilization

The agreement between the point cloud methods and biomass change field method was not as robust as the ungrazed plant method. At the aggregated transect scale, the agreement between the point cloud and biomass change estimates of utilization was modest ($R^2 = 0.46$; b=0.61; Fig. 3C); and differences between the point cloud and biomass change estimates of utilization ranged from an overestimation of 9.8% to an underestimation of 10.6%, and median absolute difference was 4.7% (Fig.3D). At the plot scale, the agreement was also modest ($R^2 = 0.51$; b=0.76; Fig. 3C); and differences between the point cloud and biomass estimates of utilization ranged from an overestimation of 8.9% to an underestimation of 8.9%, and median absolute difference was 3.6% (Fig.3D). As occurred with the ungrazed plant results, at both the aggregated transect and plot scales, the biomass change estimates of utilization was underestimated when the point cloud estimate was <15% utilization and overestimated when >15% (Figs. 3C).

The utilization of all 6 plots combined was estimated at 23.3% using the biomass change method (Table 3). The point cloud method with 5 aggregated transects had utilization of 20.8%, while the entire plot point cloud method estimated a total utilization of 22.8% for all 6 plots. Utilization rank order using the biomass change method was a bit different than the other methods (Table 3). Most notably, it estimated plot 3 to have the highest utilization (37.5%), 15% higher than the ungrazed plant method, 11% higher than the aggregated transect point cloud method, and 9% higher than the entire plot point cloud method.

Accuracy of point cloud maximum plant heights

On average, the point maximum plant heights were 45% of ground measured heights with SD of 12% (Fig. 4; Appendix Table 1). Under-estimation of grass plant height is likely a function of imagery that is too coarse to detect and match features in the diffuse canopy and possible movement of that canopy caused by wind.

Discussion

Our 'proof of concept' assessment provides results that support the use of photogrammetric point cloud differencing as a viable alternative to ground-based estimates of forage utilization in a semi-arid mixed shrub savanna ecosystem. There was strong agreement between utilization estimates using drone-based point cloud differencing of plant height and the ground-based ungrazed plant method (developed at SRER) for which it was expected to mimic. There was also good agreement with the biomass change ground-method. This suggests that the point cloud method of detecting change in plant height could provide reliable estimates of utilization in other rangeland ecosystems, and more importantly represent utilization over a larger spatial extent with shorter field-time than the traditional ground-based estimates.

The approach of simply estimating change in plant height is advantageous compared with other remote sensing approaches that must estimate forage biomass at multiple points in time. Specifically, our method should be more stable across seasons than a 2D imagery spectra approach (e.g., Wang et al. 2014) where spectra/biomass relationships can differ among seasons for the same amount of mass. Additionally, our approach should be more replicable than a 3D representation of biomass which is reliant on making DTMs and canopy height models (e.g., Cunliffe et al. 2016). For example, our approach could be especially advantageous in ecosystems with large amounts of herbaceous cover (e.g., Great Plains) that would make it difficult to sense the ground elevation.

Agreement between ground-based and point cloud methods were stronger at plot scale than transect scale. Some of this can be attributed to the central limit theorem, which suggests that as more measurements are aggregated, the distribution will better represent the central tendency of a normal distribution leading to better agreement between the methods. In addition, the mechanics of performing the measures could contribute to the improved relationship at the plot-scale. In the ungrazed plant method, the absence of a plant at the point of observation causes the observer to seek the nearest plant, perhaps away from the transect line. This can create a mismatch in the exact ground footprint being sampled by the two methods. Also, the ground-based method is taking a sample of 20 individual plants along the transect. The point cloud method cannot distinguish individual plants and is instead taking a census of all herbaceous points in the 3 cm radius core point (~120-200 core points per m^2). If there is a large plant consisting of multiple core points, some points may be classified as grazed and others as ungrazed, leading to different estimates of utilization compared to the ground-based method which would have classified that entire plant as grazed.

Interestingly, the strong relationship between the point cloud and both the ungrazed plant and biomass change estimates of utilization occurred in spite of the point cloud representing on average 45% of grass height. We propose that the strong relationship exists because 1) grass mass is disproportionately concentrated at the lower portions of the plant (Nafus et al., 2009; Schmutz et al., 1963), and 2) we considered any plant with ≤ 10% utilization as 'ungrazed' in our ground estimates. Based on the agreement between the field and point cloud methods, it appears that our ability to model the bottom 45% of plant height was sufficient for the level of grazing intensity in this study. For studies or management goals that require a more sensitive detection of grazing, it would possible to reconstruct the top of grass canopies better by flying lower to the ground or using a sensor with higher spatial resolution.

We defined grazing in this study as a modeled grass height reduction with 90% confidence interval. The confidence interval can be changed to better meet management goals. Relaxing this threshold will likely increase the points that are identified as grazed which in turn will increase utilization estimates. This could increase Type I errors of identifying grass as being grazed when it was not. Consequences of this could be the pasture is grazed less than desired. Strengthening the threshold will reduce the number of points we identified as grazed which will lower utilization estimates. This could increase Type II errors (true grazing that is not detected) for this application. Consequences of this could be the pasture is grazed more than desired.

There are a few potential limitations of the point cloud utilization method. First, it assumes any reduction in herbaceous height past the threshold is due to grazing. Vegetation height could also be reduced by wind, rain, animal trampling, or sagging under their own weight. It may be appropriate to consider and inspect these occurrences before assuming all height reduction is due to grazing. Second, the point cloud method, along with the field methods we compared it to, are conservative estimates of utilization. It is possible that some utilization was not detected due to

grass growth after being grazed. This was likely an infrequent occurrence because we timed the grazing to coincide with peak biomass. Third, it is unlikely that herbaceous species (e.g., native vs. non-native) can be distinguished with high-resolution imagery. Therefore, an estimate of *what* is being utilized will be very challenging. Because the vegetation community was fairly simple at SRER, separating woody vegetation, herbaceous vegetation, and non-vegetation features was achievable. However, further parsing of vegetation composition will become extremely challenging when using RGB sensors.

Expanding Spatial Coverage of Point Cloud Analysis

This study demonstrated an ability to measure forage utilization at plot scales (0.25 ha). With this proof of concept established, the method must be expanded and tested over larger areas. The real advantage of drone data is to cover greater extents of land and capture more indicator variability than can be realistically sampled with ground methods.

An additional benefit of a drone approach is generating a spatial explicit map of forage utilization across a pasture. These image products will be used to better understand the response to management practices intended to change grazing intensity and location (Brock and Owensby, 2000; Guenther et al., 2000). Utilization maps will improve our knowledge of herbivore behavior in relation to habitat characteristics such as distance from drinking water, slope, previously grazed patches, and neighboring non-forage vegetation (e.g., Bailey et al. 1996; Washington-Allen et al. 2004). A utilization map also enables a reverse assessment of the accuracy of utilization estimates based on a few ground-based estimates to represent pasture- and landscape-scale patterns. The implication being that we are able to ask how well 'key areas' represent the response of utilization at the pasture-scale to changes in the management practices and growing conditions. This could especially be useful when two or more herbivore species are grazing, such

as elk and cattle, and a 'key area' designed for cattle may not represent the spatial use pattern of elk (Laca et al., 2010)

With a few workflow and technological improvements, we think it is feasible to estimate point cloud utilization over the entire pasture (150 ha) and potentially even larger areas. Here, we identify critical improvements to the workflow that will speed estimates of utilization measurements and increase the likelihood of adoption by practitioners.

First, we can reduce the number of images per area needed for herbaceous vegetation reconstruction. We only used the nadir images (~190 per plot) for dense point cloud generation, and therefore could have avoided the time spent collecting and processing the 760 oblique images. Woodlands or other ecosystems with more tree cover may benefit from more oblique images to view forage change at the base of the trees. The more open canopy of mesquite savanna made it possible to view herbaceous vegetation change at the base of most mesquite trees with just nadir images. Future acquisitions at SRER should consist of nadir images along with a modest amount (a few dozen) of oblique images which have been shown to improve scene geometry in the initial alignment (James et al., 2017). Fewer images and flight lines per area will free up our flights to cover larger areas.

Second, we should use higher resolution sensors (more megapixels or longer focal lengths) to allow higher flight elevation and greater spatial coverage per flight time without loss of data resolution (3000-5000 points$\cdot$m^{-2} in our study). Higher resolution sensors are already available for the Phantom series (Phantom 4 Pro with 20 mpx) while other studies have demonstrated the use of higher-resolution RGB cameras on other drone aircrafts (Bendig et al., 2014; Gillan et al., 2017; Li et al., 2016). We should also consider flying more than one drone at a time, which

currently requires a special waiver from the United States Federal Aviation Administration (CFR 107.35).

Third, we need more precise and differentially correctable GNSS onboard the drones to precisely capture the coordinates of each exposure station (location of camera when image was taken) to streamline direct georeferencing and reduce reliance on ground control. The success of our point cloud differencing method depends on the point clouds being very well co-registered in 3 dimensions. Horizontal (xy) co-registration is important in order to difference the height of same grass plant. Vertical (z) co-registration is important because it drives the vertical repeatability error and thus sets the threshold for detection of vegetation height change. We achieved very good co-registration with the RTK surveyed ground control points (0.9 cm horizontal, 1.4 cm vertical). However, the survey added an entire day of field work and hours of post-processing in Photoscan spent locating targets in the imagery.

With enough precision, direct georeferencing with RTK GNSS has the potential to greatly reduce the cost of measuring utilization over larger areas by reducing ground control requirements. Early results from drone-mounted RTK report accuracies of 2-4 cm (x, y) and 2-9 cm (z) among a variety of systems (Forlani et al., 2018; Hugenholtz et al., 2016; Rehak et al., 2013). Given that our accuracies are were better than the drone-mounted RTK tests suggests that establishing permanent ground control points and RTK base stations may provide a greater return on investment for range and pastures that are routinely measured.

Alternatively, there is a little known photogrammetric technique that can be used to ensure good co-registration between multi-temporal imagery products without differential GNSS. Raw images from before and after a grazing event can actually be processed within the same project 'chunk'(Gillan et al., 2016; Korpela, 2006). The initial alignment should be conducted with all

images from both time periods, while the dense point clouds should be created with images from just one time period. This multi-temporal approach should produce point clouds co-registered to within a few cm. The drawback, is that the absolute georeferencing accuracy of the products will still depend on the references used (GCPs or GNSS). Also, doubling the image count in a project chunk will increase processing demands in the initial alignment.

Reducing the processing time of point clouds is the final improvement needed to expand the use of drone-based photogrammetry to estimate utilization of forage on rangelands. Measuring indicators over entire pastures will require tens of thousands of images, and processing them is a big data problem that quickly overwhelms the model of using a single powerful desktop computer. To achieve the goal of creating useable imagery products and analysis summaries in 1 or 2 days, we must shift to a cloud computing or network computing model where super computers or many regular computers tackle the problem with parallel processing nodes. Projects such as NSF funded Cyverse (Goff et al., 2011) and Google Earth Engine (Gorelick et al., 2017) show that big data processing is accessible now to anyone with an internet connection, though advanced computing skills is often required. Removing the technical barriers for mass adoption will likely require a 'software-as-a service' model where users upload images to a server and get an automated product (e.g., point cloud) in return. This shifts the burden of photogrammetry expertise as well as purchasing and maintaining hardware. Commercial companies (e.g., DroneDeploy and Agisoft) are offering cloud-based image product creation, but they are likely to be expensive over large extents and not specific for rangeland applications. Researchers and resource agencies should partner to develop cloud-based image processing tools specifically for estimating forage utilization and other rangeland monitoring applications.

Implications

We focus on three implications that emerge from this successful 'proof of concept' assessment showing that drone-based estimates of forage utilization can replicate estimates from traditional ground-based methods. First, there is promise to provide confident estimates of forage utilization patterns over large pastures and landscapes, at levels of spatial precision that are consistent with ground-based methods, and that promise will only increase as the technology becomes more affordable and easy to use.

The second implication is related to the clear benefit of adopting 21st century technology to assess site-specific resource conditions at exceptional precision and extent. This implies that training for rangeland managers (or at least geospatial specialists) is likely to include operation of drones for data collection and use of cloud-computing resources to handle data processing demand. Adopting these technologies may be similar to the proliferation of global positioning systems (GPS) and geographic information systems (GIS) in the later 20th century, where the initial high computing costs were reduced, use of the technologies became the norm, and the availability of more precise spatial patterns was applied to prescribe and evaluate management practices.

The third implication is that these technologies do not replace field skills in plant identification, knowledge of phenological patterns of growth, and ability to associate utilization patterns with the distribution of soils and geomorphic surfaces. Common sense and field setting acuity will remain critical to logical interpretation and application of the extensive and precise information available from these new technologies.

References

Anderson, K., Gaston, K.J., 2013. Lightweight unmanned aerial vehicles will revolutionize spatial ecology. Front. Ecol. Environ. 11, 138–146. https://doi.org/10.1890/120150

Bailey, D.W., Gross, J.E., Laca, E.A., Rittenhouse, L.R., Coughenour, M.B., Swift, D.M., Sims, P.L., 1996. Mechanisms That Result in Large Herbivore Grazing Distribution Patterns. J. Range Manag. 49, 386. https://doi.org/10.2307/4002919

Beeri, O., Phillips, R., Hendrickson, J., Frank, A.B., Kronberg, S., 2007. Estimating forage quantity and quality using aerial hyperspectral imagery for northern mixed-grass prairie. Remote Sens. Environ. 110, 216–225. https://doi.org/10.1016/j.rse.2007.02.027

Bendig, J., Bolten, A., Bennertz, S., Broscheit, J., Eichfuss, S., Bareth, G., 2014. Estimating biomass of barley using crop surface models (CSMs) derived from UAV-based RGB imaging. Remote Sens. 6, 10395–10412. https://doi.org/10.3390/rs61110395

Booth, D., Cox, S., 2011. Art to science: Tools for greater objectivity in resource monitoring. Rangelands 33, 27–34. https://doi.org/10.2111/1551-501x-33.4.27

Booth, D., Tueller, P., 2003. Rangeland monitoring using remote sensing. Arid L. Res. Manag. https://doi.org/10.1080/713936105

Brasington, J., Langham, J., Rumsby, B., 2003. Methodological sensitivity of morphometric estimates of coarse fluvial sediment transport. Geomorphology 53, 299–316. https://doi.org/10.1016/S0169-555X(02)00320-3

Brock, B.L., Owensby, C.E., 2000. Predictive Models for Grazing Distribution : A GIS Approach. Rangelands 53, 39–46.

Cunliffe, A.M., Brazier, R.E., Anderson, K., 2016. Ultra-fine grain landscape-scale quantification of dryland vegetation structure with drone-acquired structure-from-motion photogrammetry. Remote Sens. Environ. 183, 129–143. https://doi.org/10.1016/j.rse.2016.05.019

Edirisinghe, a., Hill, M.J., Donald, G.E., Hyder, M., 2011. Quantitative mapping of pasture biomass using satellite imagery. Int. J. Remote Sens. 32, 2699–2724. https://doi.org/10.1080/01431161003743181

Eltner, A., Kaiser, A., Castillo, C., Rock, G., Neugirg, F., Abellan, A., 2016. Image-based surface

reconstruction in geomorphometry – merits, limits and developments of a promising tool for
geoscientists. Earth Surf. Dyn. Discuss. 1445–1508. https://doi.org/10.5194/esurfd-3-1445-2015

Feng, X.M., Zhao, Y.S., 2011. Grazing intensity monitoring in northern China steppe: Integrating
CENTURY model and MODIS data. Ecol. Indic. 11, 175–182.
https://doi.org/10.1016/j.ecolind.2009.07.002

Forlani, G., Asta, E.D., Diotri, F., Morra, U., Roncella, R., Santise, M., 2018. Quality Assessment of DSMs
Produced from UAV Flights Georeferenced with On-Board RTK Positioning 1–22.
https://doi.org/10.3390/rs10020311

Gillan, J.K., Karl, J.W., Barger, N.N., Elaksher, A., Duniway, M.C., 2016. Spatially Explicit Rangeland
Erosion Monitoring Using High-Resolution Digital Aerial Imagery. Rangel. Ecol. Manag. 69.
https://doi.org/10.1016/j.rama.2015.10.012

Gillan, J.K., Karl, J.W., Elaksher, A., Duniway, M.C., 2017. Fine-resolution repeat topographic surveying
of dryland landscapes using UAS-based structure-from-motion photogrammetry: Assessing accuracy
and precision against traditional ground-based erosion measurements. Remote Sens. 9.
https://doi.org/10.3390/rs9050437

Goff, S.A., Vaughn, M., McKay, S., Lyons, E., Stapleton, A.E., Gessler, D., Matasci, N., Wang, L.,
Hanlon, M., Lenards, A., Muir, A., Merchant, N., Lowry, S., Mock, S., Helmke, M., Kubach, A.,
Narro, M., Hopkins, N., Micklos, D., Hilgert, U., Gonzales, M., Jordan, C., Skidmore, E., Dooley, R.,
Cazes, J., McLay, R., Lu, Z., Pasternak, S., Koesterke, L., Piel, W.H., Grene, R., Noutsos, C.,
Gendler, K., Feng, X., Tang, C., Lent, M., Kim, S.-J., Kvilekval, K., Manjunath, B.S., Tannen, V.,
Stamatakis, A., Sanderson, M., Welch, S.M., Cranston, K.A., Soltis, P., Soltis, D., O'Meara, B., Ane,
C., Brutnell, T., Kleibenstein, D.J., White, J.W., Leebens-Mack, J., Donoghue, M.J., Spalding, E.P.,
Vision, T.J., Myers, C.R., Lowenthal, D., Enquist, B.J., Boyle, B., Akoglu, A., Andrews, G., Ram, S.,
Ware, D., Stein, L., Stanzione, D., 2011. The iPlant Collaborative: Cyberinfrastructure for Plant
Biology. Front. Plant Sci. 2, 34. https://doi.org/10.3389/fpls.2011.00034

Gorelick, N., Hancher, M., Dixon, M., Ilyushchenko, S., Thau, D., Moore, R., 2017. Google Earth Engine:
Planetary-scale geospatial analysis for everyone. Remote Sens. Environ. 202, 18–27.
https://doi.org/10.1016/j.rse.2017.06.031

Guenther, K.S., Guenther, G.E., Redick, P.S., 2000. Expected-Use GIS maps. Rangelands 22, 18–20.

Heady, H.F., 1949. Methods of Determining Utilization of Range Forage. J. Range Manag. 2, 53–63.

Hugenholtz, C., Brown, O., Walker, J., Barchyn, T., Nesbit, P., Kucharczyk, M., Myshak, S., 2016. Spatial
    Accuracy of UAV-Derived Orthoimagery and Topography: Comparing Photogrammetric Models
    Processed with Direct Geo-Referencing and Ground Control Points. GEOMATICA 70, 21–30.
    https://doi.org/10.5623/cig2016-102

James, M.R., Robson, S., 2014. Mitigating systematic error in topographic models derived from UAV and
    ground-based image networks. Earth Surf. Process. Landforms 39, 1413–1420.
    https://doi.org/10.1002/esp.3609

James, M.R., Robson, S., D'Oleire-Oltmanns, S., Niethammer, U., 2017. Optimising UAV topographic
    surveys processed with structure-from-motion: Ground control quality, quantity and bundle
    adjustment. Geomorphology 280, 51–66. https://doi.org/10.1016/j.geomorph.2016.11.021

James, M.R., Robson, S., Smith, M.W., 2017. 3-D uncertainty-based topographic change detection with
    structure-from-motion photogrammetry: precision maps for ground control and directly
    georeferenced surveys. Earth Surf. Process. Landforms 42, 1769–1788.
    https://doi.org/10.1002/esp.4125

Kawamura, K., Akiyama, T., Yokota, H.O., Tsutsumi, M., Yasuda, T., Watanabe, O., Wang, S., 2005.
    Quantifying grazing intensities using geographic information systems and satellite remote sensing in
    the Xilingol steppe region, Inner Mongolia, China. Agric. Ecosyst. Environ. 107, 83–93.
    https://doi.org/10.1016/j.agee.2004.09.008

Korpela, I., 2006. Geometrically accurate time series of archived aerial images and airborne lidar data in a
    forest environment. Silva Fenn. 40, 109–126.

Laca, E.A., Sokolow, S., Galli, J.R., Cangiano, C.A., 2010. Allometry and spatial scales of foraging in
    mammalian herbivores. Ecol. Lett. 13, 311–320. https://doi.org/10.1111/j.1461-0248.2009.01423.x

Lague, D., Brodu, N., Leroux, J., 2013. Accurate 3D comparison of complex topography with terrestrial
    laser scanner: Application to the Rangitikei canyon (N-Z). ISPRS J. Photogramm. Remote Sens. 82,
    10–26. https://doi.org/10.1016/j.isprsjprs.2013.04.009

Li, W., Niu, Z., Chen, H., Li, D., Wu, M., Zhao, W., 2016. Remote estimation of canopy height and

aboveground biomass of maize using high-resolution stereo images from a low-cost unmanned aerial

vehicle system. Ecol. Indic. 67, 637–648. https://doi.org/10.1016/j.ecolind.2016.03.036

Louhaichi, M., Borman, M.M., Johnson, D.E., 2001. Spatially Located Platform and Aerial Photography

for Documentation of Grazing Impacts on Wheat. Geocarto Int. 16, 65–70.

https://doi.org/10.1080/10106040108542184

Marsett, R.C., Qi, J., Heilman, P., Biedenbender, S.H., Watson, M.C., Amer, S., Weltz, M., Goodrich, D.,

Marsett, R., 2006. Remote Sensing for Grassland Management in the Arid Southwest. Rangel. Ecol.

Manag. 59, 530–540. https://doi.org/10.2111/05-201R.1

McClaran, M.P., Wei, H., 2014. Recent drought phase in a 73-year record at two spatial scales:

Implications for livestock production on rangelands in the Southwestern United States. Agric. For.

Meteorol. 197, 40–51. https://doi.org/10.1016/j.agrformet.2014.06.004

Montealegre, A.L., Lamelas, M.T., De La Riva, J., 2015. A Comparison of Open - Source LiDAR Filtering

Algorithms in a Mediterranean Forest Environment. IEEE J. Sel. Top. Appl. Earth Obs. Remote Sens.

8, 4072–4085. https://doi.org/10.1109/JSTARS.2015.2436974

Nafus, A.M., McClaran, M.P., Archer, S.R., Throop, H.L., 2009. Multispecies allometric models predict

grass biomass in semidesert rangeland. Rangel. Ecol. Manag. 62, 68–72. https://doi.org/10.2111/08-

003

Quilter, M.C., Anderson, V. a L.J.O., 2001. A proposed method for determining shrub utilization using (

LA / LS) imagery. J. Range Manag. 54, 378–381.

Rango, A., Laliberte, A., Herrick, J.E., Winters, C., Havstad, K., Steel, C., Browning, D., 2009. Unmanned

aerial vehicle-based remote sensing for rangeland assessment, monitoring, and management. J. Appl.

Remote Sens. 3, 033542. https://doi.org/10.1117/1.3216822

Rehak, M., Mabillard, R., Skaloud, J., 2013. a Micro-Uav With the Capability of Direct Georeferencing.

Int. Arch. Photogramm. Remote Sensing, Beijing, China XL, 4–6.

https://doi.org/10.5194/isprsarchives-XL-1-W2-317-2013

Roach, M.E., 1950. Estimating Perennial Grass Utilization on Semidesert Cattle Ranges by Percentage of

Ungrazed Plants. J. Range Manag. 3, 182–185.

Schmutz, E.M., Holt, G.A., Michaels, C.C., 1963. Grazed-Class Method of Estimating Forage Utilization.

J. Range Manag. 16, 54–60.

Schucknecht, A., Meroni, M., Kayitakire, F., Boureima, A., 2017. Phenology-Based Biomass Estimation to Support Rangeland Management in Semi-Arid Environments. Remote Sens. 9, 463. https://doi.org/10.3390/rs9050463

Smith, L., Ruyle, G., Maynard, J., Barker, S., Meyer, W., Stewart, D., 2016. Principles of Obtaining and Interpreting Utilization Data on Rangelands.

Smith, M.W., Carrivick, J.L., Quincey, D.J., 2015. Structure from motion photogrammetry in physical geography. Prog. Phys. Geogr. 40, 247–275. https://doi.org/10.1177/0309133315615805

Snavely, N., Seitz, S.M., Szeliski, R., 2008. Modeling the world from Internet photo collections. Int. J. Comput. Vis. 80, 189–210. https://doi.org/10.1007/s11263-007-0107-3

Swetnam, T.L., Gillan, J.K., Sankey, T.T., McClaran, M.P., Nichols, M.H., Heilman, P., McVay, J., 2018. Considerations for Achieving Cross-Platform Point Cloud Data Fusion across Different Dryland Ecosystem Structural States. Front. Plant Sci. 8, 2144. https://doi.org/10.3389/fpls.2017.02144

Todd, S.W., Hoffer, R.M., Milchunas, D.G., 1998. Biomass estimation on grazed and ungrazed rangelands using spectral indices. Int. J. Remote Sens. 19, 427–438. https://doi.org/10.1080/014311698216071

USDI Bureau of Land Management, 1999. Sampling Vegetation Attributes Interagency. Technical Reference.

USDI Bureau of Land Management, 1997. Idaho standards for rangeland health and guidelines for livestock grazing management.

Vautherin, J., 2016. Photogrammetric Accuracy and Modeling of Rolling Shutter Cameras. EuroCOW 2016, Eur. Calibration Orientat. Work. (presentation), 10–12 Febr. 2016, Lausanne, Switz. https://doi.org/10.5194/isprsannals-III-3-139-2016

Veblen, K.E., Pyke, D. a., Aldridge, C.L., Casazza, M.L., Assal, T.J., Farinha, M. a., 2014. Monitoring of Livestock Grazing Effects on Bureau of Land Management Land. Rangel. Ecol. Manag. 67, 68–77. https://doi.org/10.2111/REM-D-12-00178.1

Wang, C., Price, K., Merwe, D. van der, An, N., Wang, H., 2014. Modeling Above-Ground Biomass in Tallgrass Prairie Using Ultra-High Spatial Resolution sUAS Imagery. Photogramm. Eng. Remote Sens. 1151–1159. https://doi.org/10.14358/PERS.80.12.10151

Washington-Allen, R.A., West, N.E., Ramsey, R.D., Efroymson, R.A., 2004. A Protocol for Retrospective Remote Sensing–Based Ecological Monitoring of Rangelands. Rangel. Ecol. Manag. 59, 19–29. https://doi.org/10.2111/04-116R2.1

Westoby, M.J., Brasington, J., Glasser, N.F., Hambrey, M.J., Reynolds, J.M., 2012. 'Structure-from-Motion' photogrammetry: A low-cost, effective tool for geoscience applications. Geomorphology 179, 300–314. https://doi.org/10.1016/j.geomorph.2012.08.021

Wheaton, J.M., Brasington, J., Darby, S.E., Sear, D. a., 2009. Accounting for uncertainty in DEMs from repeat topographic surveys: improved sediment budgets. Earth Surf. Process. Landforms 156, 136–156. https://doi.org/10.1002/esp.1886

Figures and Tables
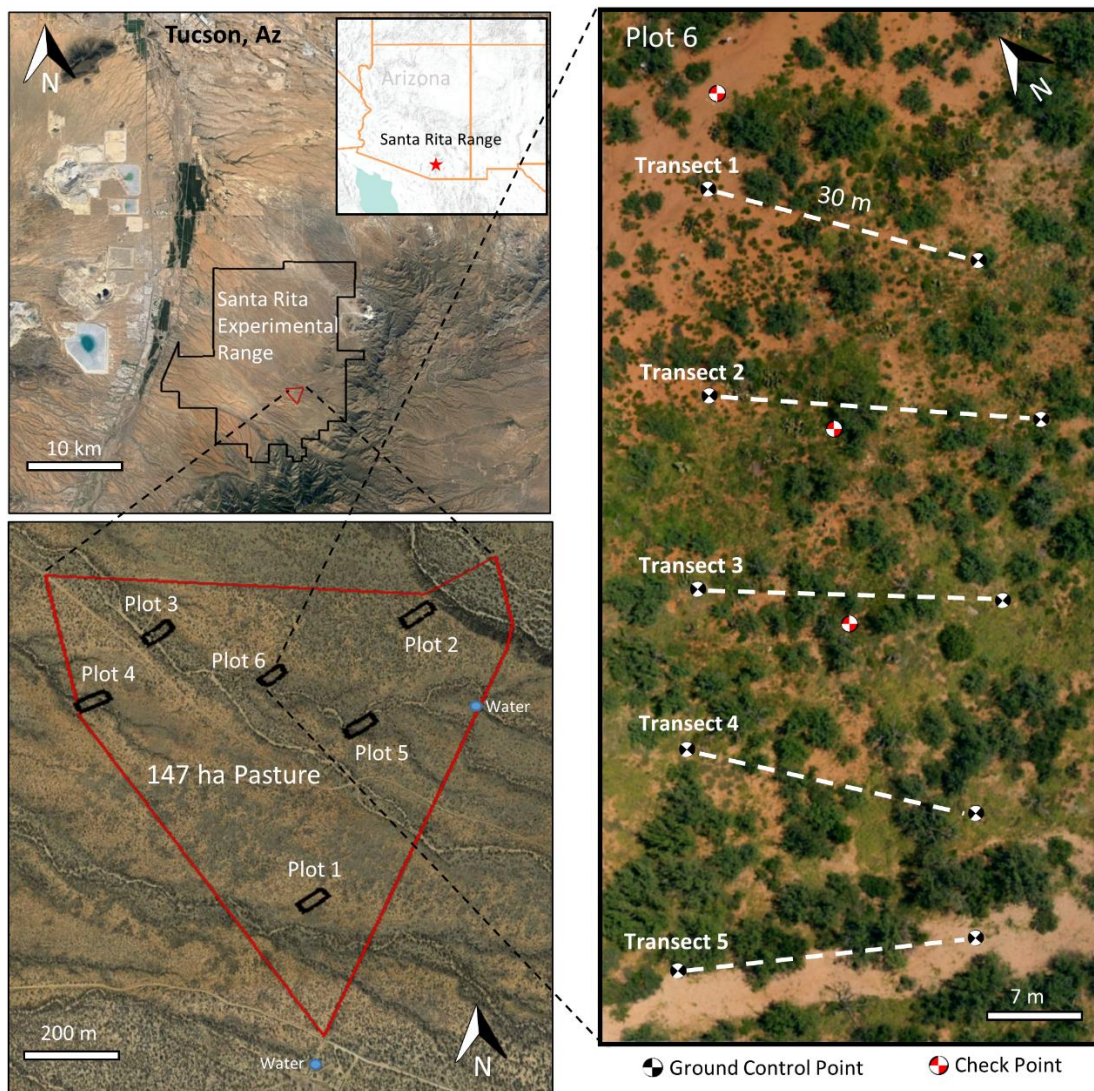
Fig. 1. Study area and plot design on the Santa Rita Experimental Range in southern Arizona, USA
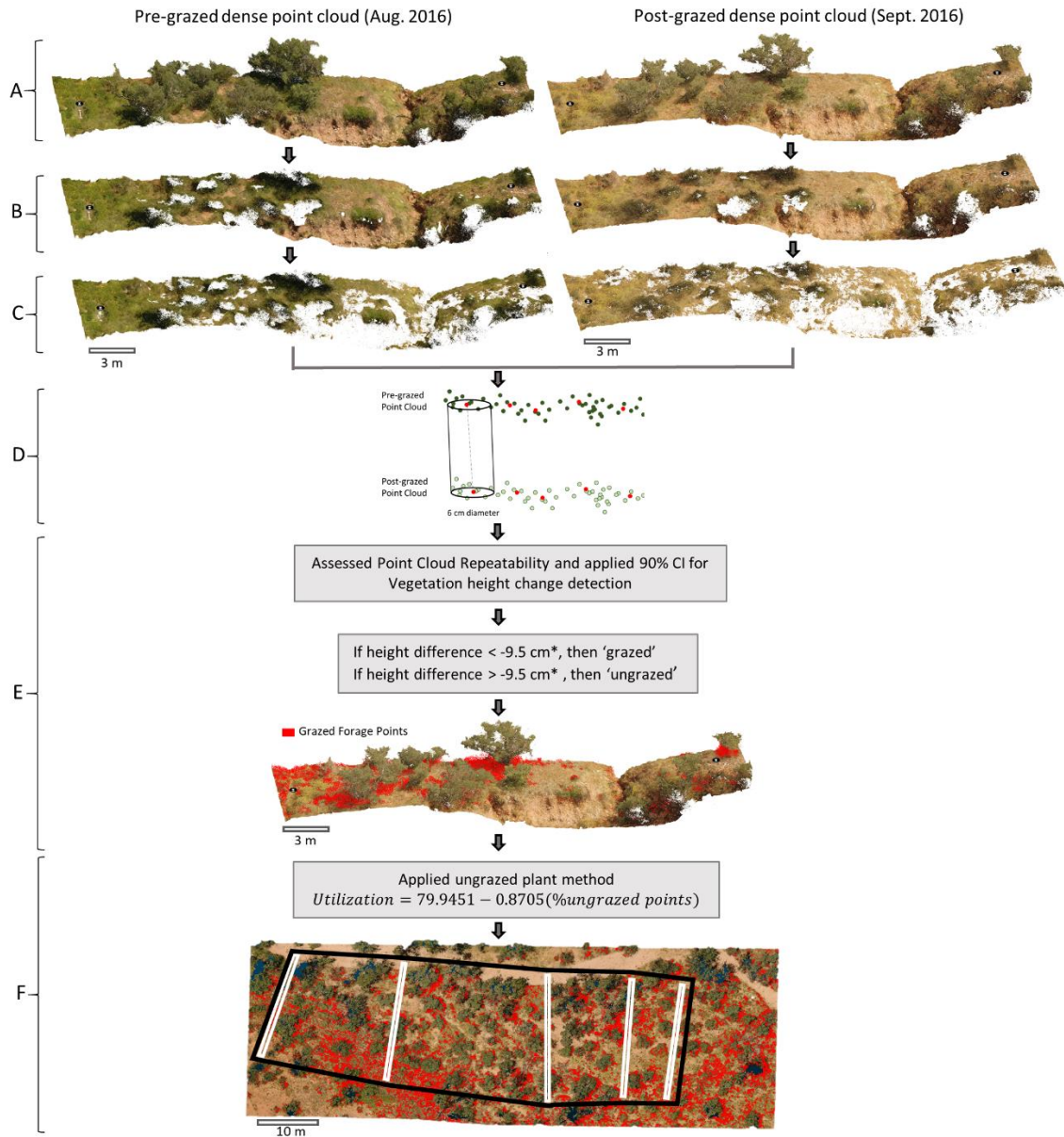
Fig. 2. Workflow to calculate forage utilization with point clouds. A) We created drone-based structure-from-motion photogrammetry point clouds before and after a month-long grazing event. Here we depict a single 30 m transect. B) Tall woody vegetation was removed using a local maximum slope threshold in Agisoft Photoscan. C) Bare-ground and woody stems were filtered with a green leaf algorithm leaving only herbaceous vegetation. D) Vertical height change estimated by subtracting pre-grazed herbaceous points from post-grazed herbaceous points using M3C2 in CloudCompare. E) Repeatability of height change estimated at each plot and applied a

90% confidence interval to set a vegetation height change detection threshold (*threshold varies per plot). Each point was labeled as 'grazed' or 'ungrazed' based on this threshold. F) The percentage of ungrazed points was entered into the ungrazed plant method equation (Eq. 1) to estimate utilization. We compared point cloud utilization with ground-based utilization at individual transects (white rectangles), plot aggregated from 5 transects, and the entire plot (black rectangle).
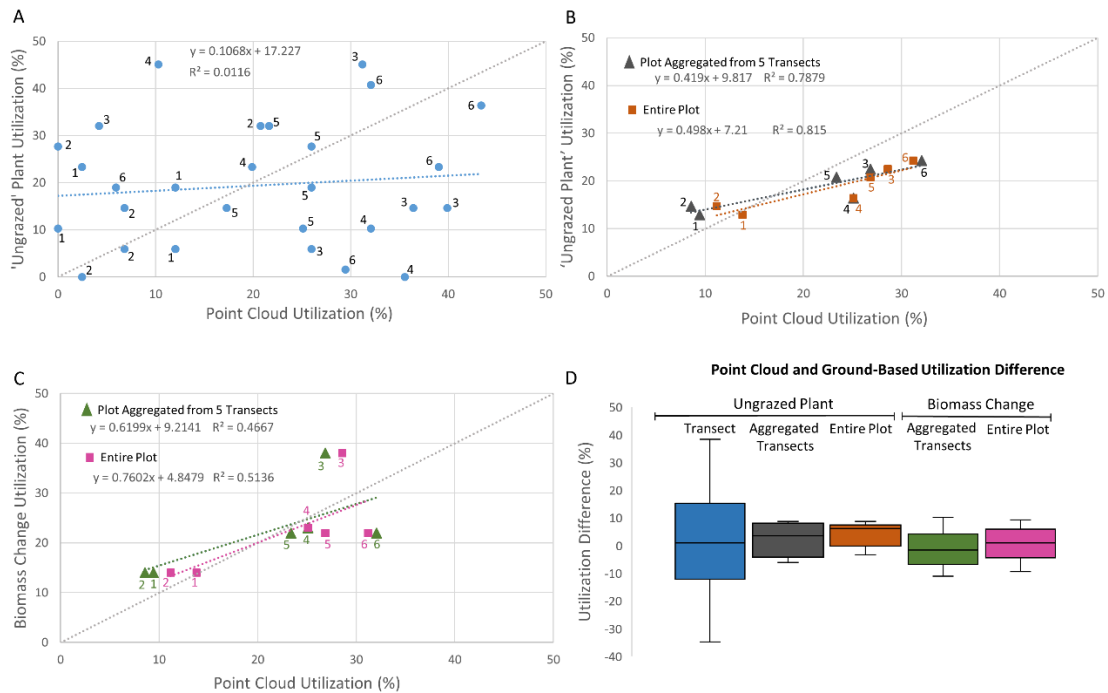
Fig. 3. A) Linear regression between point cloud and ungrazed plant method estimates of utilization with transects as the sample unit. Plot numbers are labeled 1-6 on the graphs. B) Linear regressions between point cloud and ungrazed plant method with the sample units being plot aggregated from 5 transects and entire plot. C) Linear regressions between point cloud and biomass change method with the sample units being plot aggregated from 5 transects and entire plot. D) Box plots showing difference between point cloud and ground-based method utilization. Whiskers show the range, boxes show the interquartile range, and the middle line represents the median.
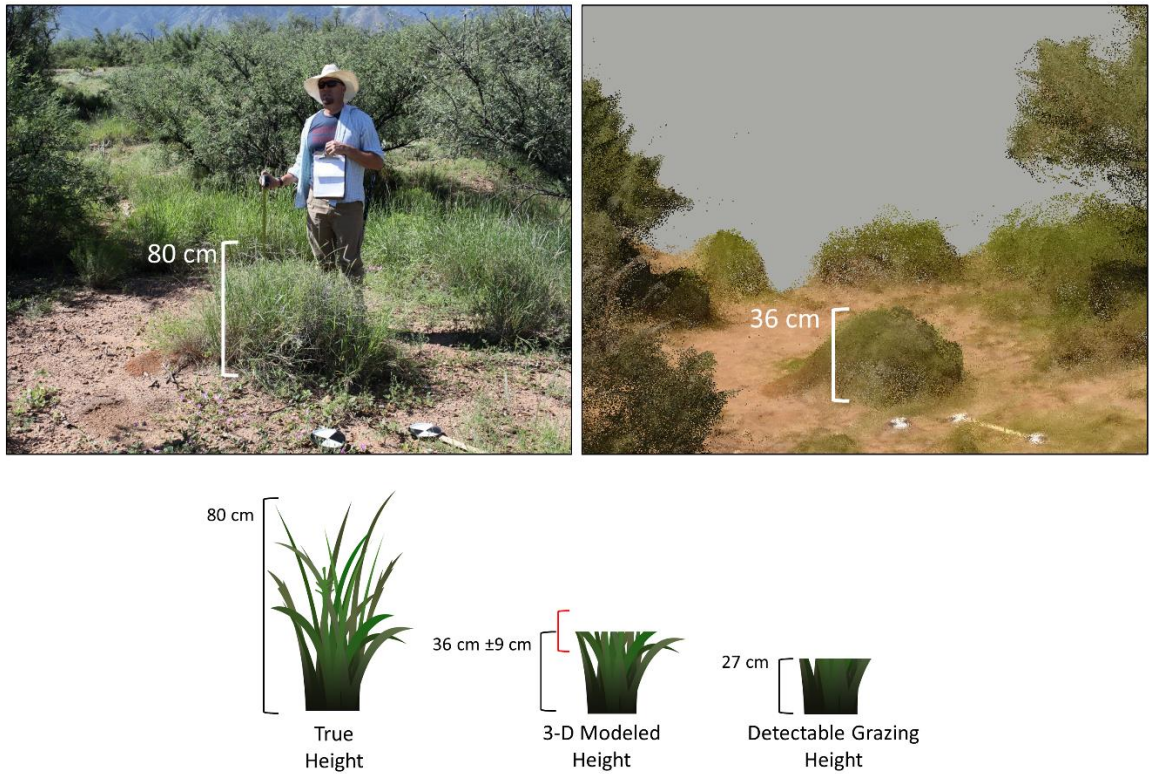
Fig. 4. Comparing the maximum height of one Arizona cottontop (*Digitaria californica*) plant as measured in the field and estimated with sUAS-based photogrammetric point clouds. The ground-measured height was 80 cm but was modeled with point clouds to be 36 cm. Combined with point cloud repeatability error 90% confidence interval of ~ 9 cm, the plant would need to be reduced to a point-cloud height of 27 cm before it could be detected as 'grazed'.

Table 1. Image acquisition specifications

Aircraft	DJI Phantom 3 Professional & Phantom 4 multi-rotors
Sensor	12 mpx; 33 millisecond rolling shutter readout; RGB
Image format	jpeg file format; 5.2 mb per image; bit depth R(8) + G(8) +B(8)
Autopilot	Altizure v 3.0 for Ipad
Flying Height	~20 m above ground level
Image dimensions	8-10 mm ground sampling; 31 m x 23 m footprints
Ground speed	4-5 m/second
Image Count per plot	~ 950 total; 190 nadir, 760 42° oblique (190 N, 190 S, 190 W, 190 E)
Image forward and side overlap	75-80%
Flying time per plot	45 min

Table 2. Check point (n=3 per plot) repeatability and vegetation height change detection threshold

Plot	Check point x repeatability RMSE (cm)	Check point y repeatability RMSE (cm)	Check point z repeatability RMSE (cm)	Check point z repeatability SD (cm)	Grass Repeatability error SD (cm)	Total Repeatability error SD (cm)	CI_{90} Height Change Threshold (cm)
1	2.0	1.8	1.7	1.2	4.7	5.9	9.7
2	0.8	1.1	0.8	1.0	4.7	5.7	9.3
3	0.8	1.5	1.9	0.5	4.7	5.2	8.5
4	2.5	1.4	2.3	2.8	4.7	7.5	12.3
5	0.8	1.1	0.9	1.1	4.7	5.8	9.5
6	0.7	0.6	0.9	1.0	4.7	5.7	9.3

Table 3. Utilization estimated with ground-based methods and point cloud differencing methods arranged from most to least utilization by plot. Normal approximation used to generate standard error and 95% confidence interval.

Forage Utilization	Ungrazed Plant Aggregated Transects	Biomass Change Aggregated Transects	Point Cloud Differencing Aggregate Transects	Point Cloud Differencing Plot Scale
Most	Plot 6 (24.2%)	Plot 3 (37.5%)	Plot 6 (32.0%)	Plot 6 (31.1%)
	Plot 3 (22.4%)	Plot 4 (23.4%)	Plot 3 (26.8%)	Plot 3 (28.5%)
	Plot 5 (20.7%)	Plot 5 (21.8%)	Plot 4 (25.1%)	Plot 5 (26.8%)
	Plot 4 (16.4 %)	Plot 6 (22.2%)	Plot 5 (23.3%)	Plot 4 (25.1%)
	Plot 2 (14.6%)	Plot 1 (13.9%)	Plot 1 (9.4%)	Plot 1 (13.7%)
Least	Plot 1 (12.9%)	Plot 2 (13.5%)	Plot 2 (8.5%)	Plot 2 (11.1%)
Avg.	18.5 ± 4.7%	23.3 ± 9.1%	20.8% ± 10.1%	22.7% ± 8.6%

Supplemental Material

Supplemental Table 1. Comparison of ground measured and point cloud modeled maximum height of 22 selected herbaceous plants.

Plant Specimen	Species	Ground measured maximum height (cm)	Point cloud maximum height (cm)	Height proportion (Point cloud height / Ground-based height)
1	*Digitaria californica*	80	36	0.45
2	*Heteropogon contortus*	80	33	0.41
3	*Bouteloua filiformis*	50	30	0.6
4	*Eragrostis lehmanniana*	80	28	0.35
5	*Digitaria californica*	50	26	0.52
6	*Eragrostis lehmanniana*	100	53	0.53
7	*Ambrosia artemisifolia*	40	13	0.32
8	*Aristida sp.*	60	10	0.16
9	*Kallstroemia grandiflora*	50	30	0.6
10	*Setaria leucopila*	58	17	0.29
11	*Heteropogon contortus*	100	44	0.44
12	*Digitaria californica*	64	40	0.62
13	*Eragrostis lehmanniana*	80	27	0.33
14	*Aristida sp.*	69	29	0.42
15	*Digitaria californica*	80	33	0.41
16	*Aristida sp.*	50	31	0.62
17	*Eragrostis lehmanniana*	75	34	0.45
18	*Eragrostis lehmanniana*	50	27	0.54
19	*Amaranthus sp.*	60	26	0.43
20	*Digitaria californica*	60	21	0.35
21	*Aristida sp.*	55	34	0.61
				Mean 0.45 **Standard Deviation 0.12**

Supplemental Table 2. Point cloud marker residuals (surveyed coordinate minus modeled coordinate)

Plot	Acquisition Date	Markers (n)	Residual RMSE (cm)			
			Easting(x)	Northing(y)	Elevation(z)	x, y, z
1	Aug. 2016	GCP (10)	2.6	0.5	0.7	2.8
		Check (3)	1.6	1.5	0.8	2.4
	Sept. 2016	GCP (10)	0.9	0.9	0.6	1.4
		Check (3)	1.4	1.0	2.2	2.8
2	Aug. 2016	GCP (10)	0.8	0.6	0.6	1.3
		Check (3)	1.1	1.4	2.2	2.9
	Sept. 2016	GCP (10)	0.5	0.4	0.3	0.8
		Check (3)	0.6	0.4	1.3	1.5
3	Aug. 2016	GCP (10)	1.5	1.3	0.4	2.1
		Check (3)	2.2	0.9	0.4	1.0
	Sept. 2016	GCP (10)	1.1	1.0	0.5	1.6
		Check (3)	0.8	1.6	1.6	2.4
4	Aug. 2016	GCP (10)	1.2	1.2	3.1	3.6
		Check (3)	0.6	0.6	1.5	1.7
	Sept. 2016	GCP (10)	1.4	1.7	2.1	3.1
		Check (3)	2.6	1.5	2.4	3.8
5	Aug. 2016	GCP (10)	1.0	0.6	1.0	1.6
		Check (3)	0.5	0.4	1.6	1.7
	Sept. 2016	GCP (10)	0.7	0.6	0.5	1.0
		Check (3)	0.5	0.8	0.9	1.4
6	Aug. 2016	GCP (10)	0.8	0.9	0.9	1.5
		Check (3)	0.9	0.5	1.8	2.0
	Sept. 2016	GCP (10)	0.9	0.5	0.7	1.3
		Check (3)	0.2	0.2	1.2	1.2
Plot Avg	**Aug. & Sept. 2016**	**GCP (60)**	**1.1**	**0.8**	**0.9**	**1.8**
		Check (18)	**1.0**	**0.8**	**1.4**	**2.0**

APPENDIX C:

TOWARD OPERATIONALIZING THE USE OF LOW COST UAS AS AN IMAGING TOOL FOR RANGELAND INVENTORY AND MONITORING

Jeffrey K. Gillan[1], Willem J.D. van Leeuwen[1,2], and Jason W. Karl[3]

[1]Arizona Remote Sensing Center, School of Natural Resources and the Environment

University of Arizona, Tucson, AZ 85721

[2]School of Geography and Development - University of Arizona, Tucson, AZ 85721

[3]Department of Forest, Rangeland, and Fire Sciences – University of Idaho, Moscow, ID 83844

Abstract

The recent availability of small and low-cost sensor carrying unmanned aerial vehicles (UAVs, commonly known as drones) coupled with advances in image processing software (i.e., structure from motion photogrammetry) have made drone-collected imagery a potentially valuable tool for range inventory and monitoring. Transitioning from research demonstrations to a suite of monitoring methods that are useful for supporting management decisions (e.g., accurate, repeatable, and cost-effective) will require additional exploration to develop best practices for image acquisition and workflow specifications that can efficiently estimate multiple indicators. The objectives of this project were to: 1) develop a unified workflow to measure three common rangeland indicators from drone imagery: fractional cover of plant functional types, canopy gaps, and vegetation height; 2) assess agreement between imagery-based and field-measured values and 3) investigate how fractional cover estimates differed between two sensor types (RGB v. multi-spectral). We embedded with a field monitoring crew in the Northern California District of the Bureau of Land Management to compare imagery-derived (using small drones) and field-measured values. The correspondence between imagery and field methods yielded encouraging agreement while revealing systematic differences between the methods. There was minimal difference in fractional cover accuracy between sensor types. Drone imagery will enable broader extent observations of fractional cover, but with a tradeoff of detail loss. For canopy gaps and vegetation heights, drone imagery was found to measure the indicators more thoroughly than field methods. Workflow best practices for producing these indicators is likely to vary by vegetation composition and phenology. An online space dedicated to sharing imagery-based workflows could spur collaboration among researchers and quicken the pace of integrating drone-imagery data with adaptive management of rangelands.

Keywords: drone, unmanned aerial system, rangelands, adaptive management, ecological inventory and monitoring, remote sensing

Introduction

Rangeland inventory and monitoring (I & M) data, used to evaluate ecosystem function and successional states, are important for adaptive management of public and private rangelands (Allen et al., 2017; Kendall and Moore, 2012; Mitchell, 2010). Because it is challenging to measure fine-scale vegetation and soil indicators (e.g., species composition, canopy gaps, vegetation heights) over entire landscapes, sampling approaches are commonly used to extrapolate limited data from field plots to estimate conditions in larger landscapes (Elzinga et al., 1998; Karl et al., 2017). On landscapes units with heterogeneous or patchy vegetation characteristics, a field sampling approach that observes a relatively small proportion of the inference area may estimate indicator values and their change with low confidence (Booth and Cox, 2011).

Range scientists and managers have long sought a remote sensing solution to extend geographic coverage of indicator observations. Satellite imagery products, however, are often too coarse to observe fine features of interest such as individual plants and the bare-ground between them (Tueller, 1996). Imagery from manned airplanes can be sufficiently fine-grained but are often cost-prohibitive. . The recent availability of small and low-cost sensor carrying unmanned aerial vehicles (UAVs, commonly known as drones) along with the codification of piloting and airspace rules have made drone-collected imagery a potentially valuable tool for range inventory and monitoring. Small drones (< 5 kg) can now be easily brought into the field and deployed to image dozens to hundreds of hectares at spatial resolutions capable of measuring fine-scale vegetation and soil indicators. They hold the promise of observing larger extents and estimating landscape I & M values with higher confidence than traditional field sampling.

Research has shown that several quantitative range indicators can be estimated from high-resolution imagery (<10 cm ground sampling distance (GSD)). Fractional cover estimates have

been demonstrated using classification algorithms (Baena et al., 2017; Cruzan et al., 2016; A. S. Laliberte et al., 2010a; Laliberte et al., 2010b; Laliberte et al., 2011b, 2011a; Laliberte and Rango, 2011; Lu and He, 2017; McGwire et al., 2013) and visual interpretation (Booth and Cox, 2009, 2008; Breckenridge et al., 2011; Duniway et al., 2012; Hardin et al., 2007; Karl et al., 2014; Moffet, 2009; Seefeldt and Booth, 2006) with high success for plant functional types and species identification. From high-resolution imagery, it is possible to estimate large inter-canopy gaps (Karl et al., 2012; Rango et al., 2009) as well as vegetation heights and structure using photogrammetry (Cunliffe et al., 2016; Gillan et al., 2014; Jensen and Mathews, 2016; Olsoy et al., 2018; Swetnam et al., 2018)

Most existing research has focused on quantifying indicator value agreement and inherent differences between imagery and traditional field methods. This is necessary for integrating drone-based indicators with existing monitoring programs and legacy field data. Transitioning from research demonstrations (i.e., one-off research projects that culminate with a peer-reviewed publication) to a suite of monitoring methods that are useful for supporting management decisions (e.g., accurate, repeatable, and cost-effective) will require additional exploration to develop best practices for image acquisition and workflow specifications that can efficiently estimate multiple indicators. Public agencies that manage rangelands often need multiple lines evidence to diagnose complex land issues (Bland et al., 2017; Michalak et al., 2017) and to carry out land health assessments (USDI Bureau of Land Management, 2001). Calculating multiple indicators from a single image acquisition and workflow helps to reduce the cost of such data.

Workflows must be customized to account for compositional and phenological differences between vegetation communities. For example, methods that successfully estimate fractional cover in a shrubland may fall short in a more biologically diverse grassland. Moreover, the timing of collecting data conducive to detecting (in the imagery) the I & M features of interest is likely

to vary between ecosystems and with precipitation regimes (Hunt et al., 2003; Lass and Calihan, 1997).

In this paper, we present the results of a pilot program to test the use of image products collected from small UAVs to produce multi-indicator rangeland inventory and monitoring data. For this test, we embedded with a Bureau of Land Management (BLM) field monitoring crew in Northern California to compare field-measured and imagery-derived indicator values and to evaluate the logistics of using small UAVs as a field-deployed tool for rangeland monitoring. We sought to develop image acquisition and processing methods specific for this study area (see details below) in part because the vegetation communities represent a large portion of other lands the BLM manages in the American West. Accordingly, the methods described in this paper could be applied to other similar vegetation communities.

Our objectives were to: 1) develop a unified workflow to measure three common rangeland indicators from drone imagery: fractional cover of plant functional types, canopy gaps, and vegetation heights; 2) assess agreement between imagery-based indicator values and field-measured values; and 3) investigate how fractional cover estimates differed between two sensor types: RGB v. multi-spectral.

Methods
Study Area

Field research was conducted at the Applegate and Eagle Lake field offices in the BLM's Northern California District (NCD), in northeastern California and across the border into Nevada (Fig. 1). The combined land area of both field offices is 11,165 km^2 and consists primarily of semi-arid sagebrush steppe, scattered mountain ranges reaching elevation of 2500 m, and extensive desert playas devoid of vegetation. Mean annual precipitation ranges from 25 to 35 cm

with 75% occurring between October and March. Typically, the warmest month is July with average temperature highs of 31.5°C and lows of 10.4°C. January is typically the coldest month of the year with average temperature highs of 4.7°C and lows of -6°C. A primary use of BLM lands in the NCD is cattle grazing. Greater sage-grouse (*Centrocercus urophasianus*), a species of conservation concern, has critical habitat within the district. The district has been heavily invaded by cheatgrass (*Bromus tectorum*) which has led to large range fires such as the Rush fire in 2012. There are also large populations of wild horses and burros which can contribute to impairment of rangeland health across the NCD and localized heavy impacts to riparian areas.

Field Data Collection

Three-person crews collected field data following the protocols of the BLM's assessment, inventory, and monitoring (AIM) strategy (MacKinnon et al., 2011). The AIM program is intended to provide long-term data on the status and trend of land health (biotic integrity, soil and site stability, hydrologic function) for multiple applications and scales on public rangelands (MacKinnon et al., 2011; Taylor et al., 2014; Toevs et al., 2011). AIM uses standardized collection methods, and randomized (i.e., probability-based) sampling designs to infer the status and trend of indicators across reporting areas that could include grazing allotments, watersheds, or entire field offices or districts. A total of 122 plots were visited and sampled in the NCD between May 22 and September 11, 2017.

At each plot, three 25-m transects were established radiating out from the plot's center to form a 'spoke' plot design, oriented at magnetic 0°, 120°, and 240°, respectively (Herrick et al., 2017; Fig. 2). The transects lines started 5 meters away from the plot center where equipment was stored and a soil pit dug to determine ecological site.

Along each transect, fractional cover was estimated using the line-point intercept method (LPI; Herrick et al., 2017). Every 0.5 m along the transect, an observer dropped a 1-mm-diameter metal pin to the ground without directing its landing location. Vegetation intercepted by the pin was recorded to species. The 'top-hit' (i.e., foliar cover) was recorded along with any lower vegetation touched by the pin. Ground surface was recorded for each pin drop as bare soil, rock, litter, or biological crust regardless of whether vegetation was also encountered. Each transect had 50 observations, and transects were aggregated to form a plot sampling unit with a total of 150 observations. To facilitate comparison with imagery fractional cover, we used just the 'top-hit' vegetation to calculate foliar cover. Cover (as a proportion) is calculated by dividing the number of observations of a given cover class by the total number of observations.

Vegetation heights were measured along the LPI transects at 2.5 m intervals (30 total measurements per plot). The height and species of the tallest herbaceous and woody vegetation within a 15 cm cylinder tangent to the transect was recorded to the nearest cm (Herrick et al., 2017). This included any dead or dormant plant. For the purposes of this study, only woody vegetation heights were compared with drone imagery.

Measures of inter-canopy gaps can help estimate magnitude of wind erosion and parameterize erosion prediction models (Okin, 2008; Webb et al., 2014). Inter-canopy gaps were measured along the three transects following Herrick et al. (2017). Field crews recorded the distances (in cm) between vegetation canopies (i.e., gaps) with only gaps > 25 cm being recorded. The canopy gap indicator was reported as the percentage of the total transect length for gap sizes of 25-50 cm, 51-100 cm, 101-200 cm, and > 200 cm as recommended by Herrick et al. (2017).

Developing a Unified Workflow for Multiple Indicators

Studies describing the use of drone-collected imagery to estimate fractional cover and vegetation heights are summarized in Fig. 3. While these studies present varied methods, collectively they represent the myriad choices for turning drone-collected imagery into quantitative estimates of ecosystem indicators. Breaking down each paper's workflow into its component parts helped to reveal the popularity of choices for each decision and identify gaps in research (i.e., viable choices that have not been tested). This literature review served as a starting point for designing a workflow tailored to the NCD study area. In addition, we documented (in graphical form) the step-by-step instructions to produce each of the indicators (Fig. 4). Taken together, the literature review and step-by-step workflow empower other researchers or land managers to understand and reproduce this workflow. It may also serve as a template to design a workflow tailored to their environment.

UAV Image Acquisition

UAV imagery was acquired at 16 AIM plots in NCD between June 16 and July 1, 2017 (Fig. 1; supplemental Table S1). At 12 of the plots, we collected the imagery 2-5 days after the field crews had collected their data. For the remaining four plots, we embedded with the field crew and acquired the imagery immediately before the field measurements. Accessing all of the plot locations required off-trail hiking across rugged terrain with the drones and associated equipment carried in backpacks. We chose the plots to cover a range of ecological sites and vegetation communities in coordination with the field crew's monitoring schedule. Drones were operated under a Part 107 sUAS license with a special use permit to conduct air operations over BLM land.

We acquired aerial imagery with Phantom 3 Professional and Phantom 4 quad-rotor drones (https://www.dji.com). Both drones have nearly identical 12 megapixel integrated RGB sensors (Table 1). We also employed a Parrot Sequoia sensor (https://www.parrot.com), which we

mounted on the Phantom 3. The Sequoia is a very small multi-spectral sensor with green, red, red-edge, and near-infrared (NIR) bands (Table 1). With its own external power supply, GNSS, and sensor-triggering capabilities, the Sequoia operated independently from the drone.

Autonomous grid pattern missions were programmed in Altizure v 3.0 (https://next.altizure.com). We flew one mission to collect nadir (vertical) imagery and four missions to collect 25°-30° oblique images because prior research has shown that the incorporation of oblique images into photogrammetry can improve scene geometry (James and Robson, 2014). We collected imagery 40 m above ground level (AGL) at each plot, yielding GSD of 1.5 cm for the Phantom imagery and 3.7 cm for the Sequoia imagery (Table 1). This resolution was chosen because it was determined resolute enough to detect the presence of bunch grasses while limiting excessive processing time typical of finer-scale data (see Gillan et al. *In Press*). Sequoia imagery was collected on only seven plots due to a manufacturer defect that caused the sensor to overheat (see Fig. 1 for plot locations and supplemental Table S1 for plot details). At each plot area we collected between 210 and 280 images per sensor. Radiometric calibration of the drone-collected images was deemed unnecessary because all classification, analysis, and interpretation was conducted within individual plots using images that were collected during a single drone flight.

Though the Phantom drones and Sequoia sensor record geographic coordinates of each acquired image with its onboard global navigation satellite system (GNSS), it is typically accurate to only a few meters, which is too coarse for our desired image products. Because we visited these remote plots only one time, it was not practical to install and survey ground control points (GCPs) to reference the scenes. To overcome this limitation, we placed a single 8 m long scale-bar in the center of each plot instead of surveying GCPs (sensu Carbonneau and Dietrich, 2016). The scale-bar consisted of two 'iron cross' targets on the ends of an 8 m collapsible rod. Informing the photogrammetry software of an object of known length (i.e., scale-bar) ensures correct horizontal

and vertical dimensions within the image products, enabling accurate estimates of fractional

cover and vegetation heights. Using this approach, however, the image products may be

systematically shifted both horizontally and vertically compared to their true location (i.e.,

georeferencing error).

Photogrammetry & Image Product Creation

We used structure-from-motion photogrammetry (SfM) software Agisoft Photoscan v. 1.3.5

(www.agisoft.com) to make point clouds and orthomosaics of each plot and sensor separately.

The general SfM process of making point clouds is well-documented (Eltner et al., 2015; Smith et

al., 2015; Snavely et al., 2008; Westoby et al., 2012) so it will be abbreviated here. The Photoscan

workflow follows the same method presented in Gillan et al. *In Press*, except the use of scale-bar

referencing. We generated point clouds with densities between 1,000-3,000 points$\cdot$m^{-2}.

Orthomosaic spatial resolutions were 1.5 cm for Phantom imagery (Fig. 2A) and 3.7 cm for

Sequoia imagery (Fig. 2B).

UAV Imagery Indicator Generation

The following section describes the workflow used to extract indicator values from drone-based

imagery products. Throughout the workflow (Fig. 4), we prioritized simple and easy to

implement methods to facilitate adoption by future users.

Classifying Fractional Cover

Orthomosaics were clipped to a consistent extent around each plot to remove photogrammetric

artifacts at the edges (i.e., stretching and blurring). Prior to classification, we simplified the

images through segmentation (i.e., grouping similar contiguous pixel together into objects;

Burnett and Blaschke, 2003). With very high spatial resolution, classification on segments (or

objects) have been shown to be more accurate than pixel-based classifications that suffer from

'salt & pepper' heterogeneity within features such as shrub canopies (Laliberte et al., 2011a). Segmentation also facilitates the use of non-color traits such as texture, size, and shape to distinguish classes, while pixel-based classifications can generally only use spectra (Navulur, 2007). Additionally, objects can be more ecologically meaningful such as representing individual plants (Laliberte et al., 2010). Using the 'segment mean shift' tool in ArcGIS 10.5 (https://www.esri.com), we attempted to group pixels into real features on the landscape (e.g., one segment for one shrub). This was quite difficult to achieve so most objects such as shrubs or large rocks often contained multiple segments.

The spectral features we used to classify the Phantom imagery were (Fig. 5): blue mean & standard deviation (SD), green mean and SD, red mean and SD, and green leaf algorithm (GLA; Louhaichi et al., 2001) mean and SD. Additionally, we used the following spatial features for classification of image segments: segment pixel count, rectangularity, and compactness. For rectangularity, values range from 0 to 1, with 1 being a rectangle. Compactness is the degree to which a segment is circular with values ranging from 0 to 1, where 1 is a circle. For Sequoia imagery, we included the red-edge and NIR bands and used normalized difference vegetation index (NDVI) instead of the green leaf algorithm. We calculated feature values for each segment.

Noticeably absent from the list of features is canopy heights which are frequently used in object-based classifications (Baena et al., 2017; Cruzan et al., 2016). In this workflow, canopy height models were created after vegetation classification and thus could not be used in the classification (details in 'Vegetation Heights' section).

The final classes were annual herb/grass, perennial herb/grass, woody, bare-ground, and shadow in some cases (Fig. 5). The bare-ground class included bare-soil, rock, and lichen. For classification training, we created individual point shapefiles for each class. We placed 50-100

points per class on the segmented orthomosaics where we opportunistically found representative samples. Identifying specific classes was aided by LPI field data and ground photos. Because features (e.g., shrubs) often consisted of multiple segments, we placed multiple training points per shrub to capture the heterogeneity of the classes. At several plots (West Ft. Sage197, Tablelands 440, Shaffer 243, Twin peaks 236, Crest 436, Snowstorm441, and Lower Lake 437), we omitted perennial herb/grass as a class because it either did not occur in the plot or the specimens were too small and indistinguishable to be useful for training.

We used R package c50 (Kuhn and Quinlan 2017) to classify the orthomosaics. The algorithm, which is an R version of SEE5 (www.rulequest.com/see5-info.html), is a machine learning decision tree used to predict discrete classes. We specified adaptive boosting with 20 trials and disabled winnowing. We used 75% of the training samples to train the classifier and withheld 25% for validation (see Supplemental Material for complete R code). C50 outputs confusion matrices and information to assess the importance of predictor features (see Supplemental Table S2 for feature importance and Table S3 for aggregated confusion matrix). We calculated fractional cover as the number of pixels per class as a proportion of total classified pixels (Fig. 2C).

Canopy Gaps

From the classified orthomosaics, we calculated canopy gaps following the general methods presented in Karl et al., (2012b). First, we digitized the three transects using markers (iron-cross targets) located at the ends as a reference. We retained the bare-ground class and removed annual herb/grass, perennial herb/grass, and woody classes. We then converted the bare-ground raster into vector polygons and used the 'intersect' tool in ArcGIS to identify the parts of lines crossing the bare-ground polygons. We calculated the length of each line and created histograms for the proportion of total line length having lengths of 25-50 cm, 51-100 cm, 101-200 cm, and >200 cm.

Vegetation Heights

We calculated vegetation heights using only the Phantom RGB imagery point clouds because the coarser Sequoia imagery would produce less detailed 3D reconstructions. Using the 'classify ground points' tool in Photoscan, We identified points representing the ground. This is a type of maximum local slope filter (Montealegre et al., 2015) where the lowest elevation point within a user defined grid cell is assumed to be the ground. All additional ground points were identified based on a user defined maximum angle and vertical distance from the origin ground point. For each plot we specified a grid cell size of 2 m while the max angle and max distance varied depending on the vegetation structure and imagery scale. We exported the original dense point clouds and the filtered point clouds (only ground points) in log ASCII format (.las) in projection WGS 84 UTM zone 10N (EPSG:32610).

In ArcMap, we converted the original point clouds into digital surface models (DSMs) with a 5 cm cell size by assigning the cell value as the highest elevation point and using natural neighbor interpolation to estimate values for cells with no points. Digital terrain models (DTMs) were created in a similar fashion with ground-only point clouds. The cell values were assigned the average value of the points with natural neighbor interpolation used for cells with no points. Using 'raster calculator', we subtracted the DTM from the DSM on a cell-by-cell basis to create a canopy height model (CHM). Due to the mechanics of interpolation, there is likely to be many small and near zero heights in the CHM that do not represent actual vegetation heights. Through exploration, we chose a threshold and removed from the CHM any values < 4 cm. In some plots, boulders were not filtered out of the point clouds because their slope resembled that of shrubs. To remove boulders from vegetation height data, we identified and deleted any height measurements that were not identified as vegetation (from the classified maps). Though this study specifically looked at woody vegetation heights, we chose not to filter herbaceous vegetation out of the CHM.

The spatial resolution of the drone imagery was generally too coarse to detect herbaceous

vegetation heights (Gillan et al. *In Press*), especially for species such as cheatgrass (*Bromus*

tectorum) and squirreltail (*Elymus elymoides*) with low-stature growth forms. Analysis of the

CHMs showed very little if any registered heights concurrent with the presence of herbaceous

vegetation. We retained all vegetation heights so to not omit any plants that were misclassified.

Finally, we used the 'aggregate' tool to compute the highest height value within a 30 x 30 cm grid

cell on the CHMs (Fig. 2D). We did this step to more closely match the field method of finding

the highest part of the plant within a 15 cm radius of the rod.

Comparison between Field and Imagery Indicators

We assessed agreement between field and imagery indicator values using the plot as the sample

unit. Imagery indicator values for fractional cover and vegetation heights were calculated within

rectangular polygons along each field transects' location approximately 0.33 m wide to contain

spatial co-registration errors with field measurements. Canopy gap values were estimated along

the three transects. For each indicator (fractional cover, canopy gaps, vegetation heights), we

assessed method agreement by comparing the mean values (with 95% confidence intervals)

across all 16 plots. Mean differences, (which include signed differences), were useful for showing

bias toward overestimate or underestimate indicator values, while absolute mean differences

(which eliminate signed differences) were computed to show true departure between methods.

Additionally, we performed least-squares regression and calculated coefficients of determination

(R^2 values) to describe linear relationships between methods. For vegetation heights, we

additionally compared maximum and standard deviation and the proportion of observations

within eight histogram bins. On a subset of plots (n=7), we compared fractional cover agreement

between Phantom and Sequoia multi-spectral imagery. Due to the relatively small sample sizes,

we did not separate analysis by ecological site which is typically done for I & M data

interpretation (see Karl and Herrick, 2010).

Results

Method Agreement - Fractional Cover

The woody vegetation cover class showed the strongest linear relationship between field and image measurements (R^2=0.82; Fig. 6), followed by annual herb/grass (R^2=0.79), bare-ground (R^2=0.69), and perennial herb/grass (R^2=0.24). Mean fractional cover across all plots was similar between field and imagery estimates for each of the four classes (Table 2). Mean method differences ranged from as small as -0.009 (perennial herb) to as large as -0.062 (bare-ground). Bare-ground had the largest absolute mean difference (0.145), followed closely by annual herb/grass (0.134). Perennial herb/grass and woody had absolute mean differences of 0.052 and 0.047, respectively. Indicator value variation between plots was higher (i.e., larger standard errors) for imagery compared with field methods for each of the cover classes.

Fractional Cover Sensor Comparison

We found minimal differences in linear relationships between the Phantom RGB camera and Sequoia multi-spectral sensor in terms of fractional cover agreement with field measurements (Fig. 7). Similarly, average fractional cover and cover differences with field methods were < 3% different for each cover class (Table 3).

Method Agreement - Canopy Gaps

Proportion of inter-canopy gaps were generally underestimated for each size class (Fig. 8A; Table 4). The greatest relative underestimations (proportional to the mean value) occurred at small gaps sizes (e.g., 25-50 cm), and steadily shrank as gap sizes increased. Variance (illustrated with confidence intervals) between field and imagery estimates were very similar. Linear relationships between field and imagery improved as the size of the gaps increased (Fig. 8B).

Method Agreement - Vegetation Heights

Imagery methods underestimated mean vegetation heights by 18 cm on average and underestimated maximum vegetation heights on average by 8 cm (Fig. 9A). Regarding the proportion of height observations within histogram bins, nearly 50% of imagery observations were within the 4-14 cm bin, while field methods had only 14% of observations within that range (Fig. 9B). Conversely, there was a much higher proportion of field observations within the height bins from 35-54 cm (29% v. 11%), 55-74 cm (8% v. 3%), and 75-94 cm (13% v. 0%). The linear relationship of mean heights was weak ($R^2=0.12$), mostly due to one plot with a dead woody plant that was too thin to be detected with imagery (Fig. 9C). Removing this one plot from analysis improved the linear relationship to $R^2=0.46$. Height standard deviation had $R^2=0.47$ (Fig. 9D) and maximum height had $R^2=0.34$ (Fig. 9E). Mean and maximum vegetation height were overpredicted (compared to field measures) at some plots because tall woody plants were not encountered with the field methods.

Discussion
Fractional Cover

Because imagery and field methods of observing vegetation cover have inherent mechanical differences (i.e., pin drops v. classified pixels) and possible co-registration error, perfect agreement between indicator values is not expected. Image-based measures should be, however, strongly related to field measures to be seen as a reliable tool worth adopting for rangeland monitoring. Though we found strong relationships between imagery and field estimates of fractional cover, some classes could be improved with small workflow adjustments detailed in the following two paragraphs.

It was difficult to find useable training specimens for perennial herb/grass at the imagery scales (1.5 cm for Phantom and 3.7 cm for Sequoia) because candidate samples were often too small and

indistinguishable from adjacent pixels. This often led to omitting the class or poor results (e.g., under- or over-prediction). The imagery resolution was generally too coarse to identify and classify perennial bunchgrasses found in this study area. We would recommend imagery ≤ 1 cm GSD to identify individual bunchgrasses and other herbaceous plants as demonstrated in other projects (Cunliffe et al., 2016; Fraser et al., 2016; Gillan et al., *In Press*). Even at this fine resolution, however, separating herbaceous species from each other will be challenging (Gearhart et al., 2013; Laliberte et al., 2010b; Lu and He, 2017).

Though the annual herb/grass and bare-ground classes had strong linear relationships with field methods, they had the highest mean absolute differences. The classifications often confused annual herb/grass (mostly cheatgrass) and bare-ground, a significant problem given the concern of cheatgrass expansion in the district. Confusion was primarily caused by cheatgrass that had senesced to a yellow/brown color making it difficult to separate from bare-ground. Separation may have been better in the spring while the cheatgrass was still green and easily distinguished from bare-ground. Imagery collected in the spring, however, may not capture other annuals such as prickly lettuce (*Lactuca serriola*) or perennials such as bottlebrush squirrel tail (*Elymus elymoides*).

Vegetation phenology is critical to identify species or functional groups within imagery, more so than identifying the same features with field methods (Hunt et al., 2003; Lass and Calihan, 1997). As with any image classification, distinguishing features of interest is highly dependent on the spectral and spatial uniqueness of the classes (Laliberte and Rango, 2011). Integrating drone imagery will require a re-thinking of when monitoring occurs to maximize feature detectability. Depending on the goal of the inventory and monitoring, multiple acquisitions may be required in a year.

We found little difference in fractional cover agreement between the Phantom RGB camera and the Parrot Sequoia multi-spectral sensor. Other research has demonstrated the ability of RGB imagery to successfully classify cover (Cruzan et al., 2016; Laliberte et al., 2010a; Meng et al., 2018). In addition to lower cost, RGB sensors generally offer higher spatial resolution compared with multi-spectral sensors, an advantage for identifying small plants and generating detailed point clouds. In theory, multi-spectral sensors offer additional bandwidth from which to separate species based on spectral differences (Laliberte et al., 2011a), though we found no discernible advantage in this study. Additionally, multi-spectral sensors can also be radiometrically calibrated to reflectance values which could improve consistency of repeat image classifications and aid the development of spectral libraries. Other sensors including LiDAR and hyperspectral have been demonstrated on drones to characterize dryland vegetation cover and structure (Mitchell et al., 2012; T. T. Sankey et al., 2017b). Their data may help to distinguish more cover classes than RGB and multi-spectral. However, the additional cost and technical challenges of these sensors may make them less desirable for mass adoption and reducing monitoring costs.

Fine-tuning spatial resolution and season of acquisition with an ideal sensor would give the best chance of accurately estimating fractional cover. However, perfecting the ability to algorithmically estimate fractional cover has its limits. For example, some plants may not be classified well due to inconsistent color, shape, or 'look' to them. In these cases, humans may be better than any algorithm at looking at images to identify objects. Humans can use knowledge of the plant's physical characteristics and the context of an entire image to identify classes in ways that algorithms cannot. Photo interpretation is an inexpensive and simple alternative to classification algorithms that can produce strong agreement with field estimate of fractional cover (Booth and Cox, 2009, 2008; Breckenridge et al., 2011; Duniway et al., 2012; Hardin et al., 2007; Karl et al., 2014; Moffet, 2009; Seefeldt and Booth, 2006). This technique, though, can be labor

intensive over large areas and does not produce a map from which to estimate other indicators such as canopy gaps.

Canopy Gaps

Similar to our findings, Karl et al. (2012b) found that correlations between imagery and field estimates improved as the gap sizes increased, and gaps > 50 cm were reliably estimated from imagery in a variety of plant communities. In this research, consistent underestimation of canopy gaps at each size class had two main causes. The first was misclassifying bare-ground as annual herb/grass. The second (and less frequent) cause was scale (specifically grain) differences between field and imagery observations. The imagery, and subsequent grouping of pixels into objects, could not see small diameter branches or sparse vegetation the field observer could see. Take, for example, a group of shrubs close to each other. The imagery classification may perceive no gaps between the shrubs, while the field observer may observe that there are in fact gaps of at least 25 cm between the branch canopies.

Canopy gaps are an example of an indicator that has the potential to be improved instead of simply replicated by drone imagery. Field-based measures of canopy gaps are a 1-dimensional representation of erosional force connectivity that is typically integrated over multiple directions in the plot to provide a composite value (Webb et al., 2014). Drone imagery could open up more meaningful 2-D or 3-D measurements of the same phenomenon. For example, with drone-based classifications, the size and configuration of bare ground patches parallel to the slope (indicator of water erosion potential) could be separated from the effects of bare ground patches in line with prevailing winds (indicator of wind erosion potential). Similarly, Ludwig et al., (2007) used two-dimensional information on bare ground distribution to create an index related to a site's ability to retain resources (i.e., a 'leakiness' index).

Vegetation Heights

The differences between imagery and field estimates of woody vegetation heights were caused primarily by the mechanics of each method. For mean height, the field method averaged 30 measurements of the tallest part of the plant that was encountered within a 15 cm radius of a rod placement. Most of these observations were high up on the plant. The point cloud/CHM methods observed all aspects of the plant, from the crown to the base. Naturally, numerous observations on the lower part of the plant brought down the average. The maximum vegetation height in a plot was generally underestimated by the imagery due to poorly modeling plant extremities that were too fine or small to detect. This is a well-known trait of photogrammetric reconstruction methods (Cunliffe et al., 2016; Gillan et al., 2014; Olsoy et al., 2018), but is not necessarily a limitation in a rangeland monitoring context. Maximum vegetation heights is a convenient trait to measure in the field, but does hold any specific ecological value. Drone-based photogrammetric point clouds can provide thousands of measurements, enabling more detailed and synoptic look at vegetation heights, including the ability to quantify observations per height bin, analyze height variance, and calculate vegetation volume. This technique will improve our ability to estimate biomass and carbon storage (Cunliffe et al., 2016), parameterize surface roughness for wind erosion modeling (Webb et al., 2014), quantify fuels for prescribed or uncontrolled fires (Leis and Morrison, 2011), and assess the quality of wildlife habitat (Olsoy et al., 2018). In NCD, for example, greater sage-grouse habitat could be assessed with drone-based vegetation structure data, including the height, cover, and shape of sagebrush (Stiver et al., 2015).

Multi-Indicator Workflow

To efficiently meet the data needs of many I & M applications, be it a single complex issue or a holistic assessment of rangeland health for a grazing permit renewal, we should strive to estimate multiple indicators from a single drone data collection (see Karl et al., 2017). Collecting data for wind erosion modeling, for example, will benefit from the efficient workflow to estimate

fractional cover, vegetation heights, and canopy gap distribution, each of which are important factors in wind erosion potential (Webb et al., 2016).

To achieve even greater efficiency, the majority of the workflow presented in this paper could be programmatically automated. By adopting real-time kinematic GNSS and eliminating the use of GCPs or scale-bars (Turner et al., 2014), we could presumably automate the photogrammetry stage of creating point clouds and orthomosaics. The workflow to estimate vegetation heights is fully automatable, though the point filtering stage (e.g., maximum local slope) would require parameter customization matched to vegetation composition. For the fractional cover and canopy gap workflow, training the imagery (i.e., identifying training samples) to detect functional groups or species is likely to require a human touch.

The AIM core field methods have been standardized to facilitate data comparison across time, space, and observer (MacKinnon et al., 2011; Toevs et al., 2011). Methods to estimate rangeland indicators from drone-based imagery, however, are more complex and require more decisions compared with their counterpart field methods. Because best practices for producing a suite of indicators is likely to vary by vegetation composition and phenology, it seems unlikely and perhaps unproductive to pursue a standard set of protocols as have been developed for field methods (e.g., AIM core indicators). Instead, we should seek workflow recommendations and best practices for given ecosystems through crowdsourcing. This has been underway since published papers began reporting their methods, but could be accelerated with an online workflow repository. Given the high interest in this technology, a website like this could spur collaboration and advancement in ways that published literature alone cannot

Documenting workflow decisions could be a useful resource for practitioners to learn the basic decisions necessary to estimate indicators, identify research gaps, and find workflow

combinations to suit particular ecosystems. A few existing protocol repositories include Protocols

Exchange (https://www.nature.com/protocolexchange) and Protocols.IO (http://protocols.io).

Cunliffe and Anderson (2019), for example, published a protocol to collect drone imagery for

biomass estimation in Protocols Exchange (doi:10.1038/protex.2018.134). Alternatively, it could

advantageous to share workflows through a website dedicated to rangeland I & M (e.g., The

Landscape Toolbox, www.landscapetoolbox.com), where drone-based monitoring could be

embedded within the larger context of rangeland data collection theory and field protocols.

Because workflows are likely to vary by geography (region, precipitation, elevation), geotagging

workflow study areas and making them discoverable in a map-based environment could help

users find appropriate methods for their area of interest (see Karl et al., 2013).

Conclusion

Due to their low cost, ability to image dozens to hundreds of hectares, and extreme portability,

small UAVs are likely to become a standard tool for rangeland inventory and monitoring. They

will be integrated with existing field efforts in order to observe larger portions of the landscape

and to measure indicators not easily measured on the ground. Developing a suite of monitoring

methods that are useful for supporting management decisions (e.g., accurate, repeatable, and cost-

effective) will require additional exploration to develop best practices for image acquisition and

workflow specifications that can efficiently estimate multiple indicators. We demonstrated a

workflow to estimate three rangeland vegetation indicators, reported agreement with their

counterpart field method, and provided recommendations for workflow improvements. These

methods could serve as a starting point for rangeland I & M data collection in other sagebrush

steppe ecosystems. However, the workflow presented in the paper is just one of many possible

paths to estimate these indicator values. Additionally, the array of choices of hardware, software,

image acquisition and processing specifications is large and growing. The effort to find the 'best'

workflows given their vegetation composition and phenology characteristics could be accelerated through an online space dedicated to the topic.

Acknowledgements

References

Allen, C.R., Angeler, D.G., Fontaine, J.J., Garmestani, A.S., Hart, N.M., Pope, K.L., Twidwell, D., 2017. Adaptive Management of Rangeland Systems, in: Rangeland Systems: Processes, Management and Challenges. pp. 373–394.

Baena, S., Moat, J., Whaley, O., Boyd, D.S., 2017. Identifying species from the air: UAVs and the very high resolution challenge for plant conservation. PLoS One 12, e0188714. https://doi.org/10.1371/journal.pone.0188714

Bendig, J., Bolten, A., Bennertz, S., Broscheit, J., Eichfuss, S., Bareth, G., 2014. Estimating biomass of barley using crop surface models (CSMs) derived from UAV-based RGB imaging. Remote Sens. 6, 10395–10412. https://doi.org/10.3390/rs61110395

Bland, L.M., Regan, T.J., Dinh, M.N., Ferrari, R., Keith, D.A., Lester, R., Mouillot, D., Murray, N.J., Nguyen, H.A., Nicholson, E., 2017. Using multiple lines of evidence to assess the risk of ecosystem collapse. Proc. R. Soc. B Biol. Sci. 284, 20170660. https://doi.org/10.1098/rspb.2017.0660

Booth, D., Cox, S., 2011. Art to science: Tools for greater objectivity in resource monitoring. Rangelands 33, 27–34. https://doi.org/10.2111/1551-501x-33.4.27

Booth, D.T., Cox, S.E., 2009. Dual-camera, high-resolution aerial assessment of pipeline revegetation.

Environ. Monit. Assess. 158, 23–33. https://doi.org/10.1007/s10661-008-0562-5

Booth, D.T., Cox, S.E., 2008. Image-based monitoring to measure ecological change in rangeland. Front. Ecol. Environ. 6, 185–190. https://doi.org/10.1890/070095

Breckenridge, R.P., Dakins, M., Bunting, S., Harbour, J.L., White, S., 2011. Comparison of Unmanned Aerial Vehicle Platforms for Assessing Vegetation Cover in Sagebrush Steppe Ecosystems. Rangel. Ecol. Manag. 64, 521–532. https://doi.org/10.2111/REM-D-10-00030.1

Burnett, C., Blaschke, T., 2003. A multi-scale segmentation/object relationship modelling methodology for landscape analysis. Ecol. Modell. 168, 233–249. https://doi.org/10.1016/S0304-3800(03)00139-X

Carbonneau, P.E., Dietrich, J.T., 2016. Cost-effective non-metric photogrammetry from consumer-grade sUAS: implications for direct georeferencing of structure from motion photogrammetry. Earth Surf. Process. Landforms 42, 473–486. https://doi.org/10.1002/esp.4012

Cruzan, M.B., Weinstein, B.G., Grasty, M.R., Kohrn, B.F., Hendrickson, E.C., Arredondo, T.M., Thompson, P.G., 2016. Small Unmanned Aerial Vehicles (Micro-Uavs, Drones) in Plant Ecology. Appl. Plant Sci. 4, 1600041. https://doi.org/10.3732/apps.1600041

Cunliffe, A.M., Brazier, R.E., Anderson, K., 2016. Ultra-fine grain landscape-scale quantification of dryland vegetation structure with drone-acquired structure-from-motion photogrammetry. Remote Sens. Environ. 183, 129–143. https://doi.org/10.1016/j.rse.2016.05.019

Duniway, M.C., Karl, J.W., Schrader, S., Baquera, N., Herrick, J.E., 2012. Rangeland and pasture monitoring: an approach to interpretation of high-resolution imagery focused on observer calibration for repeatability. Environ. Monit. Assess. 184, 3789–804. https://doi.org/10.1007/s10661-011-2224-2

Eltner, A., Kaiser, A., Castillo, C., Rock, G., Neugirg, F., Abellan, A., 2015. Image-based surface reconstruction in geomorphometry – merits, limits and developments of a promising tool for geoscientists. Earth Surf. Dyn. Discuss. 3, 1445–1508. https://doi.org/10.5194/esurfd-3-1445-2015

Elzinga, C.L., Salzer, W., Willoughby, J.W., 1998. Measuring and Monitoring Plant Populations. U.S. Department of the Interior, Bureau of Land Management, Denver, CO.

Fraser, R.H., Olthof, I., Lantz, T.C., Schmitt, C., 2016. UAV Photogrammetry for Mapping Vegetation in the Low-Arctic. Arct. Sci. 102, 1–51. https://doi.org/10.1139/as-2016-0008

Gearhart, A., Booth, D.T., Sedivec, K., Schauer, C., 2013. Use of Kendall's coefficient of concordance to

assess agreement among observers of very high resolution imagery. Geocarto Int. 28, 517–526. https://doi.org/10.1080/10106049.2012.725775

Gillan, J.K., Karl, J.W., Duniway, M., Elaksher, A., 2014. Modeling vegetation heights from high resolution stereo aerial photography: an application for broad-scale rangeland monitoring. J. Environ. Manage. 144, 226–35. https://doi.org/10.1016/j.jenvman.2014.05.028

Gillan, J.K., McClaran, M.P., Swetnam, T.L., Heilman, P., In Press. Estimating forage utilization with drone-based photogrammetric point clouds. Rangel. Ecol. Manag. https://doi.org/10.1016/j.rama.2019.02.009

Hardin, P., Jackson, M., Anderson, V., Johnson, R., 2007. Detecting Squarrose Knapweed (Centaurea virgata Lam. Ssp. squarrosa Gugl.) Using a Remotely Piloted Vehicle: A Utah Case Study. GIScience Remote Sens. 44, 203–219. https://doi.org/10.2747/1548-1603.44.3.203

Herrick, J.E., Zee, J.W. Van, McCord, S.E., Courtright, E.M., Karl, J.W., Burkett, L.M., 2017. Monitoring Manual for Grassland, Shrubland, and savanna ecosystems 2nd Edition. Volume 1: Core Methods.

Hunt, E.R., Everitt, J.H., Ritchie, J.C., Moran, M.S., Booth, D.T., Anderson, G.L., Clark, P.E., Seyfried, M.S., 2003. Applications and Research Using Remote Sensing for Rangeland Management. Photogramm. Eng. Remote Sens. 69, 675–693. https://doi.org/10.14358/PERS.69.6.675

James, M.R., Robson, S., 2014. Mitigating systematic error in topographic models derived from UAV and ground-based image networks. Earth Surf. Process. Landforms 39, 1413–1420. https://doi.org/10.1002/esp.3609

Jensen, J.L.R., Mathews, A.J., 2016. Assessment of Image-Based Point Cloud Products to Generate a Bare Earth Surface and Estimate Canopy Heights in a Woodland Ecosystem. Remote Sens. 8. https://doi.org/10.3390/rs8010050

Johansen, K., Raharjo, T., Mccabe, M.F., 2018. Using Multi-Spectral UAV Imagery to Extract Tree Crop Structural Properties and Assess Pruning Effects 1–22. https://doi.org/10.20944/preprints201804.0198.v1

Karl, J.W., Duniway, M.C., Schrader, T.S., 2012. A Technique for Estimating Rangeland Canopy-Gap Size Distributions From High-Resolution Digital Imagery. Rangel. Ecol. Manag. 65, 196–207. https://doi.org/10.2111/REM-D-11-00006.1

Karl, J.W., Gillan, J.K., Barger, N.N., Herrick, J.E., Duniway, M.C., 2014. Interpretation of high-resolution imagery for detecting vegetation cover composition change after fuels reduction treatments in woodlands. Ecol. Indic. 45, 570–578. https://doi.org/10.1016/j.ecolind.2014.05.017

Karl, J.W., Gillan, J.K., Herrick, J.E., 2013. Geographic searching for ecological studies: a new frontier. Trends Ecol. Evol. 28, 383–4. https://doi.org/10.1016/j.tree.2013.05.001

Karl, J.W., Herrick, J.E., 2010. Monitoring and Assessment Based on Ecological Sites. Rangelands 32, 60–64. https://doi.org/10.2111/RANGELANDS-D-10-00082.1

Karl, J.W., Herrick, J.E., Pyke, D.A., 2017. Monitoring Protocols: Options, Approaches, Implementation, Benefits, in: Briske, D. (Ed.), Rangeland Systems: Processes, Management and Challenges. Springer, p. 664.

Kendall, W.L., Moore, C.T., 2012. Maximizing the utility of monitoring to the adaptive management of natural resources, in: Gitzen, R.A., Milspaugh, J.J., Cooper, A.B., Licht, D.S. (Eds.), Design and Analysis of Long-Term Ecological Monitoring Studies. University of Cambridge Press.

Laliberte, A.S., Browning, D.M., Herrick, J.E., Gronemeyer, P., 2010. Hierarchical object-based classification of ultra-high-resolution digital mapping camera (DMC) imagery for rangeland mapping and assessment. J. Spat. Sci. 55, 101–115. https://doi.org/10.1080/14498596.2010.487853

Laliberte, A.S., Goforth, M. a., Steele, C.M., Rango, A., 2011a. Multispectral Remote Sensing from Unmanned Aircraft: Image Processing Workflows and Applications for Rangeland Environments. Remote Sens. 3, 2529–2551. https://doi.org/10.3390/rs3112529

Laliberte, A.S., Herrick, J.E., Rango, A., Winters, C., 2010. Acquisition, Orthorectification, and Object-based Classification of Unmanned Aerial Vehicle (UAV) Imagery for Rangeland Monitoring. Photogramm. Eng. Remote Sens. 76, 661–672. https://doi.org/10.14358/PERS.76.6.661

Laliberte, A.S., Rango, A., 2011. Image Processing and Classification Procedures for Analysis of Sub-decimeter Imagery Acquired with an Unmanned Aircraft over Arid Rangelands. GIScience Remote Sens. 48, 4–23. https://doi.org/10.2747/1548-1603.48.1.4

Laliberte, A.S., Winters, C., Rango, A., 2011b. UAS remote sensing missions for rangeland applications. Geocarto Int. 26, 141–156. https://doi.org/10.1080/10106049.2010.534557

Lass, L.W., Calihan, R.H., 1997. Effects of Phenological Stage on Detectability of Yellow Hawkweed

(Hieracium Pratense) and Oxeye Daisy (Chrysanthemum Leucanthemum) with Remote Multispectral Digital Imagery. Weed Technol. 11, 248–256.

Leis, S. a., Morrison, L.W., 2011. Field Test of Digital Photography Biomass Estimation Technique in Tallgrass Prairie. Rangel. Ecol. Manag. 64, 99–103. https://doi.org/10.2111/REM-D-09-00180.1

Li, W., Niu, Z., Chen, H., Li, D., Wu, M., Zhao, W., 2016. Remote estimation of canopy height and aboveground biomass of maize using high-resolution stereo images from a low-cost unmanned aerial vehicle system. Ecol. Indic. 67, 637–648. https://doi.org/10.1016/j.ecolind.2016.03.036

Louhaichi, M., Borman, M.M., Johnson, D.E., 2001. Spatially Located Platform and Aerial Photography for Documentation of Grazing Impacts on Wheat. Geocarto Int. 16, 65–70. https://doi.org/10.1080/10106040108542184

Lu, B., He, Y., 2017. Species classification using Unmanned Aerial Vehicle (UAV)-acquired high spatial resolution imagery in a heterogeneous grassland. ISPRS J. Photogramm. Remote Sens. 128, 73–85. https://doi.org/10.1016/j.isprsjprs.2017.03.011

Ludwig, J.A., Bastin, G.N., Chewings, V.H., Eager, R.W., Liedloff, A.C., 2007. Leakiness: A new index for monitoring the health of arid and semiarid landscapes using remotely sensed vegetation cover and elevation data. Ecol. Indic. 7, 442–454. https://doi.org/10.1016/j.ecolind.2006.05.001

MacKinnon, W.C., Karl, J.W., Toevs, G.R., Taylor, J.J., Karl, M., Spurrier, C.S., Herrick, J.E., 2011. BLM core terrestrial indicators and methods. Tech Note 440.

McGwire, K.C., Weltz, M.A., Finzel, J.A., Morris, C.E., Fenstermaker, L.F., McGraw, D.S., 2013. Multiscale assessment of green leaf cover in a semi-arid rangeland with a small unmanned aerial vehicle. Int. J. Remote Sens. 34, 1615–1632. https://doi.org/10.1080/01431161.2012.723836

Meng, B., Gao, J., Liang, T., Cui, X., Ge, J., Yin, J., Feng, Q., Xie, H., 2018. Modeling of Alpine Grassland Cover Based on Unmanned Aerial Vehicle Technology and Multi-Factor Methods: A Case Study in the East of Tibetan Plateau, China. Remote Sens. 10, 320. https://doi.org/10.3390/rs10020320

Michalak, J.L., Withey, J.C., Lawler, J.J., Case, M.J., 2017. Future climate vulnerability - evaluating multiple lines of evidence. Front. Ecol. Environ. 15, 367–376. https://doi.org/10.1002/fee.1516

Mitchell, J.E., 2010. Criteria and Indicators of Sustainable Rangeland Management. University of Wyoming Cooperative Extension Publication No. SM-56.

Mitchell, J.J., Glenn, N.F., Anderson, M.O., Hruska, R.C., Charlie, A.H., 2012. Unmanned Aerial Vehicle ({UAV}) Hyperspectral Remote Sensing for Dryland Vegetation Monitoring Hyperspectral Image and Signal Sensing. Idaho Natl. Lab. Prepr.

Moffet, C. a., 2009. Agreement Between Measurements of Shrub Cover Using Ground-Based Methods and Very Large Scale Aerial Imagery. Rangel. Ecol. Manag. 62, 268–277. https://doi.org/10.2111/08-244R.1

Montealegre, A.L., Lamelas, M.T., De La Riva, J., 2015. A Comparison of Open - Source LiDAR Filtering Algorithms in a Mediterranean Forest Environment. IEEE J. Sel. Top. Appl. Earth Obs. Remote Sens. 8, 4072–4085. https://doi.org/10.1109/JSTARS.2015.2436974

Navulur, K., 2007. Multi-spectral image analysis using the object-oriented paradigm. CRC Press, Taylor and Francis Group, Boca Raton, FL.

Okin, G.S., 2008. A new model of wind erosion in the presence of vegetation. J. Geophys. Res. 113, F02S10. https://doi.org/10.1029/2007JF000758

Olsoy, P.J., Shipley, L.A., Rachlow, J.L., Forbey, J.S., Glenn, N.F., Burgess, M.A., Thornton, D.H., 2018. Unmanned aerial systems measure structural habitat features for wildlife across multiple scales. Methods Ecol. Evol. 9, 594–604. https://doi.org/10.1111/2041-210X.12919

Rango, A., Laliberte, A., Herrick, J.E., Winters, C., Havstad, K., Steel, C., Browning, D., 2009. Unmanned aerial vehicle-based remote sensing for rangeland assessment, monitoring, and management. J. Appl. Remote Sens. 3, 033542. https://doi.org/10.1117/1.3216822

Sankey, T., Donager, J., McVay, J., Sankey, J.B., 2017. UAV lidar and hyperspectral fusion for forest monitoring in the southwestern USA. Remote Sens. Environ. 195, 30–43. https://doi.org/10.1016/j.rse.2017.04.007

Sankey, T.T., McVay, J., Swetnam, T.L., McClaran, M.P., Heilman, P., Nichols, M., 2017. UAV hyperspectral and lidar data and their fusion for arid and semi-arid land vegetation monitoring. Remote Sens. Ecol. Conserv. 1–14. https://doi.org/10.1002/RSE2.44

Seefeldt, S.S., Booth, D.T., 2006. Measuring plant cover in sagebrush steppe rangelands: a comparison of methods. Environ. Manage. 37, 703–11. https://doi.org/10.1007/s00267-005-0016-6

Smith, M.W., Carrivick, J.L., Quincey, D.J., 2015. Structure from motion photogrammetry in physical

geography. Prog. Phys. Geogr. 40, 247–275. https://doi.org/10.1177/0309133315615805

Snavely, N., Seitz, S.M., Szeliski, R., 2008. Modeling the world from Internet photo collections. Int. J. Comput. Vis. 80, 189–210. https://doi.org/10.1007/s11263-007-0107-3

Stiver, S.J., Thomas Rinkes, E., Naugle, D.E., 2015. Sage-Grouse Habitat Assessment Framework: A multiscale assessment tool. Technical Reference 6710-1. Denver, CO.

Swetnam, T.L., Gillan, J.K., Sankey, T.T., McClaran, M.P., Nichols, M.H., Heilman, P., McVay, J., 2018. Considerations for Achieving Cross-Platform Point Cloud Data Fusion across Different Dryland Ecosystem Structural States. Front. Plant Sci. 8, 2144. https://doi.org/10.3389/fpls.2017.02144

Taylor, J., Kachergis, E., Toevs, G., Karl, J., Bobo, M., Karl, M. "Sherm," Miller, S., Spurrier, C., 2014. AIM-Monitoring: A component of the BLM Assessment, Inventory, and Monitoring Strategy. Tech Note 445. Denver, CO.

Toevs, G.R., Karl, J.W., Taylor, J.J., Spurrier, C.S., Karl, M.S., Bobo, M.R., Herrick, J.E., 2011. Consistent Indicators and Methods and a Scalable Sample Design to Meet Assessment, Inventory, and Monitoring Information Needs Across Scales. Rangelands 33, 14–20. https://doi.org/10.2111/1551-501X-33.4.14

Tueller, P.T., 1996. Near-earth monitoring of range condition and trend. Geocarto Int. 11, 53–62. https://doi.org/10.1080/10106049609354548

Turner, D., Lucieer, A., Wallace, L., 2014. Direct georeferencing of ultrahigh-resolution UAV imagery. IEEE Trans. Geosci. Remote Sens. 52, 2738–2745. https://doi.org/10.1109/TGRS.2013.2265295

USDI Bureau of Land Management, 2001. H-4180-1 Rangeland Health Standards.

Webb, N.P., Herrick, J.E., Duniway, M.C., 2014. Ecological site-based assessments of wind and water erosion : informing accelerated soil erosion management in rangelands. Ecol. Appl. 24, 1405–1420. https://doi.org/10.1890/13-1175.1

Webb, N.P., Herrick, J.E., Van Zee, J.W., Courtright, E.M., Hugenholtz, C.H., Zobeck, T.M., Okin, G.S., Barchyn, T.E., Billings, B.J., Boyd, R., Clingan, S.D., Cooper, B.F., Duniway, M.C., Derner, J.D., Fox, F.A., Havstad, K.M., Heilman, P., LaPlante, V., Ludwig, N.A., Metz, L.J., Nearing, M.A., Norfleet, M.L., Pierson, F.B., Sanderson, M.A., Sharratt, B.S., Steiner, J.L., Tatarko, J., Tedela, N.H., Toledo, D., Unnasch, R.S., Van Pelt, R.S., Wagner, L., 2016. The National Wind Erosion Research

Network: Building a standardized long-term data resource for aeolian research, modeling and land management. Aeolian Res. 22, 23–36. https://doi.org/10.1016/j.aeolia.2016.05.005

Westoby, M.J., Brasington, J., Glasser, N.F., Hambrey, M.J., Reynolds, J.M., 2012. 'Structure-from-Motion' photogrammetry: A low-cost, effective tool for geoscience applications. Geomorphology 179, 300–314. https://doi.org/10.1016/j.geomorph.2012.08.021

Zarco-Tejada, P.J., Diaz-Varela, R., Angileri, V., Loudjani, P., 2014. Tree height quantification using very high resolution imagery acquired from an unmanned aerial vehicle (UAV) and automatic 3D photo-reconstruction methods. Eur. J. Agron. 55, 89–99. https://doi.org/10.1016/j.eja.2014.01.004
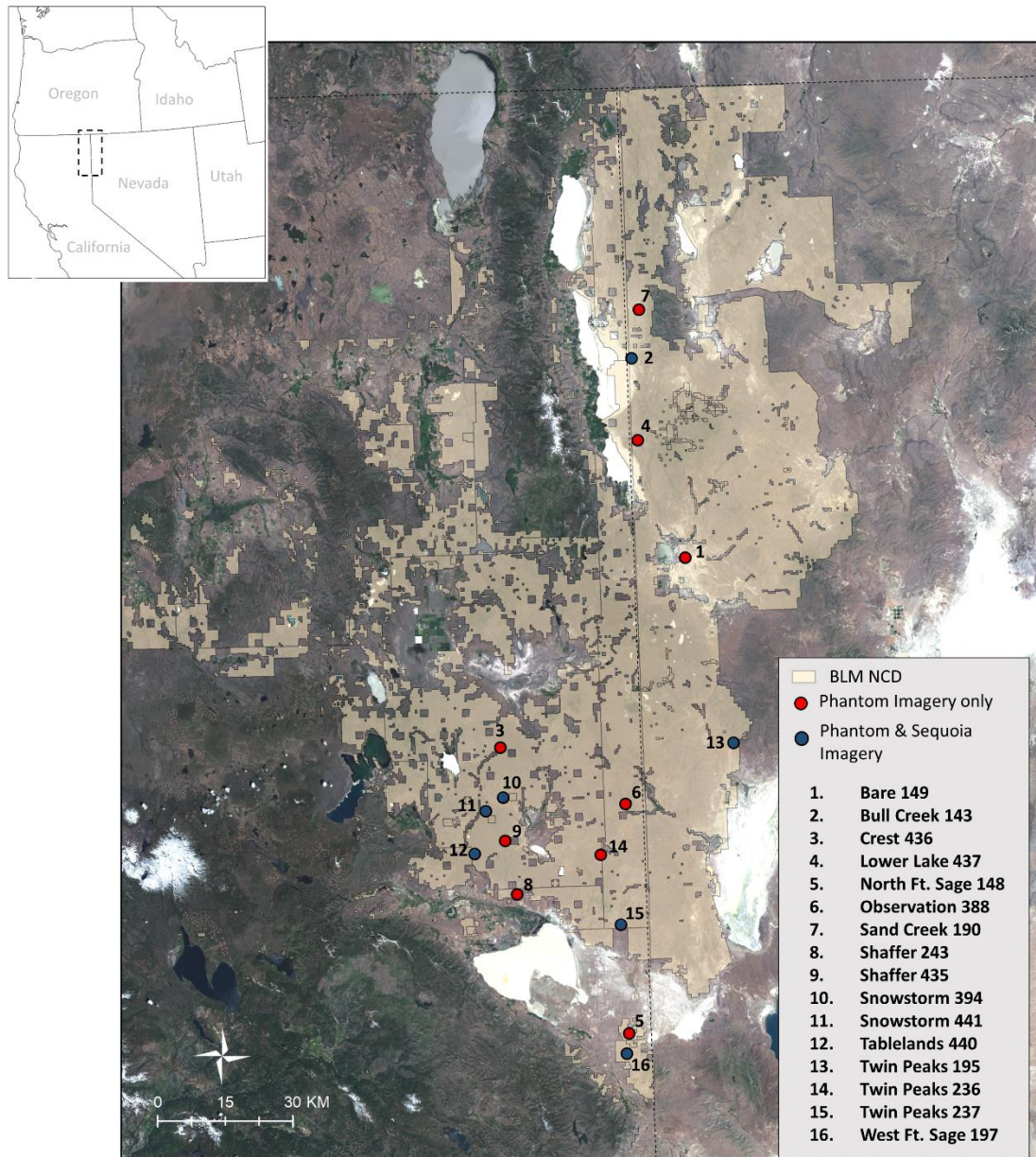
Figures and Tables

Fig. 1. Study area at the Northern California District (NCD) of the Bureau of Land Management. BLM land is highlighted in tan. Red circles indicate sample locations where only Phantom imagery was collected, while blue circles are sample locations where Phantom and Sequoia imagery were acquired. The background imagery is from Landsat 8, acquired June 2017.
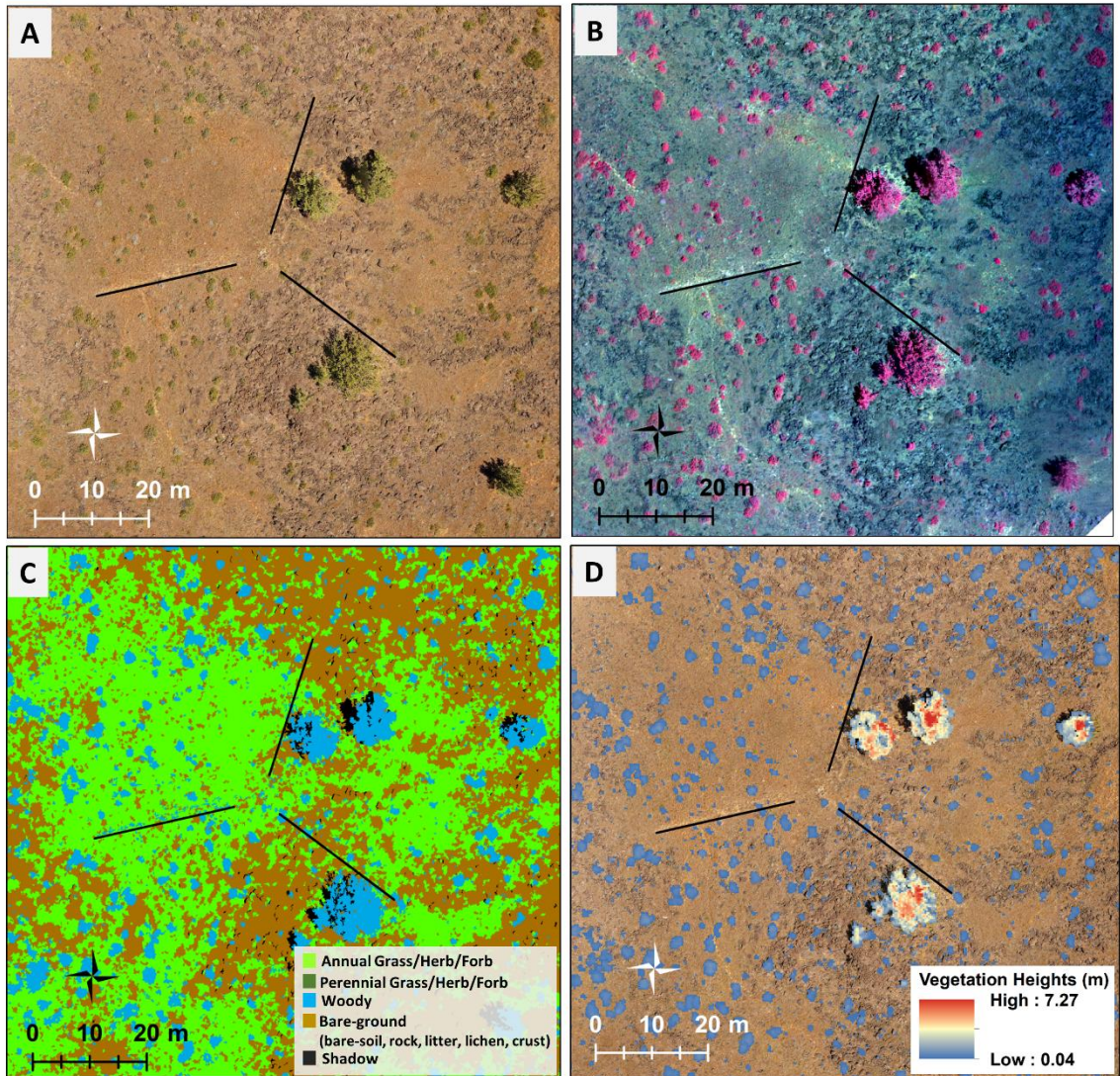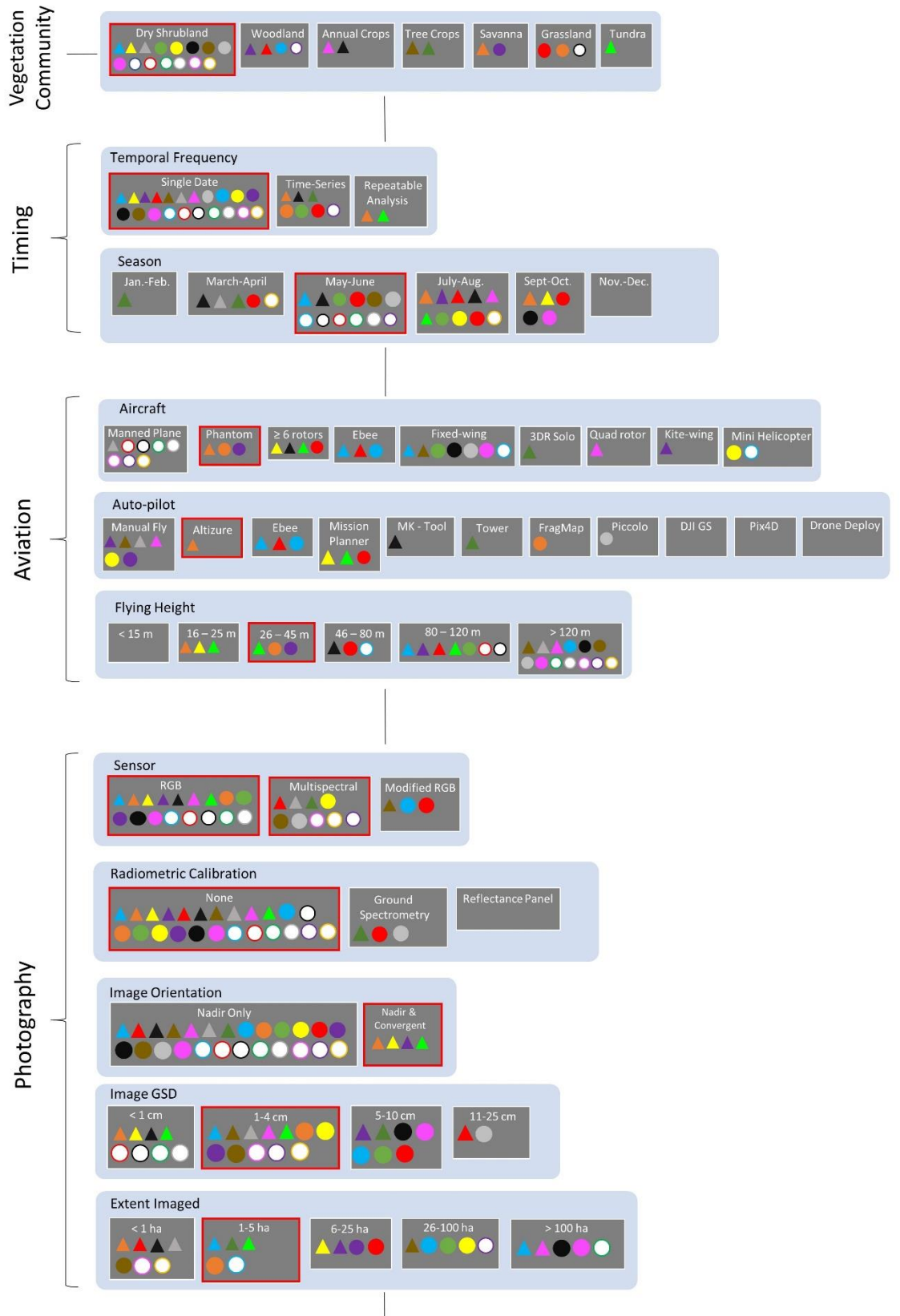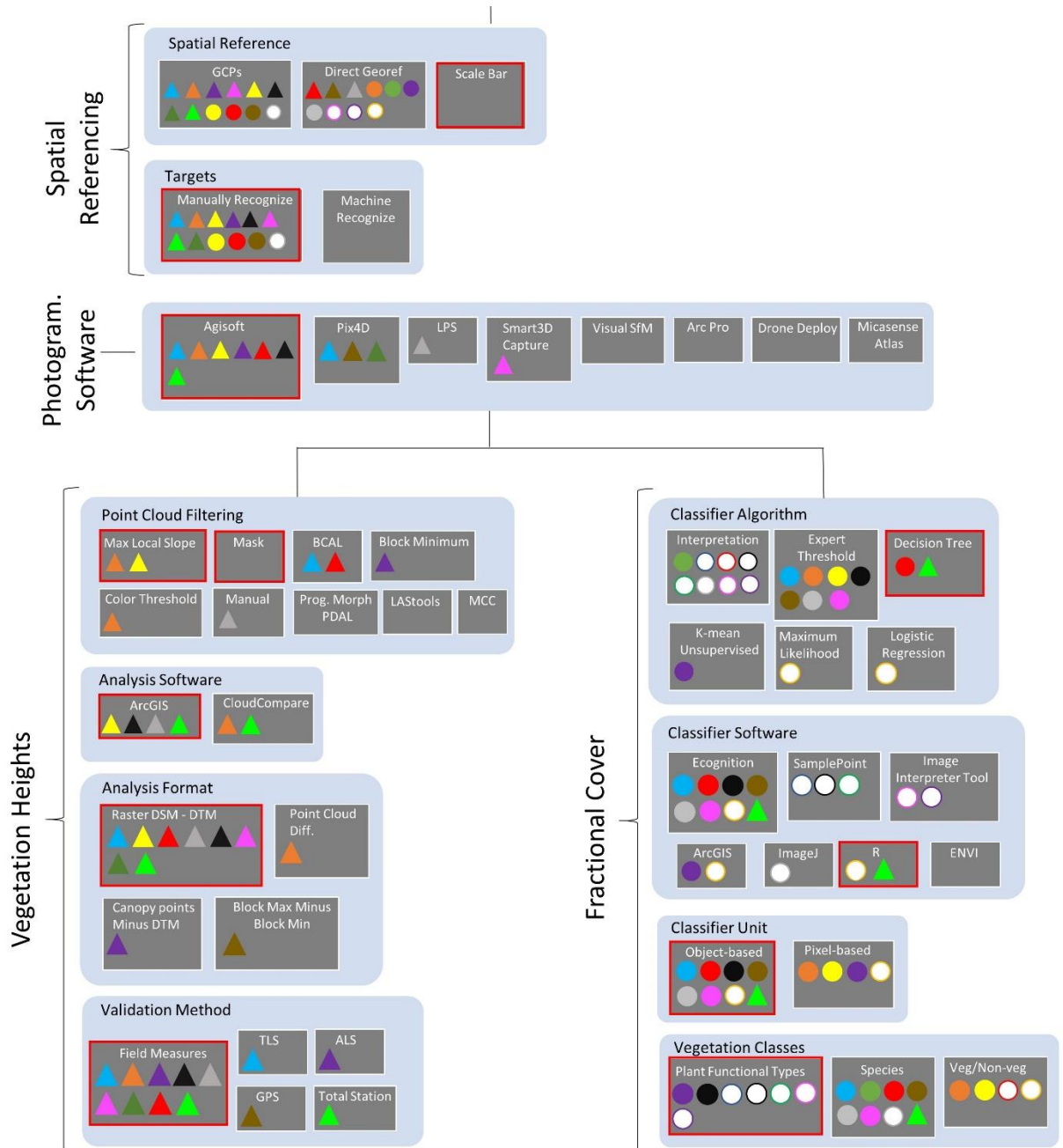
Fig. 2. Data for this study were collected at field plots consisting of three 25 m transects (black lines). Shown here is plot Tablelands 440. A) Orthomosaic made with Phantom RGB imagery, B) false-color composite orthomosaic made with Sequoia multi-spectral imagery, C) an orthomosaic thematically classified into plant functional types, D) woody vegetation heights.

Spatial Referencing

Spatial Reference
GCPs
Direct Georef
Scale Bar

Targets
Manually Recognize
Machine Recognize

Photogram. Software
Agisoft · Pix4D · LPS · Smart3D Capture · Visual SfM · Arc Pro · Drone Deploy · Micasense Atlas

Vegetation Heights

Point Cloud Filtering
Max Local Slope · Mask · BCAL · Block Minimum
Color Threshold · Manual · Prog. Morph PDAL · LAStools · MCC

Analysis Software
ArcGIS · CloudCompare

Analysis Format
Raster DSM - DTM · Point Cloud Diff.
Canopy points Minus DTM · Block Max Minus Block Min

Validation Method
Field Measures · TLS · ALS
GPS · Total Station

Fractional Cover

Classifier Algorithm
Interpretation · Expert Threshold · Decision Tree
K-mean Unsupervised · Maximum Likelihood · Logistic Regression

Classifier Software
Ecognition · SamplePoint · Image Interpreter Tool
ArcGIS · ImageJ · R · ENVI

Classifier Unit
Object-based · Pixel-based

Vegetation Classes
Plant Functional Types · Species · Veg/Non-veg

Vegetation Heights Literature
▲ Olsoy et al. 2018
▲ Gillan et al. *In Press*
▲ Cunliffe et al. 2016
▲ Jensen & Mathews 2016
▲ Sankey et al. 2017
▲ Bendig et al. 2014
▲ Zarco-Tejada et al. 2014
▲ Gillan 2014
▲ Li et al. 2016
▲ Johansen et al. 2018
▲ Fraser et al. 2016

Fractional Cover Literature
● Baena et al. 2017
● Meng et al. 2018
● Hardin et al. 2007
● McGwire et al. 2013
● Cruzan et al. 2016
● Lu & He 2017
● Laliberte et al. 2010a
● Laliberte et al. 2010b
● Laliberte et al. 2011
● Laliberte & Rango 2011
○ Breckenridge et al. 2011
○ Seefeldt & Booth 2006
○ Booth & Cox 2008
○ Booth & Cox 2009
○ Duniway et al. 2012
○ Karl et al. 2014
○ Moffet 2009
○ Karl et al. 2012
▲ Fraser et al. 2016

Fig. 3. Workflow decisions based on a review of 29 published studies using high-resolution aerial photography (drone and manned aircraft) to estimate vegetation fractional cover and height. The focus was on rangeland type environments (e.g., grasslands, shrublands) but also included some research in crop systems. The options used in this project are highlighted with red boxes.
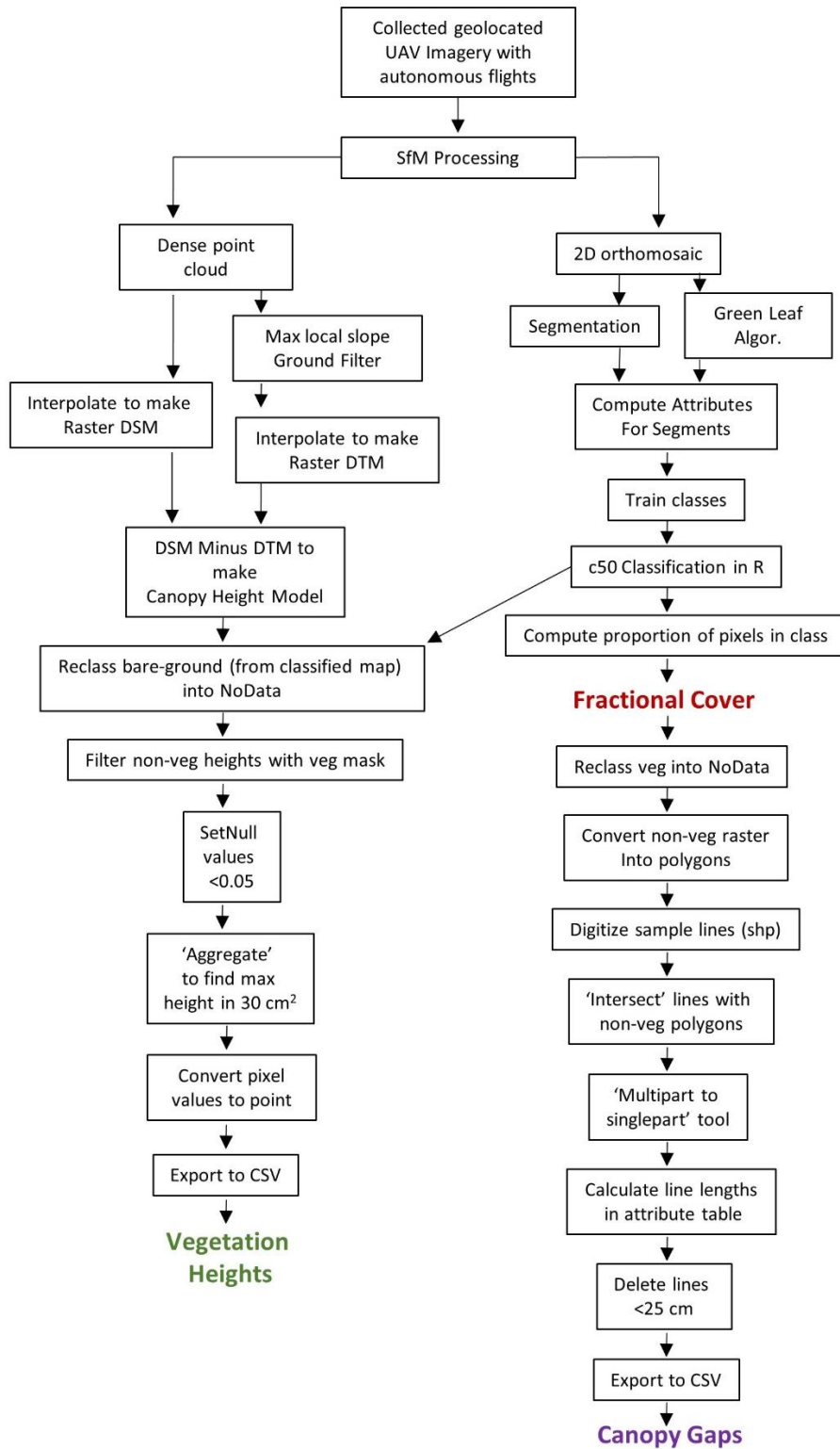
Fig. 4. Step-by-step workflow to calculate vegetation fractional cover by plant functional types, canopy gaps, and vegetation heights from orthomosaics and point clouds.

Predictor Features	
Phantom Imagery	**Sequoia Imagery**
Blue mean, SD	Green mean, SD
Green mean, SD	Red mean, SD
Red mean, SD	Red edge mean, SD
---	NIR mean, SD
Pixel count	Pixel count
Rectangularity	Rectangularity
Compactness	Compactness
Green leaf algorithm mean, SD	NDVI mean, SD

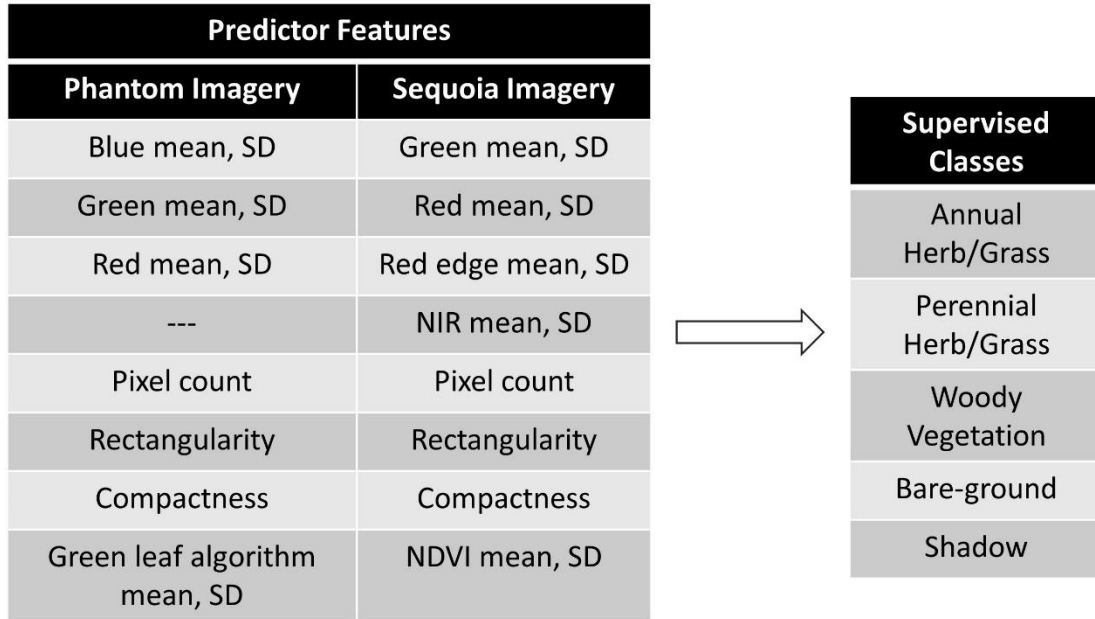| Supervised Classes |
|---|
| Annual Herb/Grass |
| Perennial Herb/Grass |
| Woody Vegetation |
| Bare-ground |
| Shadow |

Fig. 5. Image features used to predict supervised classes in c50 decision tree classification
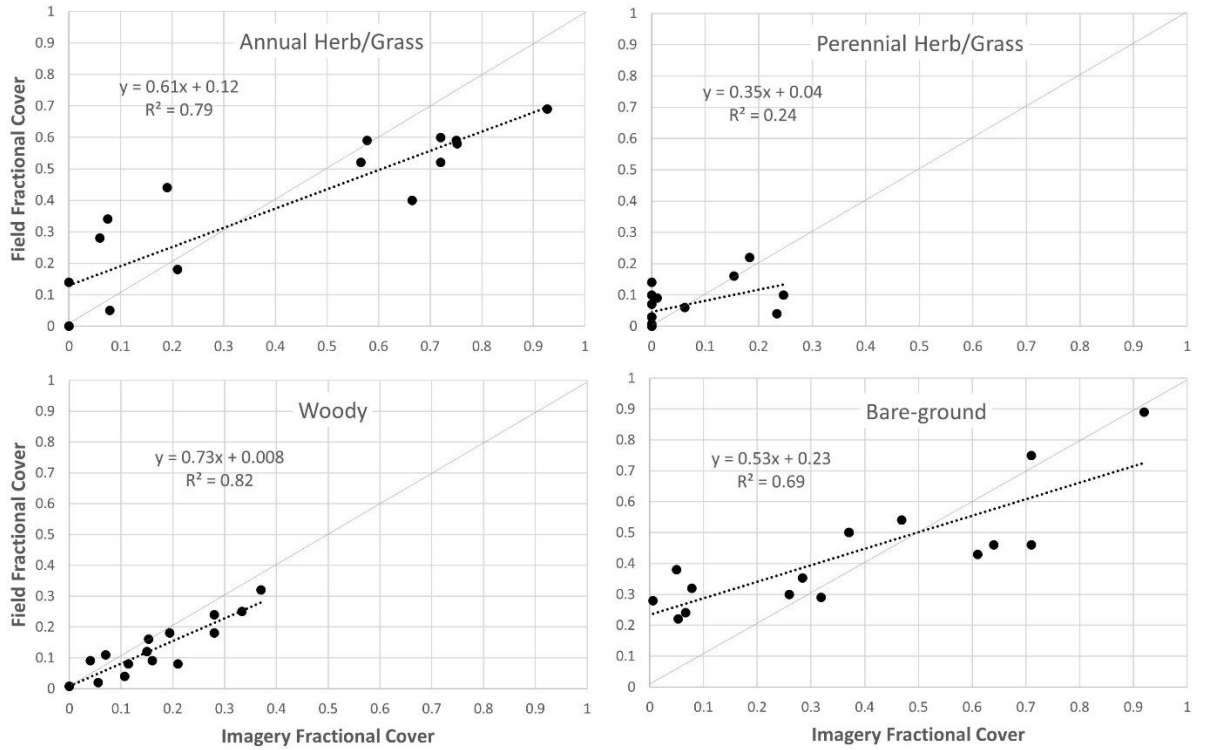
Fig. 6. Scatter plots and linear regression (dotted lines) show the comparison between field and

imagery estimates of fractional cover (n=16). Solid grey lines represent a 1:1 agreement.
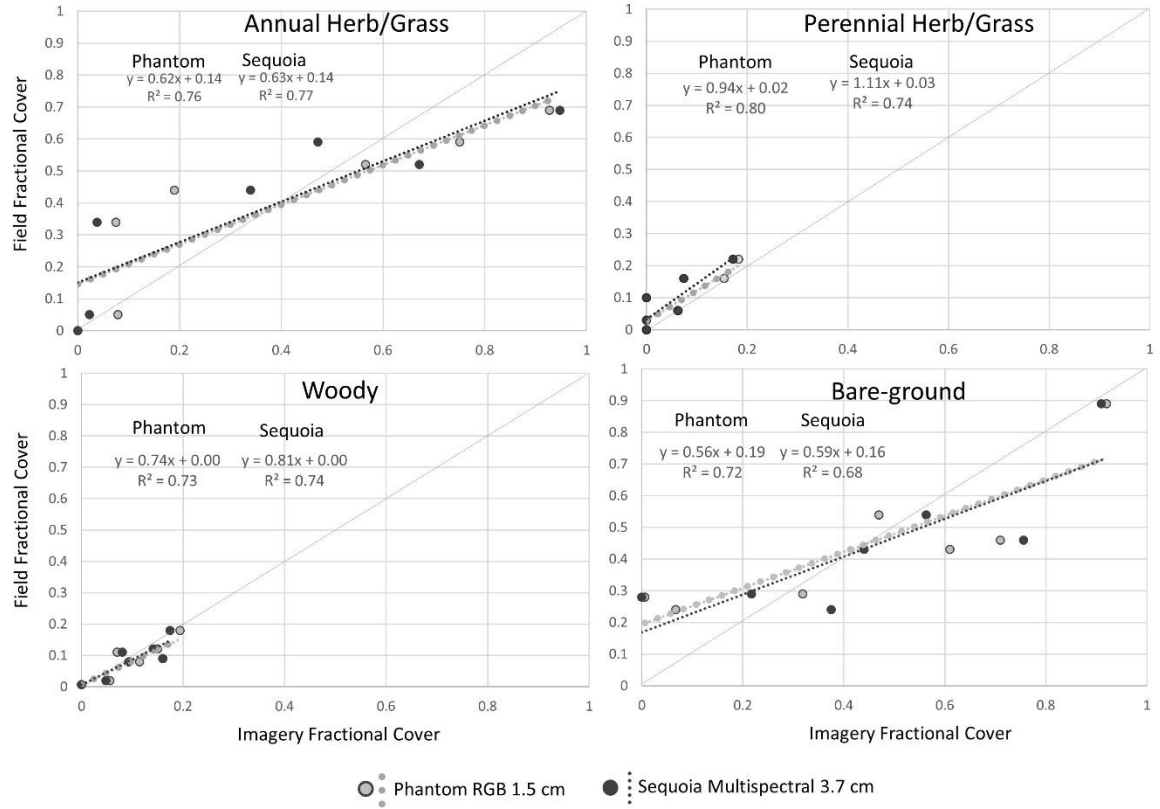
Fig. 7. Fractional cover scatter plots and regression lines showing linear relationships between Phantom RGB imagery and field methods (n=7), and Sequoia multi-spectral imagery and field methods (n=7). Solid lines represent 1:1 agreement.
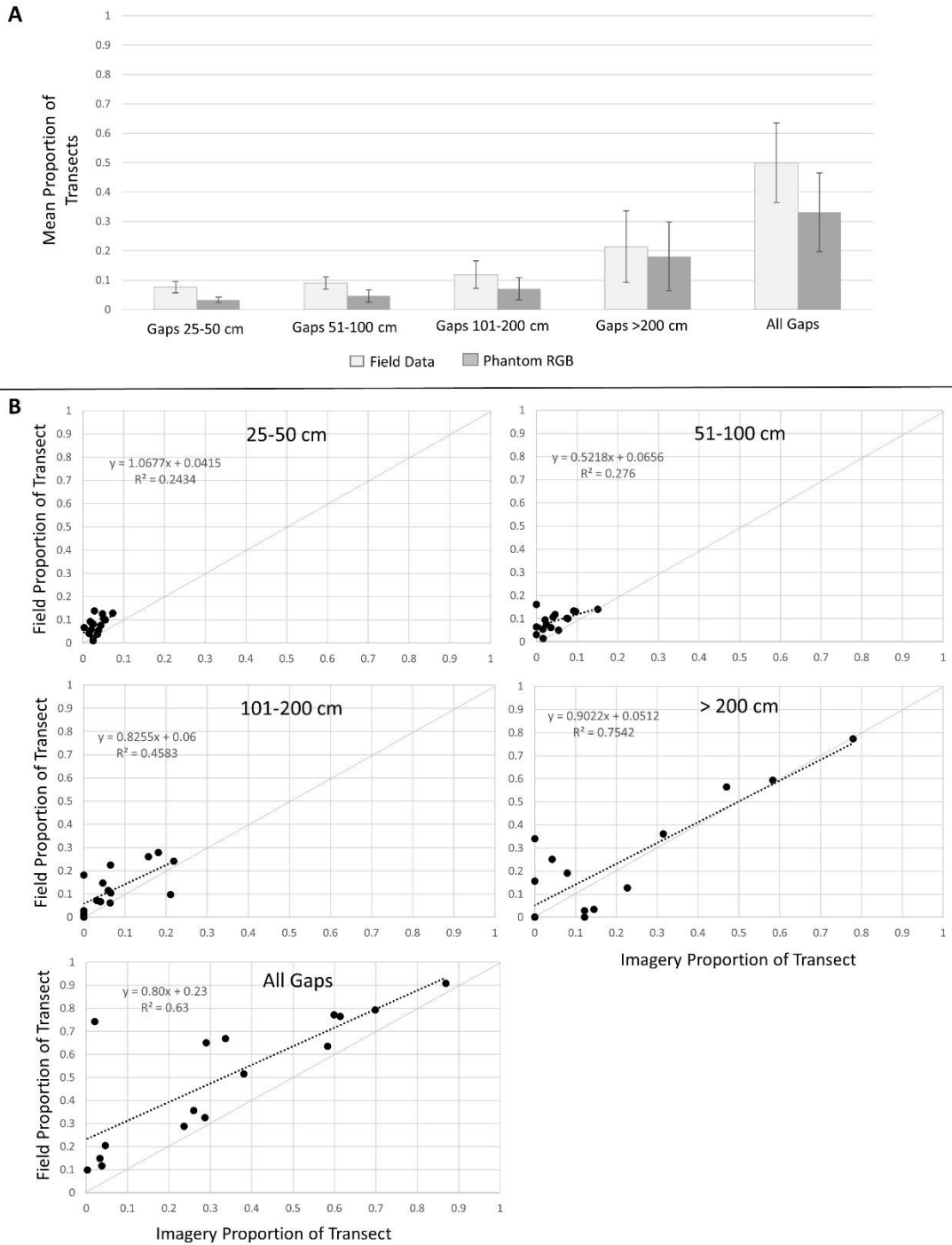
Fig. 8. Canopy gaps comparison between field measurements and imagery. A) Bars indicate mean proportion of transect with associated gap sizes. Error bars indicate 95% confidence intervals. B) Scatterplots and linear regression (dotted lines) comparing field and imagery estimates of canopy gaps. Solid lines represent 1:1 agreement.
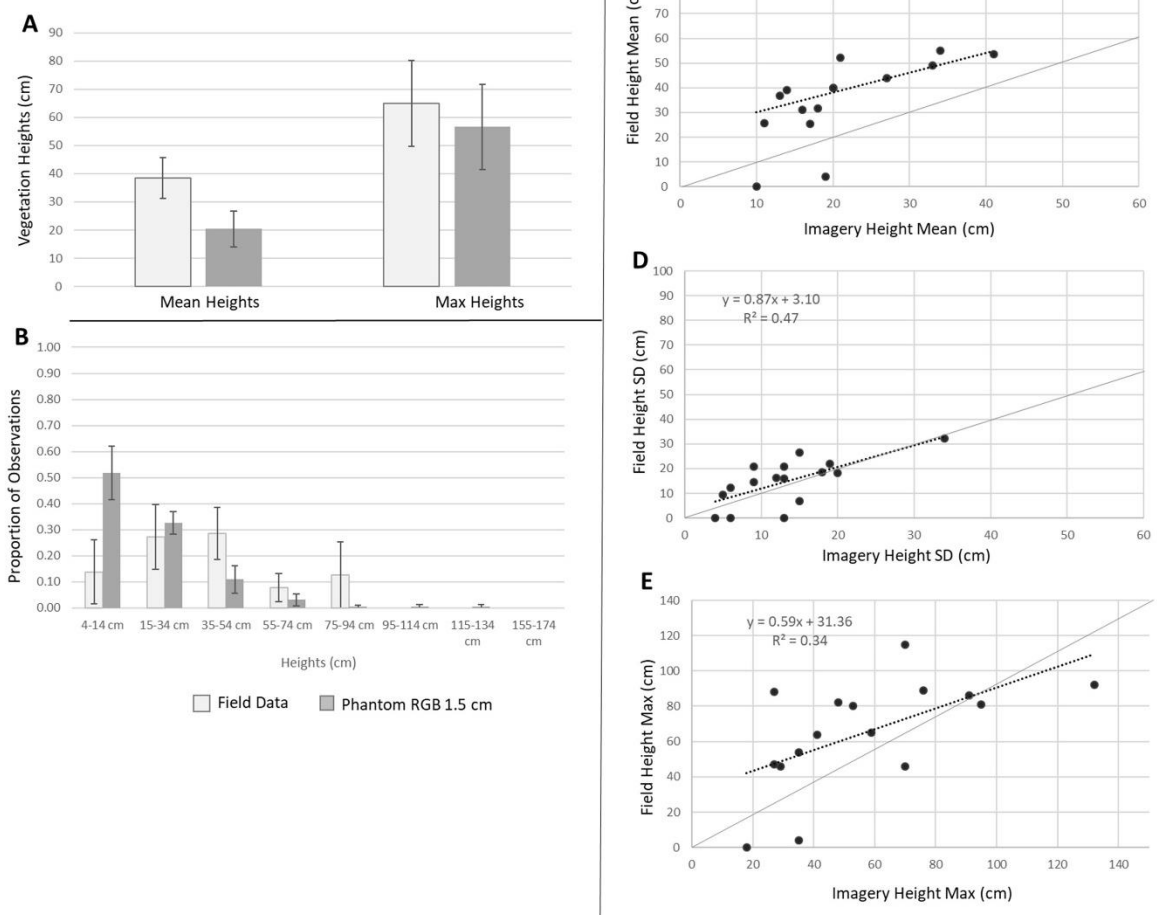
Fig. 9. Agreement between field and imagery methods of estimating vegetation heights. A) Bar graphs show mean and maximum vegetation heights across all plots with 95% confidence intervals (n=16), B) Histogram showing proportion of values within height bins with 95% confidence intervals, C) scatterplot and linear regression for mean height, D) scatterplot and linear regression for height standard deviation, and E) scatterplot and linear regression (dotted lines) for maximum vegetation heights. Solid lines represent 1:1 agreement.

Table 1. Phantom 3 and 4 camera and Parrot Sequoia sensor specifications

	Spectral Characteristics	Sensor Pixels	Shutter	Radiometric Resolution	Image Format	Image Overlap	GSD at 40 m AGL
Phantom 3 & 4	Red, Green, Blue	4000 horizontal x 3000 vertical (12 mpx)	Rolling with 33 millisecond readout	8 bit (256 BVs)	jpeg	75-80%	1.5 cm
Parrot Sequoia	Green 530-570 nm Red 640-680 nm Red-edge 730-740 nm NIR 770-810 nm	1280 horizontal x 960 vertical (1.2 mpx)	Global	10 bit (1,024 BVs) stored as 16 bit (65,536 BVs)	Tiff	75-80%	3.7 cm

Table 2. Fractional cover for field data and Phantom RGB imagery. Standard errors are shown in parenthesis.

	Data	Annual Herb/Grass	Perennial Herb/Grass	Woody	Bare-ground	Shadow
Mean	Field	0.37(0.05)	0.06(0.01)	0.12(0.02)	0.43(0.04)	0
	Phantom	0.39(0.08)	0.05(0.02)	0.15(0.02)	0.36(0.07)	0.017
	Difference	0.02(0.04)	0.00(0.02)	0.03(0.01)	-0.06(0.04)	0.017
Absolute Mean	Difference	0.13(0.02)	0.05(0.01)	0.04(0.00)	0.14(0.02)	0.017

Table 3. Comparing fractional cover estimated with Phantom RGB and Sequoia multi-spectral imagery (n=7). Standard errors shown in parenthesis.

	Data	Annual Herb/Grass	Perennial Herb/Grass	Woody	Bare-ground	Shadow
Mean	Field	0.37(0.09)	0.08(0.03)	0.08(0.02)	0.44(0.08)	0
	Phantom	0.36(0.14)	0.05(0.03)	0.10(0.02)	0.44(0.12)	0.01
	Sequoia	0.35(0.13)	0.04(0.02)	0.09(0.02)	0.46(0.11)	0.02
Mean Difference with Field Methods	Phantom	-0.00(0.07)	-0.02(0.01)	0.01(0.01)	-0.00(0.07)	0.01
	Sequoia	-0.01(0.06)	-0.03(0.01)	0.01(0.01)	0.01(0.06)	0.02
Absolute Mean Difference with Field Methods	Phantom	0.14(0.04)	0.02(0.01)	0.03(0.00)	0.14(0.03)	0.01
	Sequoia	0.13(0.04)	0.03(0.01)	0.02(0.00)	0.11(0.04)	0.02

Table 4. Comparison of canopy gap data as measured by field and imagery (Phantom) methods.

	Data	25-50 cm	51-100 cm	101-200 cm	>200 cm	All Gaps >25 cm
Mean	Field	0.07(0.00)	0.09(0.01)	0.11(0.02)	0.21(0.06)	0.49(0.06)
	Phantom	0.03(0.00)	0.04(0.01)	0.071(0.01)	0.18(0.05)	0.33(0.06)
	Difference	-0.04(0.00)	-0.04(0.01)	-0.04(0.01)	-0.03(0.03)	-0.16(0.04)
	Phantom/Field	0.42	0.44	0.63	0.85	0.67
Absolute Mean	Difference	0.04(0.00)	0.04(0.00)	0.06(0.01)	0.08(0.02)	0.16(0.04)

Supplemental Material

Table S1. Location and description of each sampling plot in the Bureau of Land Management

Northern California District.

Plot	Date Acquired	Coordinates Elevation	Ecological Site Eco Clusters	Precip (mm)	1.5 cm Phantom	3.7 cm Sequoia
Bare 149	7/1/2017	41.05865° N 119.86897° W 1453 m	R024XY020NV DROUGHTY LOAM 8-10 P.Z. **Loamy Slope 6-12"**	230	✓	
Bull Creek 143	6/30/2017	41.46002° N 119.99275° W 1380 m	R024XY003NV SODIC TERRACE 6-8 P.Z. **Arid/Sodic**	178	✓	✓
Crest 436	6/22/2017	40.69162° N 120.37149° W 1651 m	R023XF093CA SHALLOW CLAY 9-16" **Vertisol**	330	✓	
Lower Lake 437	7/1/2017	41.29594° N 119.98383° W 1602 m	R024XY002NV LOAMY 5-8 P.Z. **Arid/Sodic**	165	✓	
North Ft. Sage 148	6/18/2017	40.11316° N 120.05794° W 1226 m	R026XF022CA GRANITIC SAND 9-12" **Sandy**	236	✓	
Observation 388	6/20/2017	40.57118° N 120.04896° W 1476 m	R023XF081CA SHALLOW STONY LOAM 9-12" **Claypan**	360	✓	
Sand Creek 190	6/30/2017	41.55683° N 119.96850° W 1664 m	R024XY020NV DROUG HTY LOAM 8-10 P.Z **Loamy Slope 6-12"**	322	✓	
Shaffer 243	6/18/2017	40.39770° N 120.33855° W 1391 m	R023XF081CA SHALLOW STONY LOAM 9-12" **Claypan**	350	✓	
Shaffer 435	6/23/2017	40.50501° N 120.3654° W 1397 m	R023XF084CA CLAY UPLAND 9-16" **Vertisol**	266	✓	
Snowstorm 394	6/22/2017	40.59154° N 120.36804° W 1651 m	R023XF081CA SHALLOW STONY LOAM 9-12" **Claypan**	270	✓	✓
Snowstorm 441	6/28/2017	40.56508° N 120.41406° W 1441 m	R023XF084CA CLAY UPLAND 9-16" **Vertisol**	330	✓	✓
Tablelands 440	6/16/2017	40.48091° N 120.44641° W 1373 m	R023XF084CA CLAY UPLAND 9-16" **Vertisol**	266	✓	✓
Twin Peaks 195	6/20/2017	40.68550° N 119.75954° W 1439 m	R023XY006NV LOAMY 8-10 P.Z**. Loamy Slope 6-12"**	230	✓	✓
Twin Peaks 236	6/20/2017	40.47117° N 120.11642° W 1474 m	R023XF082CA STONY LOAM 9-12" **Loamy Slope 6-12"**	266	✓	
Twin Peaks 237	6/23/2017	40.33000° N 120.06989° W 1636 m	R023XF082CA STONY LOAM 9-12" **Loamy Slope 6-12"**	266	✓	✓
West Ft. Sage 197	6/19/2017	40.07272° N 120.06603° W 1541 m	R026XF052CA GRANITIC UPLAND 9-12" P.Z. **Sandy**	246	✓	✓

Table S2. Importance of predictor features in c50 decision tree classifications

Feature	Mean Usage %	Feature	Mean Usage %
1 GLA mean	94.57	10 Rededge mean	72.15
2 NDVI mean	94.55	11 NIR SD	64.53
3 Blue mean	93.06	12 Compactness	58.71
4 Red mean	90.59	13 Green SD	57.97
5 GLA SD	89.27	14 Red SD	57.80
6 NDVI SD	88.96	15 Blue SD	56.95
7 Green mean	87.90	16 Rectangularity	51.14
8 NIR mean	85.69	17 Rededge SD	49.91
9 Pixel count	83.77		

Table S3. Classification confusion matrix for Phantom imagery with 1.5 cm ground sampling distance.

	Annual herb/grass	Perennial herb/grass	Bare-ground	Woody	Shadow	Total	User's Accuracy
Annual herb/grass	190	8	16	5	1	220	0.86
Perennial herb/grass	10	83	6	14	1	114	0.72
Bare-ground	11	2	269	15	4	301	0.89
Woody	9	6	8	293	7	323	0.90
Shadow	3	0	1	4	96	104	0.92
Total	223	99	300	331	109	1062	
Producer's Accuracy	0.85	0.83	0.90	0.88	0.88		0.87

Figure S1. R code for using c50 decision tree classification with segmented objects

```
setwd("F:\\gillan_sfm\\Norcal_aim_SfM\\projects_products\\lowerlake437_40agl_stuff\\exploration")
library(C50)
library(partykit)
library(mvtnorm)
library(raster)
library(shapefiles)
library(sp)
library(rgdal)
library(caret)
library(class)
library(e1071)
library(maptools)
library(doParallel)
registerDoParallel(cores = 20)
library(snow)
### Read in the raster images(the feature predictor variables)
 img<- stack("segment_pixelcount.tif","segment_CHM_SD.tif", "segment_CHM_mean.tif",
"segment_GLA_SD.tif", "segment_GLA_mean.tif", "segment_red_SD.tif", "segment_red_mean.tif",
"segment_green_SD.tif", "segment_green_mean.tif", "segment_blue_mean.tif", "segment_blue_SD.tif")
##Read in the training shapefiles, one for each class. The file names must end with 'train.shp'
train.files <- list.files(pattern="*train.*shp")
train.full <- NULL
for (x in seq_along(train.files)) {
  ### Read in the a shapefile
  train.locations <- readShapePoints(train.files[x])
  ### Extract values from the rasters at the shapefile point locations.
  train.predictors <- extract(img, train.locations, df = TRUE)
  ### Add a column for the class type and populate it.
  train.by.class <- cbind(train.predictors, "types" = substr(train.files[x], 1, nchar(train.files[x])-9))
  ### Combine the data with data from previous loops.
  train.full <- rbind(train.full, train.by.class)
}
#Training the c50 model with the training data
X <- train.full[,2:12]
Y <- train.full[,13]
testmodel<- C5.0(X, Y, trials = 20, rules = FALSE, control = C5.0Control(winnow=FALSE,
sample=0.75))
summary(testmodel)
#Predict classes on raster image
beginCluster(20)
#NAvalue(img) <- x
clusterR(img,raster::predict, args=list(model=testmodel),
      filename="rgb_classified", format="HFA", datatype="INT1U" ,
      overwrite=TRUE, na.action=na.omit)
endCluster()
#Describe Predictor Variable importance
importance_usage <- C5imp(testmodel, metric = "usage", pct = TRUE)
importance_splits <- C5imp(testmodel, metric = "splits", pct = TRUE)
importance_usage
importance_splits
#Visualize the decision trees
plot(testmodel, trial = 19, subtree = NULL)
```